



HAL
open science

Observation and diagnosis for trucks

Donatien Dubuc

► **To cite this version:**

Donatien Dubuc. Observation and diagnosis for trucks. Automatic. Université Grenoble Alpes, 2018. English. NNT : 2018GREAT098 . tel-02122227

HAL Id: tel-02122227

<https://theses.hal.science/tel-02122227>

Submitted on 7 May 2019

HAL is a multi-disciplinary open access archive for the deposit and dissemination of scientific research documents, whether they are published or not. The documents may come from teaching and research institutions in France or abroad, or from public or private research centers.

L'archive ouverte pluridisciplinaire **HAL**, est destinée au dépôt et à la diffusion de documents scientifiques de niveau recherche, publiés ou non, émanant des établissements d'enseignement et de recherche français ou étrangers, des laboratoires publics ou privés.

THÈSE

pour obtenir le grade de

**DOCTEUR DE LA COMMUNAUTE
UNIVERSITE GRENOBLE ALPES**

Spécialité : **Automatique-Productique**

Arrêté ministériel : 25 mai 2016

Présentée par
Donatien DUBUC

Thèse dirigée par **Olivier SENAME** et
co-encadrée par **Delphine BRESCH-PIETRI**

préparée au sein du **GIPSA-Lab**
dans l'**Ecole Doctorale d'Electronique, Electrotechnique,
Automatique, Traitement du Signal (EEATS)**

Observation and diagnosis for trucks

Thèse soutenue publiquement le **10 Décembre 2018**,
devant le jury composé de:

M. Didier THEILLIOL

Professeur, Université de Lorraine, Président

M. Jimmy LAUBER

Professeur, Université Polytechnique Hauts-de-France,
Rapporteur

M. Guillaume COLIN

Maître de Conférences, Université d'Orléans, Rapporteur

M. Olivier SENAME

Professeur, Grenoble INP, Directeur de thèse

Mme Delphine BRESCH-PIETRI

Maître-assistante, Mines Paritech, Co-encadrante de thèse

M. Adrien HALLÉ

Ingénieur, Volvo Group, Examineur

M. Christophe GAUTHIER

Ingénieur, JTEKT Europe, Invité



Remerciements

Tout d'abord, un chaleureux merci à l'initiateur de la thèse en la personne de Christophe Gauthier sans qui rien ne serait arrivé. Un merci équivalent à mes chers encadrants scientifiques Olivier Sename et Delphine Bresch-Pietri qui ont su donner inspiration, motivation et persévérance. Merci encore à Adrien Hallé qui a excellemment repris la relève de Christophe en apportant expertise technique et nouveaux regards sur le sujet.

Merci à Jimmy Lauber et Guillaume Colin d'avoir accepté d'être rapporteurs et pour leurs retours enrichissant. Merci également à Didier Theilliol pour la présidence du jury.

Ma gratitude aussi à toute l'équipe de management de Volvo qui m'a accompagné tout au long de la thèse.

Des mercis spéciaux à tous ceux qui ont anéanti ma productivité pendant ces trois années. J'accuse mes camarades doctorants du Gipsa : Kazusa, Diego, Nadia, Tan, Sandra, Hung, Phong. Les piliers, les rocs de feu AT&R : Francesco, Elodie, Johana, Yoan, Wilfried, Thomas, Xavier. Les (ex)tôliers de "control" : Mickaël, Jérôme, Tanguy, Nicolas, Gabriel. Vous méritez amour et sympathie.

Et enfin, je me dois de remercier une certaine personne qui mérite toute ma gratitude. Bisous ma p'tite roussette.

Contents

Table of Acronyms	xv
Résumé (in French)	xvii
Preamble	1
Introduction	3
1 Some theoretical background	9
1.1 Dynamical systems under consideration	9
1.1.1 Nonlinear systems	10
1.1.2 Linear Time Invariant systems	10
1.1.3 LPV systems	11
1.1.3.1 Representation of LPV systems	12
1.1.4 Stability of LPV systems	13
1.2 Observer design	14
1.2.1 LPV polytopic systems	15
1.2.1.1 Pole placement method	15
1.2.1.2 \mathcal{H}_∞ performance method	18
1.2.1.3 FAFE design method	19
1.2.1.4 \mathcal{H}_∞ filtering method	22
1.2.1.5 Implementation issues	25
1.2.2 For nonlinear systems	29
1.2.2.1 Kalman observer	29
1.2.2.2 Adaptive observer	30

2	Belt tensioner diagnosis	33
2.1	Introduction	33
2.2	Cooling System Modeling	34
2.2.1	Thermal modeling of the engine block	35
2.2.1.1	Engine block thermal balance	36
2.2.1.2	Coolant thermal balance	37
2.2.1.3	Final second-order model	37
2.2.2	Flow modeling	38
2.2.3	Model validation	39
2.3	Observer-based fault estimation	40
2.3.1	Fault diagnosis problem statement	40
2.3.2	Adaptive observer	41
2.3.3	Extended Kalman filter	43
2.4	Simulation results	43
2.4.1	Fault scenario	44
2.4.2	First simulation case: constant engine speed and torque	44
2.4.3	Second simulation case: constant engine speed and time-varying torque	45
2.4.4	Third simulation case: more realistic profiles	46
2.5	Conclusion	47
3	CAC and EGR cooler diagnosis	49
3.1	Introduction	49
3.2	Subsystems modeling	51
3.2.1	Gas mixture modeling inside the intake manifold	51
3.2.2	Charge air cooler modeling	52
3.2.3	T_{2A} estimation	53
3.2.4	EGR cooler modeling	54

3.2.5	Summary of the considered model and measurements	55
3.3	Observers design	56
3.3.1	Observer design for k_{cac}	56
3.3.2	LPV observer design for k_{egr}	57
3.3.2.1	LPV modeling	57
3.3.2.2	LPV observer design	58
3.4	Estimation results	59
3.4.1	Heat transfer coefficients expression	59
3.4.1.1	k_{cac} estimation	60
3.4.1.2	k_{egr} estimation	61
3.4.2	k_{cac} observer evaluation	62
3.4.3	k_{egr} observer evaluation	63
3.5	Sensitivity with respect to input uncertainties	64
3.6	Conclusion	67
4	EGR mass flow rate Estimation	69
4.1	Introduction	69
4.2	Intake manifold modeling	71
4.3	Observers design	72
4.3.1	Pole placement design	73
4.3.2	FAFE design	75
4.3.3	\mathcal{H}_∞ filter design	77
4.3.4	Kalman filter design	78
4.3.5	Adaptive observer design	79
4.3.6	Sliding mode observer design	80
4.4	Experimental setup	83
4.4.1	ECU implementation	83

4.4.2	Test cell description	84
4.4.3	EGR mass flow rate measurement	85
4.5	Experimental results	85
4.5.1	Medium duty 5L engine	86
	Case 1: WHSC.	86
	Case 2: Part load.	86
4.5.2	Medium duty 8L engine	87
	Case 3: WHSC.	87
	Case 4: Part load.	87
4.5.3	Analysis of the estimation errors	89
4.5.4	Computational performance	91
4.6	Conclusion	92
5	Exhaust Pressure Estimation	93
5.1	Introduction	94
5.2	Mean value model of the engine	95
5.2.1	Exhaust manifold dynamics	96
5.2.2	Turbocharger dynamics	97
	5.2.2.1 Rotor speed modeling	97
	5.2.2.2 Compressor power	98
	5.2.2.3 Turbine power	99
5.2.3	Turbine flow modeling	101
	5.2.3.1 Orifice flow equation	101
	5.2.3.2 Hammerstein-Wiener model	101
	5.2.3.3 Identification results	102
5.2.4	Summary of the nonlinear model of ω_{tc} and P_3	102
5.3	Observer design	103

5.3.1	LPV modeling	104
5.3.2	Problem formulation	105
5.3.3	Synthesis	106
5.4	Simulation results	108
5.4.1	Case 1: D_t defined by the orifice equations (5.13)-(5.15)	109
5.4.2	Case 2: D_t defined by HW model	109
5.5	Some ongoing studies	110
5.5.1	Pressure and EGR mass flow estimation	110
5.5.2	Turbocharger efficiency estimation	111
5.6	Conclusion	112
6	Engine mass flow rates estimation submitted to a sensor delay	115
6.1	Introduction	115
6.2	Time-delay system modeling	118
6.2.1	O_2 concentration in the intake manifold	119
6.2.2	O_2 concentration in the exhaust manifold	119
6.2.2.1	After the DPF	120
6.2.3	Delay modeling	121
6.2.4	Summary of time-delay system modeling	122
6.3	Time-delay observer synthesis	123
6.3.1	Analysis and LPV formulation	123
6.3.2	Design of LPV time-delay observers	127
6.4	Results for EGR and Inlet air mass flow rates estimation	132
6.4.1	Synthesis based on Theorem 6.1	133
	Case 1.	133
	Case 2.	135
6.4.2	Synthesis based on Theorem 6.2	137

Case 3.	137
Case 4.	137
Case 5.	138
6.5 Conclusion	141
Conclusion	143
A Performance index	149
B World harmonized cycles	151
C Air mass flow aspirated by the cylinders	153
Bibliography	154

List of Figures

1	Exemples de systèmes complexes	xvii
2	European legislation emission limits for diesel engines [Martin 2010]	3
1.1	Different classes of systems	10
1.2	Pole placement area example	17
1.3	Generalized \mathcal{H}_∞ problem	23
1.4	Bloc scheme for fault estimation	25
1.5	Generalized \mathcal{H}_∞ problem for fault estimation	25
1.6	Matrix polytopic interpolation	28
2.1	Components driven by the belt	34
2.2	Architecture of the cooling system	36
2.3	Flows and temperatures of the engine block	37
2.4	Heat flow from the gas to the engine block	38
2.5	Block diagram to validate the simplified model	39
2.6	Torque and engine speed profiles	39
2.7	Comparison between the reference and the simplified model	40
2.8	Block diagram to evaluate the developed observers	44
2.9	Estimation results obtained in the first case	45
2.10	Torque profile in the second case	46
2.11	Estimation results obtained in the second case	46
2.12	Estimation results obtained in the third case	47
3.1	Schematic view of the air path in the considered engine	50
3.2	Intake manifold volume	51
3.3	Heat exchanges inside the Charge Air Cooler (CAC)	53

3.4	Block diagram to evaluate T_{2A} modeling (3.9)	54
3.5	Evolution of the temperature after the compressor T_{2A}	54
3.6	Heat exchanges inside the EGR cooler	55
3.7	Pole placement area	59
3.8	Interpolation of the identified k_{cac} data	61
3.9	Time-domain results of the identified data k_{cac}	61
3.10	Interpolation of the identified k_{egr} data	62
3.11	Time-domain results of the identified data k_{egr}	63
3.12	k_{cac} estimation for a WHSC	63
3.13	k_{cac} estimation for a WHTC	64
3.14	k_{egr} estimation for a WHSC	64
3.15	k_{egr} estimation for a WHTC	65
3.16	Box plot for k_{cac} estimation	67
3.17	Box plot for k_{egr} estimation	68
4.1	Schematic view of the air path in the considered engine	70
4.2	Intake manifold volume	71
4.3	Pole placement area	74
4.4	FAFE parameters optimization using a Genetic Algorithm	76
4.5	Block scheme for \mathcal{H}_∞ filter design	77
4.6	Generalized \mathcal{H}_∞ problem	78
4.7	Bode diagram of S_{f,e_f} at each vertex	79
4.8	Sliding mode observer parameters optimization using a Genetic Algorithm	82
4.9	Process of the ECU implementation	84
4.10	Test cell description	85
4.11	Part load profile for the engine speed and torque	86
4.12	WHSC for 5L engine (case 1)	87

4.13	Partial results for the part load cycle - 5L (case 2)	88
4.14	Relative error for different operating points - 5L (case 2)	88
4.15	WHSC for 8L engine (case 3)	89
4.16	Partial results for the part load cycle - 8L (case 4)	89
4.17	Relative error for different operating points - 8L (case 4)	90
4.18	Inlet air mass flow rate (top) - Absolute errors of D_{air} and D_{egr} (bottom) . .	90
4.19	Execution time of the function containing the observers	92
5.1	Schematic view of the air path in the considered engine	96
5.2	Scheme of a turbocharger	98
5.3	Interpolated compressor efficiency map	99
5.4	Interpolated turbine efficiency map	100
5.5	Hammerstein-Wiener model block diagram	102
5.6	Identification results for transient cycle	103
5.7	Identification results for stationary cycle	104
5.8	Roots locus of T_{wez}	108
5.9	Frequency response of $T_{ezw}(\rho)$	109
5.10	Scheme of the simulation tests	110
5.11	Case 1: WHSC cycle with D_t defined by orifice equations (5.13)-(5.15)	111
5.12	Case 1: WHTC cycle with D_t defined by orifice equations (5.13)-(5.15)	112
5.13	Case 2: WHSC cycle with D_t defined by the Hammerstein-Wiener model . .	113
5.14	Case 2: WHTC cycle with D_t defined by the Hammerstein-Wiener model . .	114
6.1	Schematic view of the air path and the after treatment system	116
6.2	Case 0: flows estimation without taking account the delay	117
6.3	Control volume	118
6.4	Intake manifold volume	119

6.5	Exhaust manifold volume	119
6.6	Exhaust volume	120
6.7	Identification results where the measure F_4 is obtained with NOx sensor and the model is (6.6)	123
6.8	Evolution of $h(t)$ defined in (6.10)	124
6.9	Results for case 1	134
6.10	Results for case 2	136
6.11	Results for case 3	138
6.12	Results for case 4	139
6.13	Results for case 5	140
6.14	TRL scale. Source: wikipedia	145
6.15	Development and readiness of the topics addressed in this thesis	147
B.1	The two standard cycles used	151

List of Tables

1	Observer frameworks used in the chapters	5
2	Features addressed along the thesis	6
2.1	Nomenclature	35
3.1	Nomenclature	51
3.2	<i>NRMS</i> obtained for the different cycles	60
3.3	Values of the considered errors on the inputs	65
4.1	Nomenclature	71
4.2	Eigenvalues of $A_i - L_i C$	75
4.3	Parameters value for the SM observer	83
4.4	Execution time of the function sorted in ascending order	91
5.1	Nomenclature	95
5.2	<i>FIT</i> obtained for the different cases	102
5.3	<i>NRMS</i> obtained for the different cases	108
6.1	Nomenclature	118
6.2	NRMS for the different cases	133

Table of Acronyms

Acronyms related to control theory

LTI	Linear Time Invariant
LPV	Linear Parameter Varying
LTV	Linear Time Varying
LMI	Linear Matrix Inequality
ODE	Ordinary Differential Equation

Acronyms related to the engine

OBD	On-Board Diagnosis
WHSC	World Harmonized Stationary Cycle
WHTC	World Harmonized Transient Cycle
EGR	Exhaust Gas Recirculation
CAC	Charge Air Cooler
ECU	Electronic Control Unit
NOx	Nitrogen Oxides

Mathematical notations

\mathbb{R}	Real values set
M^T	Transpose of the real matrix M
$M \prec 0$	Matrix M is symmetric and negative definite
$M \succ 0$	Matrix M is symmetric and positive definite
$\text{Co}(X)$	Convex hull of set X
*	Symmetric element of the opposite bloc in a matrix
I_n	$n \times n$ identity matrix
\hat{x}	Estimation of the variable x
$\ \cdot\ _2$	Norm 2
$\ \cdot\ _\infty$	Norm ∞

Résumé (in French)

Cette thèse est le fruit d'une convention CIFRE (Conventions Industrielles de Formation par la REcherche) en collaboration avec le laboratoire Gipsa-lab et le groupe Volvo. Les travaux portent sur la conception d'observateurs, appliquée à plusieurs systèmes du camion, dans un objectif de diagnostic et d'estimation de variables.

Enjeux de la thèse

De nos jours, nous faisons face à importante complexification des objets de la vie courante. Ceci est particulièrement frappant dans l'industrie automobile qui, pour répondre à la fois aux exigences des clients en terme de confort, sécurité etc... mais aussi pour répondre aux nouvelles normes, a dû ajouter de nombreux systèmes supplémentaires.

Cela a pour conséquence d'augmenter le risque de défaillance du moteur, puisqu'il y a plus d'éléments susceptibles de subir une panne, mais aussi un besoin accru de contrôle avancé pour piloter ces nouveaux systèmes de manière la plus optimale possible. Comme nouveaux systèmes notables chez Volvo, citons par exemple : le système de post-traitement qui a rencontré de nombreuses nouvelles défaillances ; ou encore la boucle de recirculation des gaz d'échappement (EGR) qui nécessite un contrôle fin pour limiter les polluants afin de respecter la législation (voir [Figure 1](#)).

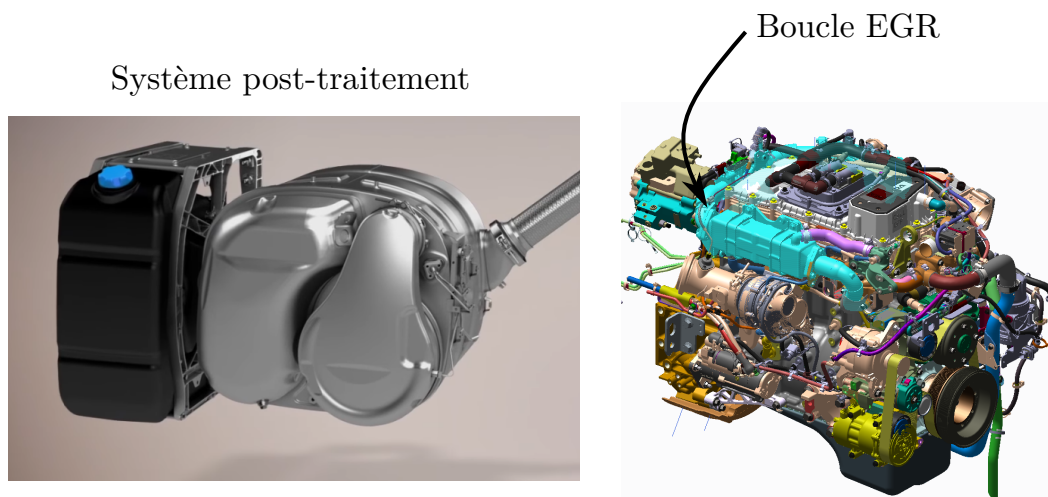


Figure 1: Exemples de systèmes complexes

Parmi les solutions disponibles pour répondre à ces nouveaux enjeux, le développement d'observateurs est une solution attractive car ils permettent de créer des fonctions de surveillance des systèmes et d'estimer plus de variables sans ajout de capteurs supplémentaires.

Résumé des contributions

Les travaux de thèse ont été présentés en 6 chapitres comme suit :

- Le chapitre 1 apporte des éléments théoriques sur la théorie du contrôle, avec un accent particulier sur la conception d'observateurs. Il présente les différentes structures d'observateur qui sont utilisées tout au long de la thèse. Deux types d'observateurs sont considérés : les observateurs dits LPV (linéaire à paramètre variant), écrits sous une forme polytopique, et les observateurs non linéaires.
- Le chapitre 2 traite de la surveillance de l'état de santé d'un tendeur de courroie de la courroie accessoire, un composant critique du moteur automobile garantissant l'efficacité du système de refroidissement du moteur. En effet, un défaut sur le tendeur de courroie affectera la transmission qui détériorera l'efficacité de la pompe à eau et, éventuellement, pourra entraîner un arrêt du moteur. Surveiller ce composant est donc primordial pour envisager de faire de la maintenance prédictive ou corrective. Dans ce chapitre, nous proposons d'estimer un paramètre qui s'avère caractéristique de l'état de santé de ce composant en utilisant un observateur adaptatif ou un filtre de Kalman étendu. Les mérites de ces solutions ont été comparés à l'aide de simulations réalisées avec GT-POWER sur un modèle haute fidélité. Même si l'observateur adaptatif a des propriétés de convergence garanties, il a été démontré que le filtre de Kalman étendu avait de meilleures performances pour cette application.
- Le chapitre 3 donne une solution de diagnostic embarqué pour le refroidisseur d'air suralimenté (CAC) et le refroidisseur EGR, qui doivent être diagnostiqués pour être conforme à la législation. Bien que ces diagnostics soient déjà réalisés chez Volvo, une autre configuration de capteurs a été envisagée pour réduire les coûts globaux de construction. Deux observateurs sont conçus pour estimer la qualité du transfert de chaleur du CAC et du refroidisseur EGR. Ils sont ensuite évalués sur des données réelles provenant d'un banc d'essai moteur. Ce chapitre permet d'établir que les solutions proposées pourraient diagnostiquer efficacement le CAC et le refroidisseur EGR.
- Le chapitre 4 compare différentes approches d'observation pour estimer une variable importante pour le contrôle des émissions de polluants : le débit massique de recirculation des gaz d'échappement (dit débit massique EGR). Ce chapitre vise à appliquer cinq approches d'observation présentées dans le chapitre 1 pour l'estimation du débit massique EGR plus une déjà présente dans la littérature. La conception de l'observateur se base sur l'utilisation du capteur de pression dans le collecteur d'admission comme mesure de référence, pour estimer ce débit massique. La validation finale consiste à implémenter sur un calculateur industriel embarqué d'un camion réel et à comparer les performances des différentes méthodes. Les essais effectués sur deux moteurs de camions montrent que, même si la structure d'observation est très différente, les performances d'estimation sont très similaires. De plus, la consommation CPU est assez faible, ce qui permet de l'utiliser dans un contexte commercial.

- Le chapitre [Chapter 5](#) propose une méthode pour estimer la pression dans le collecteur d'échappement. La connaissance de cette variable est essentielle pour remplir des fonctions telle que la commande du frein moteur. Cependant, bien que dans la plupart des cas la pression soit mesurée directement, le capteur peut rencontrer des défaillances puisque soumis à de fortes variations de pression et de température. Son estimation est donc important pour des objectifs de diagnostic et de conception de lois de commande tolérantes aux fautes. Sur la base de modèles simplifiés du turbocompresseur et du collecteur d'échappement, un observateur polytopique LPV est conçu pour fournir une estimation de la pression. Les mérites de cette solution sont illustrés grâce au simulateur haute fidélité GT-POWER. Les résultats montrent que la méthode développée est un moyen prometteur d'estimer la pression avec une erreur relative raisonnable.
- Le chapitre [Chapter 6](#) traite de l'estimation du débit massique EGR et du débit massique d'air à l'entrée du moteur avec une sonde mesurant la quantité de NOx (oxydes d'azote) située dans le système de post-traitement du moteur. Le problème est qu'il existe un retard important entre la sonde NOx et la sonde lambda qui est actuellement utilisée pour estimer les deux débits massiques. Pour prendre en compte ce retard, des observateurs LPV à retard sont conçus à partir d'une méthode existante et d'une nouvelle méthode déduite du lemme de Finsler. La validation et la comparaison des différentes méthodes sont effectuées avec des données réelles provenant d'un banc d'essai. Même avec un important retard, les observateurs développés réussissent à bien estimer les débits, en particulier le débit massique d'air à l'entrée du moteur.

Perspectives

En guise de perspectives pour de futurs travaux au sein de Volvo, il est apparu que les sujets suivants méritent d'être étudiés de manière approfondie :

- *Estimer la température du collecteur d'échappement.* En raison de la température élevée et des fortes oscillations de pression, la mesure de cette variable est trop coûteuse pour le constructeur. Ainsi, à l'heure actuelle, un modèle en boucle ouverte donne une approximation de la température. En revanche ce modèle est soumis à des incertitudes et ses inexactitudes causent des problèmes de contrôle. En effet, la stratégie mise en place impose, lorsque la température du collecteur est trop élevée, de réduire la quantité de carburant injectée et donc le couple produit par le moteur. Il est donc nécessaire de connaître la température aussi précisément que possible, pour ne pas inutilement restreindre le moteur. Suivant la même modélisation que celle décrite dans [Chapter 3](#), un observateur pourrait estimer cette température.
- *Fournir une solution de diagnostic pour le démarreur.* Le démarreur est un dispositif électrique utilisé pour faire tourner le vilebrequin du moteur afin d'atteindre la vitesse de rotation requise pour que l'allumage ait lieu. Il a été identifié que ce système subit une usure prématurée. Ainsi, une solution à base d'observateur pourrait être conçue pour

surveiller un écart trop important. Le composant principal du démarreur est un moteur à courant continu, ce qui permet, par exemple, d'appliquer les travaux de [Christophe 2001] (qui traite du diagnostic non linéaire des systèmes appliqué aux machines électriques).

- *Détecter une faute dans l'injection d'urée.* Pour réduire les émissions d'oxyde d'azote, le système de post-traitement injecte de l'urée pour déclencher une réaction chimique. La législation exige une solution OBD pour certifier que ce système fonctionne correctement. Pour cette raison, les fabricants doivent s'assurer que la solution injectée est bien de l'urée. Des solutions basées sur des modèles pourraient être étudiées pour résoudre ce problème.
- *Estimer la température de la paroi à l'intérieur du système de post-traitement.* Afin d'assurer que les différentes réactions chimiques dans le système de post-traitement aient lieu, une certaine température doit être atteinte. Bien que ce système soit équipé de nombreux capteurs de température, en raison de la nature distribuée du flux de température de départ, l'optimum n'est pas atteint. Dans un premier temps, des travaux doivent être consacrés à la modélisation, puis, en fonction des capteurs disponibles, on pourrait envisager de faire appel à des observateurs.

Preamble

This thesis has been developed thanks to a CIFRE (Conventions Industrielles de Formation par la REcherche) agreement, a program of the agency ANRT (Association Nationale de la Recherche et de la Technologie). This agreement funds any French company that engages a PhD student to carry out a research project inside the company and in collaboration with a public laboratory. This thesis has been carried out between Renault Trucks (which belongs to Volvo Group) in Lyon and GIPSA-lab in Grenoble. It is the result of a three years work (from December 2015 to December 2018), under the supervision of Olivier Senname and Delphine Bresch-Pietri, on the academic side, and of Christophe Gauthier then Adrien Hallé, on the company side.

Volvo Group is one of the world's largest manufacturers of trucks, buses, construction equipment and marine and industrial engines. It has divided its trucks sales into four major brands which are: Volvo Trucks, Renault Trucks, Mack (for North America market) and UD Trucks. Among the development sites around the world, the one in Lyon is mainly focused on the development of the medium duty diesel engines used for local or regional delivery and public services for example.

Introduction

General introduction

Due to both production planning and urbanization, the role of the transport sector has increased dramatically over the last decades. This has led to many undesirable consequences such as the increase of fuel consumption, greenhouse gases emissions and greater exposure of people to air pollutants. This last point has a serious impact on the human's health. For example, in European countries, [Künzli et al. 2000] has shown that about half of all mortality caused by air pollution was attributed to motorized traffic.

Thus, since January 1993, with the Euro 1 standard, car manufacturers have been subject of increasingly stringent emission standards over time. Figure 2 shows the evolution of emission regulations. For example, the Euro 6 standard, the current one, has required a 95% reduction in particulate emissions (PM) compared to the Euro 1 one. In addition to reducing pollutants, future legislation will require the control of greenhouse gas emissions.

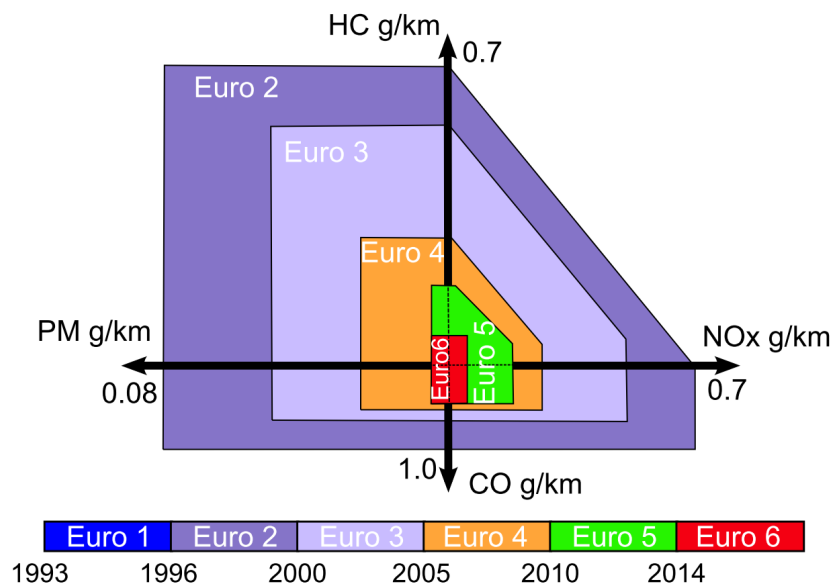


Figure 2: European legislation emission limits for diesel engines [Martin 2010]

From the customer point of view, the truck has to be operated at the lowest possible cost. This means that the fuel consumption must be the lowest possible. However, for combustion engines, reducing both pollutants and consumption require to add new components such as Exhaust Gas Recirculation (EGR) loop or after treatment system. Therefore, to meet both new legislative standards and customer requirements, the complexity of trucks has increased significantly as well as the engine control and so the risk of failure.

To ensure the reliable functionality of the anti-pollution system, legislation also requires

to develop on-board diagnosis (OBD) solutions to monitor the components achieving these functions [Mohammadpour et al. 2012]. It appears that manufacturers have to add new equipment such as sensors to create a diagnosis solution, which increases again the complexity.

Initially, OBD solutions have been developed to comply with the law. But today, the maximization of the uptime of the truck is a major priority for the manufacturers to increase the truck's productivity and so the customer satisfaction. This goal can be achieved with a set of strategies that include, but are not limited to: predictive and planning maintenance, Fault Detection and Isolation (FDI) and usage of top quality components. The FDI problem consists of determining the location as well as the nature of the fault [Hwang et al. 2010]. FDI methods utilize the concept of redundancy, which is, in general, analytical redundancy. The basic concept of analytical redundancy is to compare real-time estimations with a mathematical model of the system. Although an OBD solution is actually an FDI's one, we will distinguish these two notions because their goal is not the same. Indeed, an OBD solution is legislatively oriented whereas an FDI one is customer-oriented which can be included in a global strategy of health monitoring of the truck.

Among FDI strategies, the observer-based approach is a popular approach [Chen and Patton 1999; Ding 2008]. An observer is an algorithm that deduces, from a model and a given set of sensors, additional information such as unknown parameters or unmeasured state variables. Therefore it is an efficient way to provide an analytical redundancy for an FDI or an OBD strategy. In addition, observers can be used as a virtual sensor in order to reduce the global cost or to have a finer control of the engine.

Consequently, this thesis is focused on the observers design for various subsystems of the engine to fulfill four main objectives:

- (1) For an FDI purpose: diagnose a component to control the truck's health.
- (2) For an OBD purpose: linked to the previous goal, but to diagnose the anti-pollution systems.
- (3) For a control purpose: estimate variables needed for the engine control.
- (4) For a cost reduction purpose: replace a sensor by an observer.

Observers design and validation

Many types of observers have been designed in the thesis. Nevertheless, they can be grouped into 3 major frameworks:

- (1) The nonlinear (NL) observers
- (2) LPV observers

(3) LPV time-delay observers

Table 1 summarizes the used frameworks for each chapter.

Table 1: Observer frameworks used in the chapters

	Frameworks		
	NL	LPV	LPV time-delay
Chapter 2	✓		
Chapter 3	✓	✓	
Chapter 4	✓	✓	
Chapter 5		✓	
Chapter 6			✓

Depending on the feasibility of the subject, these developed observers have been validated following 3 simulation or experimental contexts:

- Validation with GT-POWER¹. GT-POWER is a software developed by Gamma Technology which consists in a set of simulation libraries for analyzing the engine behavior and it enables to obtain a high-fidelity simulator. This context represents first significant step to test the developed observers. It has been used in Chapter 2 and Chapter 5.
- Validation with data from test-bench. The observers are implemented in a simulation environment (most of the time, Simulink) and fed with data obtained with a real engine mounted on a test-bench. This context is very representative of the performance that could be obtained on an industrial application. Test-bench data are used in for the topics in Chapter 3 and Chapter 6.
- Validation on an embedded computer. The developed observers are implemented in the real calculator of the truck and tested in a test-cell. This context is the most representative since it is the closest one to industrial applications. Chapter 4 presents this context.

Thesis Structure

This study focused mainly on two sets of the Volvo's medium duty: the cooling system, which regulates the engine block temperature and the air path of the engine. Chapter 2 is devoted to the cooling system and Chapters 3 to 6 deal with the air path. In detail, the manuscript is organized as follows:

¹www.gtisoft.com

- [Chapter 1](#) provides some theoretical background on control theory with a particular focus on observer design. It presents the different observer structures that will be used along the thesis. Two types of observers are considered there: LPV systems, put into a polytopic form, and nonlinear systems.
- [Chapter 2](#) proposes a observer-based solution to estimate the degradation of a belt tensioner. Through the analysis of the engine cooling system, a characteristic parameter has been identified to be a good candidate to represent the belt tensioner's health.
- [Chapter 3](#) gives an OBD solution for two components of the air path that need to be diagnosed to meet the legislation but with a different sensor configuration for cost saving. Two observers are designed to estimate the heat transfer quality of the charge air cooler and the EGR cooler.
- [Chapter 4](#) compares different observer approaches to estimate an important air path variable for the pollutant emissions control: the EGR mass flow rate. Six observers have been implemented on a real truck calculator and evaluated on a test bench.
- [Chapter 5](#) presents an LPV observer to estimate the pressure inside the exhaust manifold of the engine. This variable is used to control an engine brake with a flap located in the exhaust line.
- [Chapter 6](#) deals with the estimation of the EGR and inlet air mass flow rates with a sensor submitted to a delay which could reduce the global cost of the engine. An LPV time-delay observer is designed to estimate these both flows, needed for the pollutant emissions control.

The features, defined in the previous section, achieved by the thesis chapters are summarized in [Table 2](#).

Table 2: Features addressed along the thesis

	Features			
	OBD	FDI	Cost reduction	Control
Chapter 2		✓		
Chapter 3	✓		✓	
Chapter 4				✓
Chapter 5		✓	✓	✓
Chapter 6			✓	✓

Publications

International Conference Papers with Proceedings

- Dubuc, D., Sename, O., Bresch-Pietri, D., Halle, A., & Gauthier, C. (2018, August). Exhaust pressure LPV observer for turbocharged diesel engine on-board diagnosis. In 10th IFAC Symposium on Fault Detection, Supervision and Safety for Technical Processes, SAFEPROCESS 2018. [Dubuc et al. 2018]
- Dubuc, D., Sename, O., Bresch-Pietri, D., & Gauthier, C. (2017, July). Observer-based fault diagnosis for trucks belt tensioner. In 20th IFAC World Congress. [Dubuc et al. 2017]

How to read the thesis

There is no strong links between the chapters, which can be understood relatively independently. Nevertheless, we recommend the reader to begin with the theoretical [Chapter 1](#) to familiarize him/herself with the observer concepts.

Note also that this thesis has been written with \LaTeX and with the package `hyperref`. Therefore we suggest to read the pdf document and use the hypertext links to ease the understanding. **Tip:** on your pdf reader (Acrobat reader for example) after clicking on a link, you can use the keyboard shortcut `Alt + ←` (left arrow) to go back in your pdf document.

Some theoretical background

Contents

1.1	Dynamical systems under consideration	9
1.1.1	Nonlinear systems	10
1.1.2	Linear Time Invariant systems	10
1.1.3	LPV systems	11
1.1.3.1	Representation of LPV systems	12
1.1.4	Stability of LPV systems	13
1.2	Observer design	14
1.2.1	LPV polytopic systems	15
1.2.1.1	Pole placement method	15
1.2.1.2	\mathcal{H}_∞ performance method	18
1.2.1.3	FAFE design method	19
1.2.1.4	\mathcal{H}_∞ filtering method	22
1.2.1.5	Implementation issues	25
1.2.2	For nonlinear systems	29
1.2.2.1	Kalman observer	29
1.2.2.2	Adaptive observer	30

This chapter is devoted to recall some theoretical tools that will be used in the next chapters of the dissertation. We first start with the definition of dynamical systems we are interested in the sequel, with a particular focus on LPV systems and their stability. Then, several design methods of observers are given for LPV polytopic and nonlinear systems. For more details about these topics, we recommend to read the books [Mohammadpour and Scherer 2012; Sename et al. 2013] which deal with LPV systems and [Besançon 2007] for nonlinear observers.

1.1 Dynamical systems under consideration

In this section, the different classes of dynamical systems that will be used in the thesis are presented. First, the definition of nonlinear and LTI systems will be recalled.

Then LPV systems will be more detailed since they are largely considered along the dissertation. Figure 1.1 gives a schematic representation of the different systems classes and their restriction in relation to the most general case.

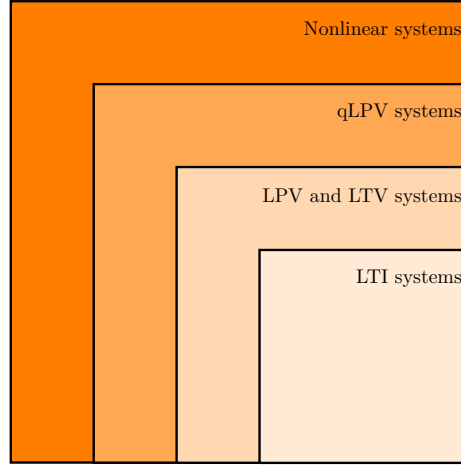


Figure 1.1: Different classes of systems

1.1.1 Nonlinear systems

We are interested in nonlinear dynamical systems that can be described by nonlinear ODEs.

Definition 1.1 (*Nonlinear system*)

A nonlinear system is described by the functions $f : \mathbb{R}^{n_x} \times \mathbb{R}^{n_u} \mapsto \mathbb{R}^{n_x}$ and $h : \mathbb{R}^{n_x} \times \mathbb{R}^{n_u} \mapsto \mathbb{R}^{n_y}$, such that:

$$\begin{cases} \dot{x}(t) = f(x(t), u(t)) \\ y(t) = h(x(t), u(t)) \end{cases} \quad (1.1)$$

where $x(t) \in \mathbb{R}^{n_x}$ is the state vector, $u(t) \in \mathbb{R}^{n_u}$ is the input vector and $y(t) \in \mathbb{R}^{n_y}$ the output (or the measurement) vector of the system.

This representation is very convenient since it is derived from the system knowledge and the physics equations so it can fit most of physical systems. However, there exist no systematic mathematical tools for identification, observation, control synthesis or analysis for these systems.

1.1.2 Linear Time Invariant systems

The LTI dynamical modeling consists in describing the system through linear ODEs.

Definition 1.2 (LTI system)

A Linear Time Invariant (LTI) system is described by the matrices $A \in \mathbb{R}^{n_x \times n_x}$, $B \in \mathbb{R}^{n_x \times n_u}$, $C \in \mathbb{R}^{n_y \times n_x}$ and $D \in \mathbb{R}^{n_y \times n_u}$ such that:

$$\begin{cases} \dot{x}(t) = Ax(t) + Bu(t) \\ y(t) = Cx(t) + Du(t) \end{cases} \quad (1.2)$$

where $x(t) \in \mathbb{R}^{n_x}$ is the state vector, $u(t) \in \mathbb{R}^{n_u}$ is the input vector and $y(t) \in \mathbb{R}^{n_y}$ the output (or the measurement) vector of the system.

Contrary to the previous class, Linear Time Invariant (LTI) systems are state-of-the-art and linear systems theory proposes many analysis and controller synthesis tools. Although this model is less accurate to describe an entire physical system than a nonlinear model, it can be seen as a local approximation around an operating point.

1.1.3 LPV systems

LPV systems are a special class of nonlinear systems (see Figure 1.1) which appears to be well suited for control of dynamic systems with parameter variations. They can be described as linear with respect to state and nonlinear with respect to parameter. Initially introduced by [Shamma and Athans 1992], LPV techniques can provide a systematic design procedure for self-scheduled systems.

Definition 1.3 (LPV system)

A Linear Parameter Varying (LPV) system is described by the linear matrix functions $A \in \mathbb{R}^{n_x \times n_x}$, $B \in \mathbb{R}^{n_x \times n_u}$, $C \in \mathbb{R}^{n_y \times n_x}$ and $D \in \mathbb{R}^{n_y \times n_u}$ such that:

$$\begin{cases} \dot{x}(t) = A(\rho)x(t) + B(\rho)u(t) \\ y(t) = C(\rho)x(t) + D(\rho)u(t) \end{cases} \quad (1.3)$$

where $x(t) \in \mathbb{R}^{n_x}$ is the state vector, $u(t) \in \mathbb{R}^{n_u}$ is the input vector, $y(t) \in \mathbb{R}^{n_y}$ the output (or the measurement) vector of the system and ρ is a vector of time-varying parameters assumed to be known (either measured or estimated) and bounded, defined in the convex set \mathcal{P}_ρ :

$$\mathcal{P}_\rho := \left\{ \rho = [\rho_1 \ \dots \ \rho_N]^T \in \mathbb{R}^N \text{ and } \rho_i \in [\underline{\rho}_i, \overline{\rho}_i], \text{ for all } i = 1 \dots N \right\} \quad (1.4)$$

Remark 1.1

In the case where:

- ρ is a constant value, (1.3) is a Linear Time Invariant (LTI) system.
- $\rho = \rho(t)$, (1.3) is a Linear Time Varying (LTV) system, where the parameter

vector is a priori known.

- $\rho = \rho(x(t))$, (1.3) is a quasi-Linear Parameter Varying (qLPV) system.

An LPV system can be viewed as a nonlinear system linearized along the varying parameters trajectories. Therefore, an LPV model allows to represent the dynamics of the nonlinear system, while keeping the linear structure. Thus, the tools deduced from the linear control theory can be used with some modifications, as we will see in the next section.

1.1.3.1 Representation of LPV systems

Based on the dependence of the system matrices on the scheduling parameters, it is possible to sort the LPV systems. In [Briat 2008], the author identified three main classes:

- (1) Affine systems
- (2) Polynomial systems
- (3) Rational systems

During this thesis only the first class of LPV systems will be considered.

Definition 1.4 (*Affine LPV system*)

An LPV system is said affine if the parameter dependence of its state-space matrices $A(\rho)$, $B(\rho)$, $C(\rho)$ and $D(\rho)$ on ρ is affine, i.e:

$$\left[\begin{array}{c|c} A(\rho) & B(\rho) \\ \hline C(\rho) & D(\rho) \end{array} \right] = \left[\begin{array}{c|c} \hat{A}_0 & \hat{B}_0 \\ \hline \hat{C}_0 & \hat{D}_0 \end{array} \right] + \sum_{i=1}^N \left[\begin{array}{c|c} \hat{A}_i & \hat{B}_i \\ \hline \hat{C}_i & \hat{D}_i \end{array} \right] \rho_i \quad (1.5)$$

where \hat{A}_i , \hat{B}_i , \hat{C}_i and \hat{D}_i are real constant matrices.

Definition 1.5 (*Matrix polytope [Apkarian et al. 1995]*)

A matrix polytope is defined as the convex hull of a finite number r of matrices M_i such that:

$$\text{Co}\{M_1, \dots, M_r\} := \left\{ \sum_{i=1}^r \mu_i M_i \mid \mu_i \geq 0, \sum_{i=1}^r \mu_i = 1 \right\} \quad (1.6)$$

Since $\rho \in \mathcal{P}_\rho$, the parameter vector evolves inside a polytope represented by 2^N vertices ω_i as:

$$\rho \in \Theta := \text{Co}\{\omega_1, \dots, \omega_{2^N}\} \quad (1.7)$$

Thus, ρ can be written as the convex combination:

$$\rho = \sum_{i=1}^{2^N} \mu_i \omega_i, \quad \mu_i \geq 0, \quad \sum_{i=1}^{2^N} \mu_i = 1 \quad (1.8)$$

where the vertices are defined by a vector $\omega_i = [\nu_{i1} \ \dots \ \nu_{iN}]^T$ and ν_{ij} equals $\underline{\rho}_j$ or $\overline{\rho}_j$.

If we substitute (1.8) into (1.5), in Definition 1.4, it is clear that $A(\rho), B(\rho), C(\rho)$ and $D(\rho)$ are delimited by four matrices polytopes the vertices of which are the images of the vertices ω_i . It leads to the following definition.

Definition 1.6 (LPV polytopic system)

An LPV system is said polytopic if the dependence of its state-space matrices on parameter vector ρ is affine and ρ evolves inside a polytope $\Theta := \text{Co}\{\omega_1, \dots, \omega_{2^N}\}$. In this case, its state-space matrices also range over polytopes the vertices of which are the images of the vertices ω_i . The following relation is then deduced:

$$\begin{aligned} \left[\begin{array}{c|c} A(\rho) & B(\rho) \\ \hline C(\rho) & D(\rho) \end{array} \right] &= \sum_{i=1}^{2^N} \mu_i(\rho) \left[\begin{array}{c|c} A_i & B_i \\ \hline C_i & D_i \end{array} \right] \\ &= \sum_{i=1}^{2^N} \mu_i(\rho) \left[\begin{array}{c|c} A(\omega_i) & B(\omega_i) \\ \hline C(\omega_i) & D(\omega_i) \end{array} \right] \end{aligned} \quad (1.9)$$

where,

$$\mu_i(\rho) \geq 0, \quad \sum_{i=1}^{2^N} \mu_i(\rho) = 1 \quad (1.10)$$

This representation is very convenient since the initial LPV system is now a convex combination of LTI systems.

1.1.4 Stability of LPV systems

Let us consider the following autonomous LPV system:

$$\dot{x}(t) = A(\rho)x(t) \quad (1.11)$$

It is possible to analyze the stability of (1.11) through the Lyapunov theory. First, if a constant Lyapunov function is used, it leads to the following definition.

Definition 1.7 (Quadratic stability)

The system (1.11) is said to be quadratically stable if there exists a Lyapunov function $V(x) = x^T P x > 0$, $P = P^T \succ 0$ satisfying:

$$A(\rho)^T P + P A(\rho) \prec 0, \quad \rho \in \mathcal{P}_\rho \quad (1.12)$$

The problem with the formulation (1.12) is that it is an infinite-dimensional problem due to infinite values of ρ . Thus, one of the challenges in the LPV framework is how to relax this infinite-dimensional constraint into a finite one. One popular and simple approach is to use the polytopic formulation.

If (1.11) is an affine LPV system, it can be turned into the following LPV polytopic system:

$$\dot{x}(t) = \sum_{i=1}^{2^N} \mu_i(\rho) A_i x(t) \quad (1.13)$$

Proposition 1.1

The LPV polytopic system (1.13) is quadratically stable if and only if there exists a matrix $P = P^T \succ 0$ such that:

$$A_i^T P + P A_i \prec 0 \quad (1.14)$$

holds for all $i = 1, \dots, 2^N$.

One of the drawbacks of the quadratic stability is its high conservatism. Thus, sometimes, it may not exist a feasible solution. To reduce the conservatism, one can use a parameter dependent Lyapunov function which leads to the following definition.

Definition 1.8 (Robust stability)

The system (1.11) is said to be robustly stable if there exists a parameter dependent Lyapunov function $V(x, \rho) = x^T P(\rho) x > 0$, $P(\rho) = P(\rho)^T \succ 0$ satisfying:

$$A(\rho)^T P(\rho) + P(\rho) A(\rho) + \dot{\rho} \frac{\partial P}{\partial \rho} \prec 0 \quad \forall \rho \in \mathcal{P}_\rho \quad (1.15)$$

Again, the previous definition leads to an infinite-dimensional problem. However, due to the product between the Lyapunov matrix and the system one, (1.15) is no more affine in ρ . To solve it, one can first define a structure for $P(\rho)$ (affine or polynomial for example), and then, use gridding (discretization) approach as in [Wu 1995] and the toolbox LPVTools developed in MATLAB [Hjartarson et al. 2013], or the sum-of-squares one [Scherer and Hol 2006].

1.2 Observer design

Most of the time, for a given plant, it is not possible to measure all the variables characterizing the system behavior due to high cost, technological constraints or physical impossibility. However, this information could be needed for identification, fault detection or control purpose. This motivates the design of an estimator, called an observer,

that deduces all the needed information from the known inputs and the outputs measured by the available sensors on the plant. It is worth noting that such a problem is of high importance for industrial systems.

This section is devoted to the observer design for two classes of systems: the LPV polytopic and the nonlinear ones. Note that we will expose the main methods that will be used in the next chapters only.

1.2.1 LPV polytopic systems

For LPV polytopic systems, the observer design methods are based on LMI constraints [Boyd et al. 1994]. In this thesis, the LMIs have been implemented with the parser YALMIP, [Löfberg 2004] associated with the SeDuMi or SDPT3 solver (see [Sturm 1999] and [Tütüncü et al. 2003] respectively).

1.2.1.1 Pole placement method

Let us consider the following LPV polytopic system:

$$\begin{aligned}\dot{x} &= \sum_{i=1}^{2^N} \mu_i(\rho) (A_i x + B_i u) \\ y &= Cx\end{aligned}\tag{1.16}$$

where $x \in \mathbb{R}^{n_x}$ is the state vector, $u \in \mathbb{R}^{n_u}$ is the known input vector, $y \in \mathbb{R}^{n_y}$ is the measurement vector, and $\rho \in \mathcal{P}_\rho$ defined in (1.4).

To estimate the state vector, the following Luenberger-like LPV polytopic observer is proposed:

$$\begin{aligned}\dot{\hat{x}} &= \sum_{i=1}^{2^N} \mu_i(\rho) (A_i \hat{x} + B_i u + L_i (y - \hat{y})) \\ \hat{y} &= C\hat{x}\end{aligned}\tag{1.17}$$

Thus, from (1.16) and (1.17), the dynamic estimation error $e = x - \hat{x}$ is governed by:

$$\dot{e} = \sum_{i=1}^{2^N} \mu_i(\rho) (A_i - L_i C) e\tag{1.18}$$

The objective, is to solve the following problem:

Problem 1.1

Find matrices $L_i \in \mathbb{R}^{n_x \times n_y}$, $i = 1, \dots, 2^N$, of the observer (1.17) for the polytopic

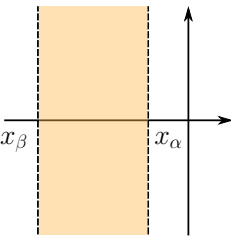
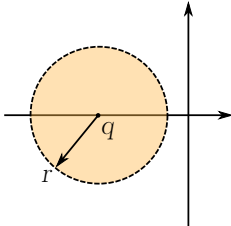
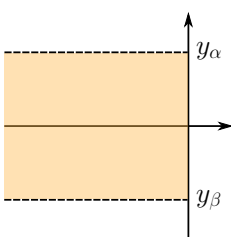
LPV system (1.16) such that:

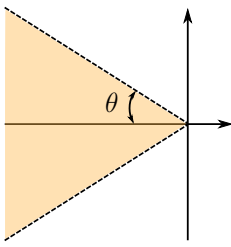
- (1) the estimation error system (1.18) is asymptotically stable i.e, $e(t) \rightarrow 0$ when $t \rightarrow \infty$.
- (2) the eigenvalues of $A_i - L_i C$, $i = 1, \dots, 2^N$, are in a chosen area of the complex plane.

Based on [Chilali and Gahinet 1996], one can establish the following proposition.

Proposition 1.2

Consider the LPV polytopic observer (1.17) for the polytopic LPV system (1.16). Problem 1.1 is solved, if there exist matrices $Y_i \in \mathbb{R}^{n_x \times n_y}$, $i = 1, \dots, 2^N$, and $P = P^T \succ 0 \in \mathbb{R}^{n_x \times n_x}$ such that the following LMIs hold for all $i = 1, \dots, 2^N$:

Pole placement area	Respective LMIs
	<p>given two positive scalars x_α and x_β,</p> $\begin{aligned} PA_i - Y_i C + A_i^T P - C^T Y_i^T + 2x_\alpha P &\prec 0 \\ PA_i - Y_i C + A_i^T P - C^T Y_i^T + 2x_\beta P &\succ 0 \end{aligned} \quad (1.19)$
	<p>given two positive scalars r and q,</p> $\begin{bmatrix} -rP & qP + PA_i - Y_i C \\ * & -rP \end{bmatrix} \prec 0 \quad (1.20)$
	<p>given two scalars y_α and y_β such that $y_\alpha > y_\beta$,</p> $\begin{aligned} j(PA_i - Y_i C + A_i^T P - C^T Y_i^T) + 2y_\alpha P &\succ 0 \\ j(PA_i - Y_i C + A_i^T P - C^T Y_i^T) + 2y_\beta P &\prec 0 \end{aligned} \quad (1.21)$ <p>where $j^2 = -1$</p>



given a positive scalar θ ,

$$\begin{bmatrix} \sin \theta (PA_i - Y_i C + A_i^T P - C^T Y_i^T) & \cos \theta (PA_i - Y_i C - A_i^T P + C^T Y_i^T) \\ * & \sin \theta (PA_i - Y_i C + A_i^T P - C^T Y_i^T) \end{bmatrix} \prec 0 \quad (1.22)$$

The gains of the observer (1.17) are deduced as $L_i = P^{-1}Y_i$.

It is possible to set more complex area by combining the different LMIs presented in Proposition 1.2.

Example 1.1

In order to ensure a desired speed and damping convergence, we wish to bring the observer poles inside a rectangle defined in Figure 1.2. A simple solution consists in combining (1.19) and (1.21) to get:

$$\begin{aligned} PA_i - Y_i C + A_i^T P - C^T Y_i^T + 2x_\alpha P &\prec 0 \\ PA_i - Y_i C + A_i^T P - C^T Y_i^T + 2x_\beta P &\succ 0 \\ j(PA_i - Y_i C + A_i^T P - C^T Y_i^T) + 2y_\alpha P &\succ 0 \\ j(PA_i - Y_i C + A_i^T P - C^T Y_i^T) + 2y_\beta P &\prec 0 \end{aligned} \quad (1.23)$$

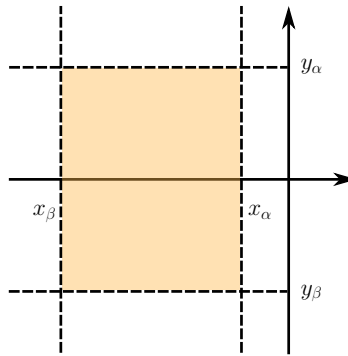


Figure 1.2: Pole placement area example

1.2.1.2 \mathcal{H}_∞ performance method

Let us consider the following LPV polytopic system subject to a disturbance:

$$\begin{aligned} \dot{x} &= \sum_{i=1}^{2^N} \mu_i(\rho) (A_i x + B_i u + E w) \\ y &= C x \\ z &= C_z x \end{aligned} \quad (1.24)$$

where $x \in \mathbb{R}^{n_x}$ is the state vector, $u \in \mathbb{R}^{n_u}$ is the known input vector, $w \in \mathbb{R}^{n_w}$ is the additive disturbance, $y \in \mathbb{R}^{n_y}$ is the measurement vector, $z \in \mathbb{R}^{n_z}$ is the signal to be estimated, and $\rho \in \mathcal{P}_\rho$.

To estimate the variable z , the Luenberger-like LPV polytopic observer is proposed hereunder:

$$\begin{aligned} \dot{\hat{x}} &= \sum_{i=1}^{2^N} \mu_i(\rho) (A_i \hat{x} + B_i u + L_i (y - \hat{y})) \\ \hat{y} &= C \hat{x} \\ \hat{z} &= C_z \hat{x} \end{aligned} \quad (1.25)$$

Thus, from (1.24) and (1.25), the dynamic estimation error $e = x - \hat{x}$ is governed by:

$$\begin{aligned} \dot{e} &= \sum_{i=1}^{2^N} \mu_i(\rho) ((A_i - L_i C) e + E w) \\ e_z &= C_z e \end{aligned} \quad (1.26)$$

The objective, is to solve the following problem:

Problem 1.2

Find matrices $L_i \in \mathbb{R}^{n_x \times n_y}$, $i = 1, \dots, 2^N$, of the observer (1.25) for the polytopic LPV system (1.24) such that:

- (1) the estimation error system (1.26) is asymptotically stable ($e(t) \rightarrow 0$ when $t \rightarrow \infty$) for $w \equiv 0$.
- (2) the upper bound γ_∞ of the induced- \mathcal{L}_2 norm from the disturbance w to e_z is minimized, i.e

$$\sup_{w \neq 0, w \in \mathcal{L}_2} \frac{\|e_z\|_2}{\|w\|_2} \leq \gamma_\infty \quad (1.27)$$

Based on the bounded real lemma [Scherer and Weiland 2000], one can establish the following proposition.

Proposition 1.3

Consider the LPV polytopic observer (1.25) for the polytopic LPV system (1.24). Problem 1.2 is solved, if there exist matrices $Y_i \in \mathbb{R}^{n_x \times n_y}$, $i = 1, \dots, 2^N$, and $P = P^T \succ 0 \in \mathbb{R}^{n_x \times n_x}$ such that the following LMIs hold for all $i = 1, \dots, 2^N$:

$$\begin{aligned} & \min \quad \gamma_\infty \\ & s.t \quad \begin{bmatrix} PA_i - Y_i C + A_i^T P - C^T Y_i^T & E & PC_z^T \\ * & -\gamma_\infty I_{n_w} & 0 \\ * & * & -\gamma_\infty I_{n_z} \end{bmatrix} \prec 0 \end{aligned} \quad (1.28)$$

The gains of the observer (1.25) are deduced as $L_i = P^{-1}Y_i$.

It is worth noting that, when the disturbance matrix E is not known, it can be arbitrarily fixed. Besides, for a loop shaping design, in order to have a finer synthesis, it is possible to add a performance weight on the input, like it has been done in [Yamamoto et al. 2015] for example.

1.2.1.3 FAFE design method

In this section, we are now looking to estimate both the states and an additive fault. An interesting solution has been developed in [Zhang et al. 2008] and [Zhang et al. 2012], where the authors proposed a Fast Adaptive Fault Estimation (FAFE) observer. As in [Rodrigues et al. 2015], the LPV polytopic FAFE formulation is presented here. Let consider the following LPV polytopic system to observe:

$$\begin{aligned} \dot{x} &= \sum_{i=1}^{2^N} \mu_i(\rho) (A_i x + B_i u + F_i f) \\ y &= Cx \end{aligned} \quad (1.29)$$

where $x \in \mathbb{R}^{n_x}$ is the state vector, $u \in \mathbb{R}^{n_u}$ is the known input vector, $y \in \mathbb{R}^{n_y}$ is the measurement vector, $f \in \mathbb{R}^{n_f}$ is the fault and $\rho \in \mathcal{P}_\rho$.

To estimate both the state and fault vectors, the following FAFE LPV polytopic observer structure is proposed:

$$\begin{cases} \dot{\hat{x}} = \sum_{i=1}^{2^N} \mu_i(\rho) (A_i \hat{x} + B_i u + L_i e_y + F_i \hat{f}) \\ \dot{\hat{f}} = \Gamma \sum_{i=1}^{2^N} \mu_i(\rho) U_i (\dot{e}_y + \sigma e_y) \\ \hat{y} = C \hat{x} \\ e_y = y - \hat{y} \end{cases} \quad (1.30)$$

where the symmetric positive matrix $\Gamma \in \mathbb{R}^{n_f \times n_f}$, and the positive scalar σ are tunable parameters.

Let us denote, $e = x - \hat{x}$ and $e_f = f - \hat{f}$, the state and fault estimation errors respectively. The objective is to solve the following problem:

Problem 1.3

Find matrices $L_i \in \mathbb{R}^{n_x \times n_y}$, $U_i \in \mathbb{R}^{n_f \times n_y}$, for all $i = 1, \dots, 2^N$ of the FAFE observer (1.30) for the polytopic LPV system (1.29) such that e and e_f are uniformly bounded.

To design (1.30), let us consider the following assumptions:

A1. $\text{rank}(CF_i) = \text{rank}(F_i)$, and the invariant zeros of (A_i, F_i, C) are in the left-half complex plane for all $i = 1, \dots, 2^N$.

A2. The fault f and its time derivative are norm bounded i.e: $0 \leq \|f\| < \beta_1$ and $0 \leq \|\dot{f}\| < \beta_2$ with $0 \leq \beta_1, \beta_2 < \infty$.

According to [Zhang et al. 2008] and adapting the solution to the polytopic case, one can establish the following proposition.

Proposition 1.4

Consider the LPV polytopic FAFE observer (1.30) for the polytopic LPV system (1.29). Under Assumptions A1-A2 and given scalars $\sigma, \mu > 0$, Problem 1.3 is solved, if there exist matrices $Y_i \in \mathbb{R}^{n_x \times n_y}$, $\forall i = 1, \dots, 2^N$ and symmetric positive matrices $P \in \mathbb{R}^{n_x \times n_x}$ and $G \in \mathbb{R}^{n_f \times n_f}$ such that the following conditions hold for all $i = 1, \dots, 2^N$:

$$\begin{bmatrix} PA_i + A_i^T P - C^T Y_i - Y_i C & -\frac{1}{\sigma} (A_i^T P F_i - C^T Y_i^T F_i) \\ * & \frac{1}{\sigma} \left(-2F_i^T P F_i + \frac{1}{\mu} G \right) \end{bmatrix} \prec 0 \quad (1.31)$$

and

$$F_i^T P = U_i C \quad (1.32)$$

The gains L_i of (1.30) are deduced as $L_i = P^{-1} Y_i$.

Remark 1.2

As mentioned in [Zhang et al. 2008], it is difficult to solve simultaneously the LMIs (1.31) and the equalities (1.32). However, it is possible to transform (1.32) into the following optimization problem for all $i = 1, \dots, 2^N$:

$$\begin{aligned} \min \quad & \eta \\ \text{s.t.} \quad & \begin{bmatrix} \eta I_{n_f} & F_i^T P - U_i C \\ * & \eta I_{n_x} \end{bmatrix} \prec 0 \end{aligned} \quad (1.33)$$

Proposition 1.4 provides a very efficient solution to estimate an additive unknown input: both implementations of the algorithm (1.30) and LMIs are easy and the convergence of the errors is relatively fast compared to other techniques. However, the method has some tuning parameters σ , μ and Γ that have to be arbitrary chosen without clear physical coherence. The scalars σ and μ are generally fixed to 1 and the learning rate matrix Γ could be taken as: $\Gamma = \lambda I_{n_f}$ with $\lambda > 0$. It shall also be mentioned that the rank condition in Assumption A1 may be very restrictive in comparison with a standard technique where the additive unknown vector f is extended in the state vector. To illustrate this problem, let us introduce the following example:

Example 1.2

Consider the following LTI system:

$$\begin{aligned} \dot{x} &= Ax + Ff \\ y &= Cx \end{aligned} \quad (1.34)$$

with,

$$A = \begin{bmatrix} 0 & 0 & 0 & 0 \\ 1.5 & 1.7 & 0 & 0 \\ 0 & -6.2 & 6.2 & 0 \\ 0 & 0 & 0 & 0 \end{bmatrix}, \quad F = \begin{bmatrix} 0.8 & 2.3 \\ 0 & 0 \\ 0 & 0 \\ 1.3 & 1.3 \end{bmatrix}, \quad C = \begin{bmatrix} 0 & 0 & 1 & 0 \\ 0 & 0 & 0 & 1 \end{bmatrix} \quad (1.35)$$

The rank computation gives: $\text{rank}(CF) = 1 \neq \text{rank}(F) = 2$. Assumption A1 is not fulfilled and thus a FAFE cannot be designed. An alternative way to estimate f is to extend (1.34) with $\dot{f} = 0$. In this case, we obtain:

$$\begin{aligned} \dot{x}_e &= A_e x_e \\ y &= C_e x_e \end{aligned} \quad (1.36)$$

with

$$x_e = \begin{bmatrix} x \\ f \end{bmatrix}, \quad A_e = \begin{bmatrix} 0 & 0 & 0 & 0 & 0.8 & 2.3 \\ 1.5 & 1.7 & 0 & 0 & 0 & 0 \\ 0 & -6.2 & 6.2 & 0 & 0 & 0 \\ 0 & 0 & 0 & 0 & 1.3 & 1.3 \\ 0 & 0 & 0 & 0 & 0 & 0 \\ 0 & 0 & 0 & 0 & 0 & 0 \end{bmatrix}, \quad C_e = \begin{bmatrix} 0 & 0 & 1 & 0 & 0 & 0 \\ 0 & 0 & 0 & 1 & 0 & 0 \end{bmatrix} \quad (1.37)$$

Now, if we compute the rank of the observability matrix of the pair (A_e, C_e) , its value is $6 = \dim(x_e)$ so an observer can be designed on (1.36) by using, for example, Proposition 1.2.

1.2.1.4 \mathcal{H}_∞ filtering method

The design of \mathcal{H}_∞ filters, is based on the standard formulation of the \mathcal{H}_∞ controller synthesis for generalized systems as illustrated in Figure 1.3 where K_f is a filter and P the generalized plant. Now, consider a generalized polytopic LPV system P such that:

$$P : \begin{cases} \dot{x} = \sum_{i=1}^{2^N} \mu_i(\rho) (A_i x + B_{1i} w + B_{2i} u) \\ z = \sum_{i=1}^{2^N} \mu_i(\rho) (C_{1i} x + D_{11i} w + D_{12i} u) \\ y = \sum_{i=1}^{2^N} \mu_i(\rho) (C_{2i} x + D_{21i} w + D_{22i} u) \end{cases} \quad (1.38)$$

where $x \in \mathbb{R}^{n_x}$ is the state vector, $w \in \mathbb{R}^{n_w}$ is the exogenous input vector, $u \in \mathbb{R}^{n_u}$ is the endogenous input vector, $z \in \mathbb{R}^{n_z}$ is the exogenous output vector and $y \in \mathbb{R}^{n_y}$ is the endogenous output vector. It is also assumed that $\rho \in \mathcal{P}_\rho$.

In addition, assume that the following statements are fulfilled for all $i = 1, \dots, 2^N$:

- A1.** P is parameter independent on the input and the output, i.e $B_{2i} = B_2$, $D_{12i} = D_{12}$, $C_{2i} = C_2$ and $D_{21i} = D_{21}$.
- A2.** The output y is independent from u , i.e $D_{22i} = 0$.
- A3.** The pairs (A_i, B_{1i}) and (A_i, B_2) are stabilizable.
- A4.** The pairs (C_{1i}, A_i) and (C_2, A_i) are detectable.

Thus, under Assumptions A1-A2, (1.38) can be rewritten as:

$$P : \begin{cases} \dot{x} = \sum_{i=1}^{2^N} \mu_i(\rho) (A_i x + B_{1i} w) + B_2 u \\ z = \sum_{i=1}^{2^N} \mu_i(\rho) (C_{1i} x + D_{11i} w) + D_{12} u \\ y = C_2 x + D_{21} w \end{cases} \quad (1.39)$$

As shown in the interconnection scheme in [Figure 1.3](#), a polytopic LPV filter K_f is investigated here, given by:

$$K_f : \begin{cases} \dot{x}_f = \sum_{i=1}^{2^N} \mu_i(\rho) (A_{fi}x_f + B_{fi}y) \\ u = \sum_{i=1}^{2^N} \mu_i(\rho) (C_{fi}x_f + D_{fi}y) \end{cases} \quad (1.40)$$

where $x_f \in \mathbb{R}^{n_{x_f}}$.

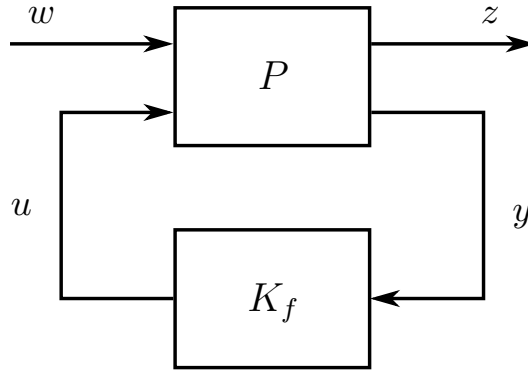


Figure 1.3: Generalized \mathcal{H}_∞ problem

Thus we aim at solving the following problem:

Problem 1.4

Find matrices $A_{fi} \in \mathbb{R}^{n_x \times n_x}$, $B_{fi} \in \mathbb{R}^{n_x \times n_y}$, $C_{fi} \in \mathbb{R}^{n_u \times n_x}$, $D_{fi} \in \mathbb{R}^{n_u \times n_y}$, $i = 1, \dots, 2^N$ of the filter (1.40) for the polytopic LPV system (1.39) such that:

- (1) the closed-loop system presented in [Figure 1.3](#) is stable.
- (2) the upper bound γ of the induced- \mathcal{L}_2 norm from the exogenous inputs w to z is minimized, i.e

$$\sup_{w \neq 0, w \in \mathcal{L}_2} \frac{\|z\|_2}{\|w\|_2} \leq \gamma_\infty \quad (1.41)$$

According to [[Scherer and Weiland 2000](#)], it is possible to synthesize the filter K_f which minimizes the effect of w on z by the following proposition:

Proposition 1.5

Consider the LPV polytopic filter (1.40) and the polytopic LPV system (1.39). Under Assumptions A1-A4, [Problem 1.4](#) is solved, if there exist matrices $Y, X \in \mathbb{R}^{n_x \times n_x}$ and $\tilde{A}_i \in \mathbb{R}^{n_x \times n_x}$, $\tilde{B}_i \in \mathbb{R}^{n_x \times n_y}$, $\tilde{C}_i \in \mathbb{R}^{n_u \times n_x}$, $\tilde{D}_i \in \mathbb{R}^{n_u \times n_y}$, $i = 1, \dots, 2^N$

such that the following LMIs hold for all $i = 1, \dots, 2^N$:

$$\begin{aligned} \min \quad & \gamma \\ \text{s.t.} \quad & \begin{bmatrix} M_{11} & * & * & * \\ M_{21} & M_{22} & * & * \\ M_{31} & M_{32} & M_{33} & * \\ M_{41} & M_{42} & M_{43} & M_{44} \end{bmatrix} \prec 0 \\ & \begin{bmatrix} X & I_{n_x} \\ I_{n_x} & Y \end{bmatrix} \succ 0 \end{aligned} \quad (1.42)$$

where,

$$\begin{aligned} M_{11} &= A_i X + X A_i^T + B_2 \tilde{C}_i + \tilde{C}_i^T B_2^T \\ M_{21} &= \tilde{A}_i + (A_i + B_2 \tilde{D}_i C_2)^T \\ M_{22} &= Y A_i + A_i^T Y + \tilde{B}_i C_2 + (\tilde{B}_i C_2)^T \\ M_{31} &= (B_{1i} + B_2 \tilde{D}_i D_{21})^T \\ M_{32} &= (Y B_{1i} + \tilde{B}_i D_{21})^T \\ M_{33} &= -\gamma I_{n_w} \\ M_{41} &= C_{1i} X + D_{12i} \tilde{C}_i \\ M_{42} &= C_{1i} + D_{12i} \tilde{D}_i C_2 \\ M_{43} &= D_{11i} + D_{12i} \tilde{D}_i D_{21} \\ M_{44} &= -\gamma I_{n_z} \end{aligned} \quad (1.43)$$

The reconstruction of the filter K_f is obtained by the following equivalent transformation,

$$\begin{cases} D_{fi} = \tilde{D}_i \\ C_{fi} = (\tilde{C}_i - \tilde{D}_i C_2 X) (M^T)^{-1} \\ B_{fi} = N^{-1} (\tilde{B}_i - Y B_2 \tilde{D}_i) \\ A_{fi} = N^{-1} (\tilde{A}_i - Y A_i X - Y B_2 \tilde{D}_i C_2 X - N \tilde{B}_i C_2 X - Y B_2 \tilde{C}_i M^T) (M^T)^{-1} \end{cases} \quad (1.44)$$

where M and N are defined such that $MN^T = I_{n_x} - XY$ which can be solved through a singular value decomposition plus a Cholesky factorization.

Of course, as in [Borges and Peres 2006; Varrier 2013] or [Yamamoto 2017], Proposition 1.5 can be used to estimate variables. To illustrate this, the following example is introduced to estimate a fault vector.

Example 1.3

Consider the system represented in the block scheme Figure 1.4. It consists of a

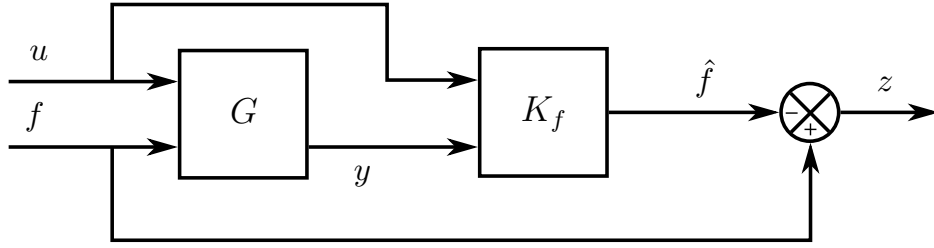
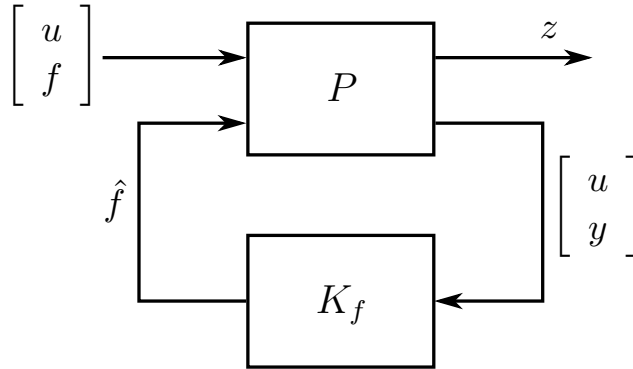


Figure 1.4: Bloc scheme for fault estimation

plant G , subject to known inputs u and unknown fault vector f , and a filter K_f which will be synthesized through the \mathcal{H}_∞ method [Proposition 1.5](#).

The first step is to construct the generalized system P as in (1.38). The variable of interest here is $z = f - \hat{f}$ and the exogenous inputs are respectively the vector $[u \ f]^T$ and \hat{f} . The input to the filter is the vector $[u \ y]^T$ and the output is the estimation of f , \hat{f} . This leads to the generalized \mathcal{H}_∞ problem depicted in [Figure 1.5](#).

Once P is deduced (one can use, for example, the MATLAB function `sysic`), [Proposition 1.5](#) can be applied to minimize the induced- \mathcal{L}_2 norm to estimate f .

Figure 1.5: Generalized \mathcal{H}_∞ problem for fault estimation

1.2.1.5 Implementation issues

We have seen in [Section 1.1.3.1](#) that, if the parameter vector $\rho \in \mathcal{P}_\rho$:

$$\mathcal{P}_\rho := \left\{ \rho = [\rho_1 \ \dots \ \rho_N]^T \in \mathbb{R}^N \text{ and } \rho_i \in [\underline{\rho}_i, \bar{\rho}_i], \text{ for all } i = 1 \dots N \right\} \quad (1.45)$$

then it evolves inside a polytope represented by 2^N vertices ω_i as:

$$\rho \in \Theta := \text{Co}\{\omega_1, \dots, \omega_{2^N}\} \quad (1.46)$$

where the vertices are defined by a vector $\omega_i = [\nu_{i1} \ \dots \ \nu_{iN}]^T$ and ν_{ij} equals $\underline{\rho}_j$ or $\bar{\rho}_j$. Thus, if a matrix $M(\rho)$ is affinely dependent on ρ , it also belongs to a polytope defined as:

$$M(\rho) \in \mathcal{M} := \text{Co}\{M_1, \dots, M_{2^N}\} \quad (1.47)$$

where the vertices $M_i = M(\omega_i)$. Therefore,

$$M(\rho) = \sum_{i=1}^{2^N} \mu_i(\rho) M_i \quad (1.48)$$

This section is devoted to the interpolation procedure for polytopic LPV systems i.e:

- (1) How to compute the vertices M_i .
- (2) How to compute the interpolation functions $\mu_i(\rho)$.

We have seen in the literature that, most of the time, the interpolation procedure for polytopic systems, when it is presented, is not explicitly formulated for a number of parameters $N > 2$. Two interesting procedures have been reported in [White et al. 2013] and [Bara et al. 2001]. The solution presented here is based on the second one where a systematic procedure easily implementable for any number N of parameters is exposed.

Let denote $(b_N^i, b_{N-1}^i, \dots, b_1^i)$, the binary representation with N bits, of the integer i . b_1^i is the least significant bit and b_N^i the most significant one. Then, each coordinate ν_k for all $k \in 1, \dots, N$ in $\omega_i = [\nu_{i1} \dots \nu_{iN}]^T$ can be computed as:

$$\nu_k = \begin{cases} \underline{\rho}_k & \text{when } b_k^{i-1} = 0 \\ \overline{\rho}_k & \text{when } b_k^{i-1} = 1 \end{cases} \quad (1.49)$$

Each vertice of \mathcal{M} in (1.47) are then deduced as: $M_i = M(\omega_i)$. The full procedure for the computation of the vertices is summarized in Algorithm 1.

Now, the interpolation functions $\mu_i(\rho)$ are given by:

$$\mu_i(\rho) = \prod_{k=1}^N \frac{\alpha_{ik} \rho_k + \beta_{ik}}{\underline{\rho}_k - \overline{\rho}_k} \quad (1.50)$$

where

$$\alpha_{ik} = \begin{cases} 1 & \text{when } b_k^{i-1} = 0 \\ -1 & \text{when } b_k^{i-1} = 1 \end{cases} \quad \text{and} \quad \beta_{ik} = \begin{cases} -\overline{\rho}_k & \text{when } b_k^{i-1} = 0 \\ \underline{\rho}_k & \text{when } b_k^{i-1} = 1 \end{cases} \quad (1.51)$$

This representation guarantees that $\mu_i(\rho) \geq 0$ and $\sum_{i=1}^{2^N} \mu_i(\rho) = 1$. The described procedure is summarized in Algorithm 2.

To see an application of the proposed algorithms, let us consider the following example.

Algorithm 1: Vertices computation of a matrix M

input : The bounds $\underline{\rho}_k$ and $\overline{\rho}_k$ of each parameter ρ_k **output:** The vertices of $M(\rho)$ **for** $i \leftarrow 1$ **to** 2^N **do** Compute the binary representation of $i - 1$: $(b_N^{i-1}, b_{N-1}^{i-1}, \dots, b_1^{i-1})$; **for** $k \leftarrow 1$ **to** N **do** **if** b_{N+1-k}^{i-1} *is equal to* 0 **then** $\nu_{ik} \leftarrow \underline{\rho}_k$; **else** $\nu_{ik} \leftarrow \overline{\rho}_k$; **end** **end** $\omega_i \leftarrow [\nu_{i1} \dots \nu_{iN}]^T$; $M_i \leftarrow M(\omega_i)$;**end**

Algorithm 2: Interpolation functions computation

input : The bounds $\underline{\rho}_k$ and $\overline{\rho}_k$ of each parameter ρ_k and the parameter vector ρ **output:** The interpolation functions $\mu_i(\rho)$ **for** $i \leftarrow 1$ **to** 2^N **do** Compute the binary representation of $i - 1$: $(b_N^{i-1}, b_{N-1}^{i-1}, \dots, b_1^{i-1})$; **for** $k \leftarrow 1$ **to** N **do** **if** b_{N+1-k}^{i-1} *is equal to* 0 **then** $\alpha_{ik} \leftarrow 1$; $\beta_{ik} \leftarrow -\overline{\rho}_k$; **else** $\alpha_{ik} \leftarrow -1$; $\beta_{ik} \leftarrow \underline{\rho}_k$; **end** $\mu_i(\rho) \leftarrow \mu_i(\rho) \left(\frac{\alpha_{ik}\rho_k + \beta_{ik}}{\underline{\rho}_k - \overline{\rho}_k} \right)$; **end****end**

Example 1.4

Given the following affine LPV matrix with $N = 2$ parameters:

$$M(\rho) = \begin{bmatrix} \rho_1 & \rho_2 \\ 1 & 0 \end{bmatrix} \quad (1.52)$$

where $\rho_1 \in [\underline{\rho}_1, \overline{\rho}_1]$ and $\rho_2 \in [\underline{\rho}_2, \overline{\rho}_2]$. We are considering the vertices M_i and the interpolation functions $\mu_i(\rho)$ such that:

$$M(\rho) = \sum_{i=1}^4 \mu_i(\rho) M(\omega_i) \quad (1.53)$$

Applying [Algorithm 1](#) and [Algorithm 2](#), one obtains:

- **For $i = 1$:**

$$(1 - 1) \xrightarrow[\text{representation}]{\text{binary}} 00 \Rightarrow \omega_1 = (\underline{\rho}_1, \underline{\rho}_2) \quad \text{and} \quad \mu_1(\rho) = \left(\frac{\rho_1 - \overline{\rho}_1}{\underline{\rho}_1 - \overline{\rho}_1} \right) \left(\frac{\rho_2 - \overline{\rho}_2}{\underline{\rho}_2 - \overline{\rho}_2} \right)$$

- **For $i = 2$:**

$$(2 - 1) \xrightarrow[\text{representation}]{\text{binary}} 01 \Rightarrow \omega_2 = (\underline{\rho}_1, \overline{\rho}_2) \quad \text{and} \quad \mu_2(\rho) = \left(\frac{\rho_1 - \overline{\rho}_1}{\underline{\rho}_1 - \overline{\rho}_1} \right) \left(\frac{-\rho_2 + \overline{\rho}_2}{\underline{\rho}_2 - \overline{\rho}_2} \right)$$

- **For $i = 3$:**

$$(3 - 1) \xrightarrow[\text{representation}]{\text{binary}} 10 \Rightarrow \omega_3 = (\overline{\rho}_1, \underline{\rho}_2) \quad \text{and} \quad \mu_3(\rho) = \left(\frac{-\rho_1 + \overline{\rho}_1}{\underline{\rho}_1 - \overline{\rho}_1} \right) \left(\frac{\rho_2 - \overline{\rho}_2}{\underline{\rho}_2 - \overline{\rho}_2} \right)$$

- **For $i = 4$:**

$$(4 - 1) \xrightarrow[\text{representation}]{\text{binary}} 11 \Rightarrow \omega_4 = (\overline{\rho}_1, \overline{\rho}_2) \quad \text{and} \quad \mu_4(\rho) = \left(\frac{-\rho_1 + \overline{\rho}_1}{\underline{\rho}_1 - \overline{\rho}_1} \right) \left(\frac{-\rho_2 + \overline{\rho}_2}{\underline{\rho}_2 - \overline{\rho}_2} \right)$$

A geometrical interpretation of the interpolation of $M(\rho)$ is depicted in [Figure 1.6](#).

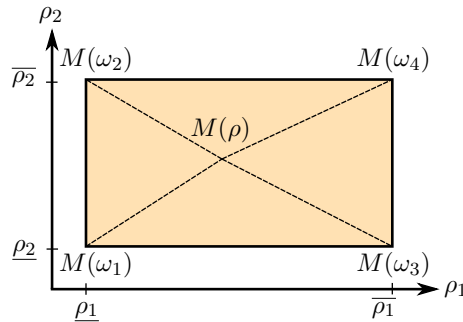


Figure 1.6: Matrix polytopic interpolation

1.2.2 For nonlinear systems

In this section, the problem of observer design for nonlinear systems [Khalil 1996] is considered. Based on [Besançon 2007], different nonlinear observers are presented hereafter. The Kalman Filter for LTV systems and its extension for nonlinear ones. Then, an adaptive observer for state affine systems is detailed.

1.2.2.1 Kalman observer

Kalman filtering is now largely used in both the academic and industrial fields. One can see for instance [Chui and Chen 2009] for the theory. Consider the following LTV system:

$$\begin{aligned}\dot{x}(t) &= A(t)x(t) + B(t) + q(t) \\ y(t) &= C(t)x + r(t)\end{aligned}\tag{1.54}$$

where $q(t)$ and $r(t)$ are white Gaussian noises following the distribution: $q(t) \sim \mathcal{N}(0, Q)$ and $r(t) \sim \mathcal{N}(0, R)$.

Although the Kalman filter is well known, it is less known that some particular conditions need to be fulfilled to guarantee its convergence. To design an observer for (1.54), we need the following definition:

Definition 1.9

The pair $(A(t), C(t))$ is said uniformly completely observable if there exist positive constants α, β, T such that, for all t , the following inequalities hold:

$$\alpha I \leq \int_t^{t+T} \Psi^T(\tau, t) C^T C \Psi(\tau, t) .d\tau \leq \beta I\tag{1.55}$$

where Ψ is the transition matrix of the autonomous system $\dot{x} = A(t)x, y = Cx$, defined by:

$$\frac{d\Psi(\tau, t)}{d\tau} = A(\tau)\Psi(\tau, t) \quad \text{and} \quad \Psi(t, t) = I\tag{1.56}$$

Then, the proposition can be established [Kalman and Bucy 1961; Hammouri and De Leon Morales 1990; Besançon 2007] which realizes a Kalman filter:

Proposition 1.6

If the pair $(A(t), C(t))$ in (1.54) is uniformly completely observable, then an observer of the form:

$$\begin{aligned}\dot{\hat{x}}(t) &= A(t)\hat{x}(t) + B(t) + K(t)(y(t) - \hat{y}(t)) \\ \hat{y}(t) &= C\hat{x}(t)\end{aligned}\tag{1.57}$$

where

$$\begin{aligned} K(t) &= P(t)C^T R^{-1} \\ \dot{P}(t) &= A(t)P(t) + P(t)A(t)^T - K(t)CP(t) + Q \\ P(0) &= P_0 = P_0^T \end{aligned} \quad (1.58)$$

minimizes the covariance matrix of the state estimation error.

The previous result can be extended for nonlinear systems which is the most well-known observer for nonlinear system: the Extended Kalman Filter (EKF).

Proposition 1.7 (*Extended Kalman Filter (EKF)*)

Given a nonlinear system of the form:

$$\begin{aligned} \dot{x}(t) &= f(x(t), u(t)) + q(t) \\ y &= Cx(t) + r(t) \end{aligned} \quad (1.59)$$

where $q(t)$ and $r(t)$ are white Gaussian noise defined as: $q(t) \sim \mathcal{N}(0, Q)$ and $r(t) \sim \mathcal{N}(0, R)$.

There exists an Extended Kalman Filter (EKF), of the form:

$$\dot{\hat{x}}(t) = f(\hat{x}(t), u(t)) + K(t)(y(t) - C\hat{x}(t)) \quad (1.60)$$

where the time-varying gain $K(t)$ is given by:

$$\begin{aligned} K(t) &= P(t)C^T R^{-1} \\ \dot{P}(t) &= F(t)P(t) + P(t)F(t)^T - K(t)CP(t) + Q \\ P(0) &= P_0 = P_0^T \\ F(t) &= \frac{\partial f}{\partial x}(\hat{x}(t), u(t)) \end{aligned} \quad (1.61)$$

Q and R are the covariance matrices of the system and measurement respectively.

This formulation is very convenient since it proposes a systematic observer for nonlinear systems. But as many authors pointed it out, as [Verhaegen and Van Dooren 1986; Besançon 2007] its convergence is just local and numerical instabilities may appear. However, it is largely used in the industry and its efficiency has been clearly demonstrated. See for example, [Boussak 2005; Janiszewski 2006] for EKF applications.

1.2.2.2 Adaptive observer

An adaptive observer design follows the method developed in [Besançon 2000; Besançon et al. 2006] and [Zhang and Clavel 2001; Li et al. 2011]. Such an observer both estimates the state and unknown constant parameters involved in the dynamical equation. The

system must be affine in the state and parameter vector as:

$$\begin{aligned}\dot{x} &= A(u, y)x + \varphi(u, y) + \Phi(u, y)\theta \\ y &= Cx\end{aligned}\tag{1.62}$$

where x , u , y classically denote the state, the input and the measured output vectors respectively and θ a vector of unknown constant parameters. The elements of the matrices $A(u, y)$ and $\Phi(u, y)$ and of the vector $\varphi(u, y)$ are assumed to be continuous and uniformly bounded functions.

Proposition 1.8

If persistent exciting conditions are verified, i.e, if there exist positive constants $\alpha_{1,2}$, $\beta_{1,2}$, $T_{1,2}$ and some bounded symmetric positive definite matrix Σ such that, for all t , the following inequalities hold:

$$\alpha_1 I \leq \int_t^{t+T_1} \Lambda^T(\tau) C^T \Sigma(\tau) C \Lambda(\tau) . d\tau \leq \beta_1 I\tag{1.63}$$

and

$$\alpha_2 I \leq \int_t^{t+T_2} \Psi^T(t, \tau) C^T \Sigma(\tau) C \Psi(t, \tau) . d\tau \leq \beta_2 I\tag{1.64}$$

where Ψ is the transition matrix of the system $\dot{x} = A(u, y)x$, $y = Cx$, then, the following system is an exponential adaptive observer for the nonlinear system (1.62),

$$\begin{aligned}\dot{\hat{x}} &= A(u, y)\hat{x} + \varphi(u, y) + \Phi(u, y)\hat{\theta} \\ &\quad + \{\Lambda S_\theta^{-1} \Lambda^T C^T + S_x^{-1} C^T\} \Sigma(y - C\hat{x}) \\ \dot{\hat{\theta}} &= S_\theta^{-1} \Lambda^T C^T \Sigma(y - C\hat{x}) \\ \dot{\Lambda} &= \{A(u, y) - S_x^{-1} C^T \Sigma C\} \Lambda + \Phi(u, y) \\ \dot{S}_x &= -\rho_x S_x - A(y, u)^T S_x - S_x A(u, y) + C^T \Sigma C \\ \dot{S}_\theta &= -\rho_\theta S_\theta + \Lambda^T C^T \Sigma C \Lambda\end{aligned}\tag{1.65}$$

with $S_x(0), S_\theta(0) \succ 0$.

Note that ρ_x and ρ_θ are the tunable parameters for the convergence rate and that Λ , S_x and S_θ are time-varying observer gains.

Belt tensioner diagnosis

Contents

2.1	Introduction	33
2.2	Cooling System Modeling	34
2.2.1	Thermal modeling of the engine block	35
2.2.1.1	Engine block thermal balance	36
2.2.1.2	Coolant thermal balance	37
2.2.1.3	Final second-order model	37
2.2.2	Flow modeling	38
2.2.3	Model validation	39
2.3	Observer-based fault estimation	40
2.3.1	Fault diagnosis problem statement	40
2.3.2	Adaptive observer	41
2.3.3	Extended Kalman filter	43
2.4	Simulation results	43
2.4.1	Fault scenario	44
2.4.2	First simulation case: constant engine speed and torque	44
2.4.3	Second simulation case: constant engine speed and time-varying torque	45
2.4.4	Third simulation case: more realistic profiles	46
2.5	Conclusion	47

The results presented in this chapter are based on [Dubuc et al. 2017].

2.1 Introduction

In trucks, multiple peripheral devices such as alternator, water pump or air conditioning compressor are driven by a common belt. This belt, connected to the engine shaft, transmits the necessary mechanical power to all components in line as depicted in Figure 2.1. During the installation, the adjustment of a belt tensioner permits to hold a predetermined amount of tension on the belt, which enables it to fulfill its role.

In case of under-tension, the belt will slip, causing noise and premature wear. More importantly, it will also degrade the operation of all driven components to a subnominal state. Among others, the water pump located in the cooling system will not provide the proper coolant flow rate to the engine. This could lead the engine to overheat and, eventually, stall.

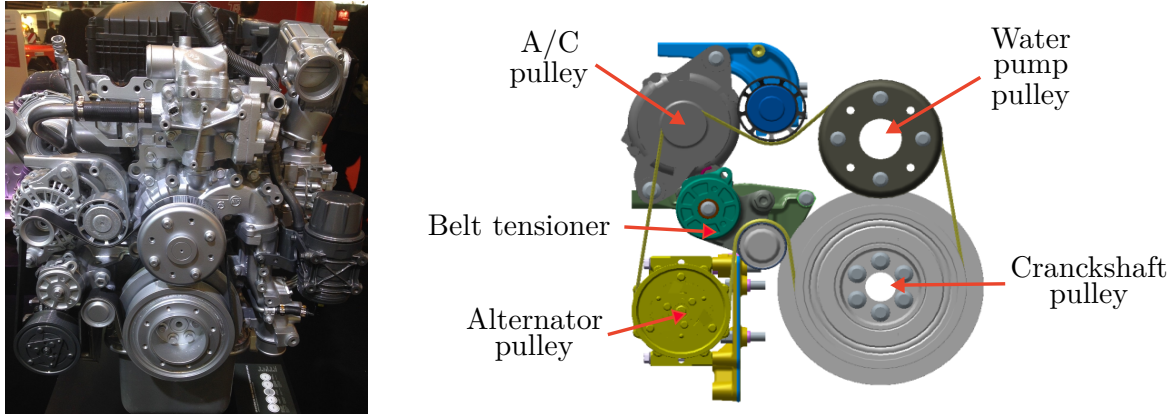


Figure 2.1: Components driven by the belt

To overcome such problems, this chapter proposes to estimate a parameter which is shown to be characteristic of the belt tensioner's health, via an analysis of the cooling system. To do so, a simplified model of the cooling system for diagnosis will be developed. To estimate the belt tensioner characteristic parameter, two observers defined in [Chapter 1](#) have been designed and compared: an Adaptive Observer (AO) and an Extended Kalman Filter (EKF). The merits of these two observer-based methods will be validated using simulation on a high-fidelity model of the cooling system designed with GT-POWER.

The chapter is organized as follows. In [Section 2.2](#), a simplified model of the cooling system is presented. In [Section 2.3](#), based on this model, an Adaptive Observer and an Extended Kalman Filter are designed to monitor the performance of the belt tensioner. Then in [Section 2.4](#) we analyze the performance of the developed solutions. Finally, conclusions are stated in [Section 2.5](#).

2.2 Cooling System Modeling

A schematic representation of the cooling system is given in [Figure 2.2](#). The water pump provides the coolant flow to remove the heat produced by the combustion in order to protect the different components from overheating and to ensure a good lubrication. In our case, the pump is driven by the engine through a belt. To reach more rapidly the optimal engine temperature, a thermostat is used to control it. It will be opened during cold start, then the flow passes through the radiator which is cooled by a fan

Table 2.1: Nomenclature

Notation	Description	Unit
N_{eng}	Engine speed	rpm
N_{pump}	Pump speed	rpm
Γ	Engine torque	N.m
$Q_{g,eb}$	Heat flow from gas in the cylinder to the engine block	W
$Q_{eb,c}$	Heat flow from the engine block to the coolant	W
A_{eb}	Heat transfer surface area inside the engine block	m ²
T_{eb}	Temperature of the engine block	K
$T_{c,\{i,o\}}$	Coolant temperature at the inlet and at the outlet	K
h_c	Coolant heat transfer coefficient	W.m ⁻² .K ⁻¹
c_{eb}	Heat capacity of the engine block	J.kg ⁻¹ .K ⁻¹
c_c	Heat capacity of the coolant	J.kg ⁻¹ .K ⁻¹
\dot{m}_c	Mass flow rate of the coolant	kg.s ⁻¹
$\dot{m}_{c,\{e,oc\}}$	Mass flow rate of the coolant through the engine and the oil cooler	kg.s ⁻¹
$m_{\{eb,c\}}$	Mass of the engine block and of the coolant in contact with the engine block	kg

and the wind speed. [Figure 2.3](#) summarizes the different heat exchanges involved the engine block.

The next section presents a simplified thermal model that will be used to design observers. The notations used in this section and in the chapter follow the nomenclature in [Table 2.1](#).

2.2.1 Thermal modeling of the engine block

To design a control-oriented model, a lumped-parameter approach is followed in the sequel, neglecting the distributed nature of the temperature of the coolant when flowing through the engine block. In details, we follow a procedure similar to [[Cortona et al. 2002](#); [Astorga-Zaragoza et al. 2008](#); [Isermann 2014](#)] where mean-value models are obtained from energy balances.

Let us consider the system presented in [Figure 2.3](#). It consists in two thermal subsystems: the engine block and the coolant.

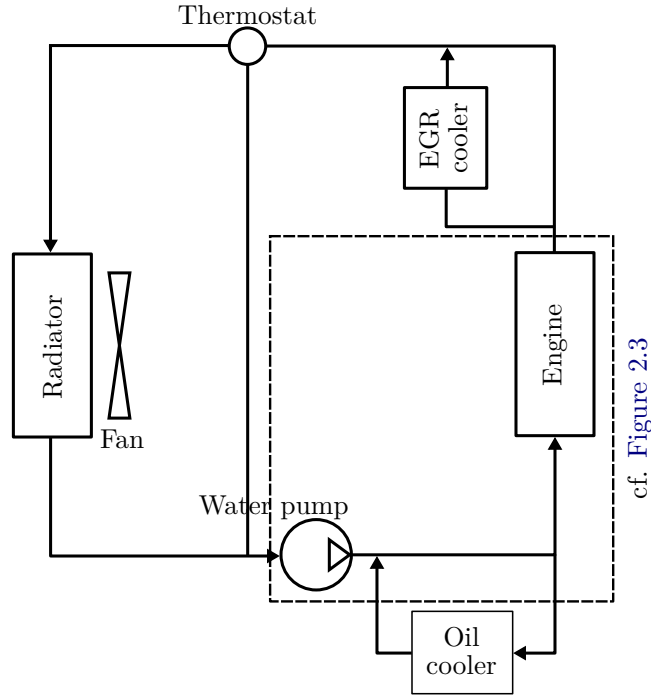


Figure 2.2: Architecture of the cooling system

2.2.1.1 Engine block thermal balance

A heat balance on the engine block gives the following temperature evolution:

$$\dot{T}_{eb} = \frac{Q_{g,eb} - Q_{eb,c}}{m_{eb}c_{eb}} \quad (2.1)$$

Note that the heat flow $Q_{g,eb}$ can be considered as an input of the model. Indeed, this flow depends on the engine operating point and its value can be obtained from a three-dimensional map (cf. Figure 2.4):

$$Q_{g,eb} = f(N_{eng}, \Gamma) \quad (2.2)$$

On the other hand, the heat transfer to the coolant originates mainly from conduction through the area A_{eb} , and thus can be expressed as:

$$Q_{eb,c} = h_c A_{eb} \left(T_{eb} - \frac{T_{c,i} + T_{c,o}}{2} \right), \quad (2.3)$$

where an average value between the inlet and outlet flow temperatures is used to account for the distributed nature of the flow temperature.

In addition, the heat transfer coefficient h_c can be expressed by phenomenological laws (see for example the Colburn analogy [Bergman and Incropera 2011]). In our case the following relation is used:

$$h_c A_{eb} = (hA)_{ref} \left(\frac{\dot{m}_{c,e}}{\dot{m}_{ref}} \right)^{0.75} \quad (2.4)$$

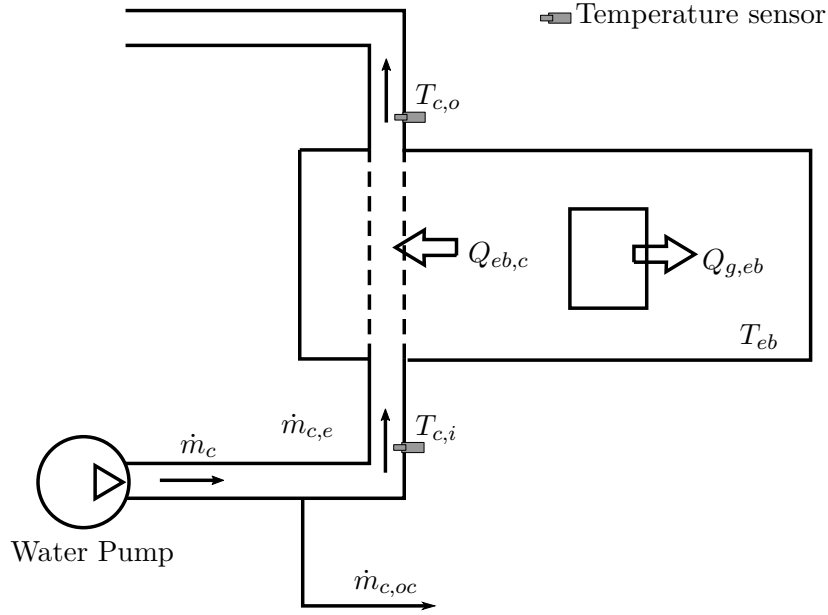


Figure 2.3: Flows and temperatures of the engine block

2.2.1.2 Coolant thermal balance

Following similar arguments, a heat balance equation gives:

$$\dot{T}_{c,o} = \frac{Q_{eb,c} - \Delta Q_c}{m_c c_c} \quad (2.5)$$

where ΔQ_c represents the heat flow due to the temperature difference at the input and the output of the engine. It can be expressed as:

$$\Delta Q_c = c_c \dot{m}_{c,e} (T_{c,o} - T_{c,i}) \quad (2.6)$$

2.2.1.3 Final second-order model

By combining (2.1), (2.3), (2.5) and (2.6), we finally get the following second order system:

$$\begin{cases} \dot{T}_{eb} = \frac{h_c(\dot{m}_{c,e})A_{eb}}{m_{eb}c_{eb}} \left(\frac{T_{c,o}}{2} - T_{eb} \right) + \frac{Q_{g,eb}}{m_w c_{eb}} + \frac{h_c(\dot{m}_{c,e})A_{eb}}{m_{eb}c_{eb}} \frac{T_{c,i}}{2} \\ \dot{T}_{c,o} = \left(-\frac{h_c(\dot{m}_{c,e})A_{eb}}{2m_c c_c} - \frac{\dot{m}_{c,e}}{m_c} \right) T_{c,o} + \frac{h_c(\dot{m}_{c,e})A_{eb}}{m_c c_c} T_{eb} + \left(\frac{\dot{m}_{c,e}}{m_c} - \frac{h_c(\dot{m}_{c,e})A_{eb}}{2m_c c_c} \right) T_{c,i} \end{cases} \quad (2.7)$$

in which h_c is defined through (2.4).

It is worth noting that, in the sequel, it is assumed that the following variables are known (measured or estimated): N_{eng} ; Γ ; $T_{c,i}$ and $T_{c,o}$.

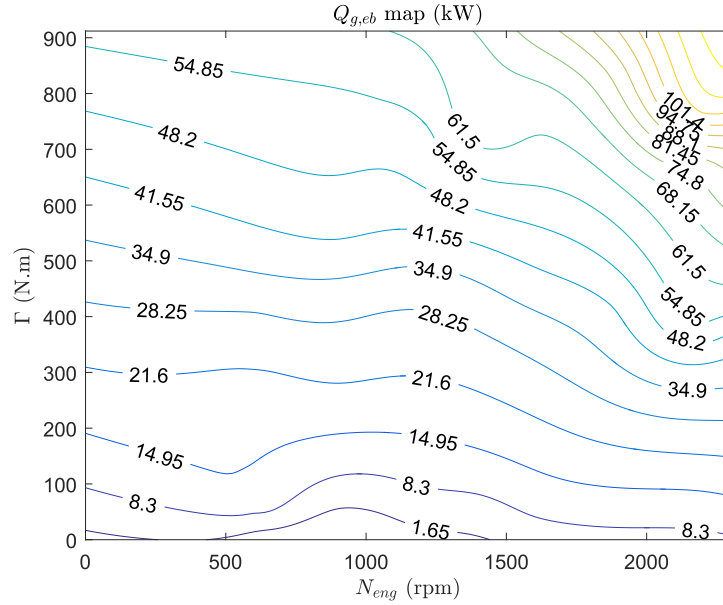


Figure 2.4: Heat flow from the gas to the engine block

2.2.2 Flow modeling

Since the water pump is mechanically connected to the engine, the provided flow is a function of the engine speed. In order to simplify the model, we will use a crude approximation of this relation by assuming that:

$$\dot{m}_c = \alpha N_{pump}, \quad \alpha \in \mathbb{R}^+ \quad (2.8)$$

For more detailed pump models see [Isermann 2014].

Since the pump speed is not measured but the engine one is, the following relation is also considered:

$$N_{pump} = r N_{eng}, \quad r \in \mathbb{R}^+ \quad (2.9)$$

Finally, a part of the coolant recirculated by the water pump actually flows through the oil cooler instead of the engine as shown in Figure 2.2. This is represented by a simplified proportional relation between the global mass flow rate and the engine block one:

$$\dot{m}_{c,e} = \beta \dot{m}_c, \quad \beta \in [0; 1] \quad (2.10)$$

Plugging together (2.8)-(2.10), we have the simple relation:

$$\dot{m}_{c,e} = \sigma N_{eng}, \quad \sigma \in \mathbb{R}^+ \quad (2.11)$$

in which $\sigma = \alpha \times \beta \times r$ is a constant¹.

¹This approximation is verified if the resistance coefficient of the cooling system is constant, that is, when the thermostat position is fixed (after engine start-up).

2.2.3 Model validation

To validate the modeling (2.7) and the assumptions (2.4) and (2.11), it is compared with one built with GT-POWER. This software, developed by Gamma Technology, consists in a set of simulation libraries for analyzing the engine behavior and is largely used in the automotive industry. As it enables to obtain a high-fidelity simulation, this model will be the reference one in the sequel.

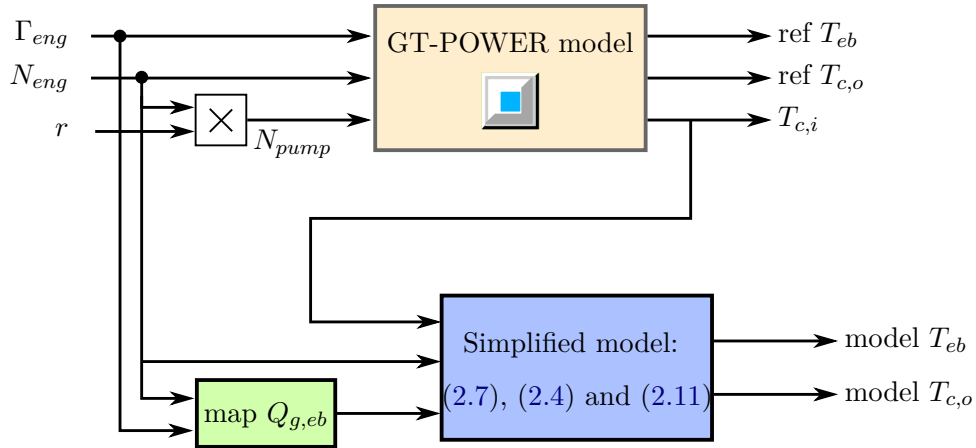


Figure 2.5: Block diagram to validate the simplified model

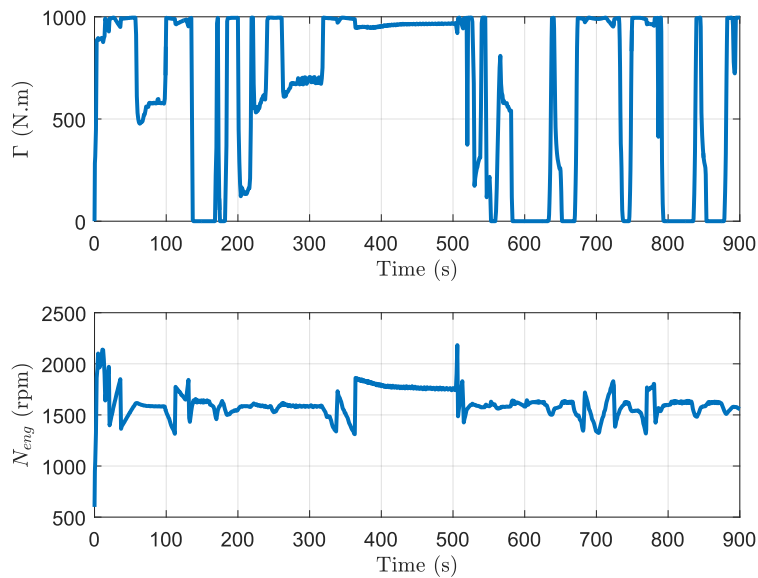


Figure 2.6: Torque and engine speed profiles

The validation consists in the comparison of the reference data from the GT-POWER and the ones obtained from the simplified model. To do so, the process described in Figure 2.5. The engine speed and load torque profiles used for the valida-

tion is the one presented in Figure 2.6.

Under these conditions, the results obtained from GT-POWER and from the developed model are given in Figure 2.7.

It can be observed that the temperatures recovered from the simplified model match almost perfectly the reference ones. This justifies the use of the simplified model to design observers.

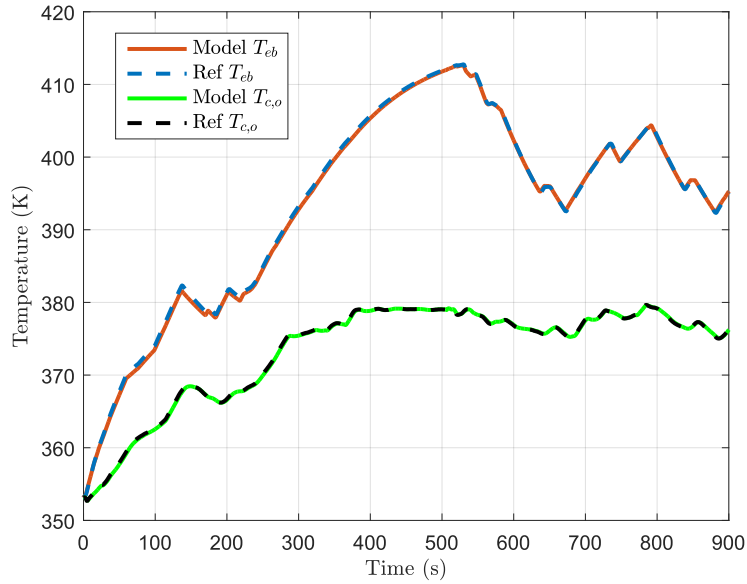


Figure 2.7: Comparison between the reference and the simplified model

2.3 Observer-based fault estimation

This section is devoted to: define a characteristic coefficient which determines the degradation of the belt tensioner and propose a observer-based solution to estimate this coefficient.

2.3.1 Fault diagnosis problem statement

The belt tensioner ensures power transmission between the engine and all the other components connected to the belt. A malfunction on the belt tensioner will affect the transmission ratio r in (2.9) which, in turn, will affect the mass flow rate in (2.8). Thus, from the cooling system (2.4), (2.7), (2.11) point of view, this malfunction will affect the nominal mass flow rate through a change of the parameter σ in (2.11). Note that this change will also affect the heat transfer coefficient h_c which depends on $\dot{m}_{c,e}$

through (2.4). Therefore, from our point of view, the coefficient σ is a good candidate to provide an indication of the belt tensioner's health.

To evaluate in real time the degradation of the transmission, observers have been designed to estimate the parameter σ which is considered to be constant (or slow-varying). Two types of observer are considered in the sequel. The first one is an Adaptive Observer (AO) and then an extended Kalman filter (EKF).

2.3.2 Adaptive observer

The adaptive observer design follows the method developed in [Besançon et al. 2006] and [Zhang and Clavel 2001]. Such an observer both estimates the state and unknown constant parameters involved in the dynamical equation. The system must be affine in the state and parameter vector as:

$$\begin{aligned} \dot{x} &= A(u, y)x + \varphi(u, y) + \Phi(u, y)\theta \\ y &= Cx \end{aligned} \quad (2.12)$$

where x , u , y classically denote the state, the input and the measured output vectors respectively and θ a vector of unknown constant parameters.

In order to apply this observer to the cooling system (2.4), (2.7), (2.11) let us note:

$$\begin{aligned} \theta_1 &= h_c A_{eb} & \theta_2 &= \dot{m}_{ce} c_c \\ a_1 &= m_{eb} c_{eb} & a_2 &= m_c c_c \end{aligned} \quad (2.13)$$

Introducing $z = [T_{eb} \ T_{c,o}]^T$; $u = [Q_{g,eb} \ T_{c,i}]^T$, one obtains the following equivalent state-space representation:

$$\begin{aligned} \dot{z} &= \begin{bmatrix} -\frac{\theta_1}{a_1} & \frac{\theta_1}{2a_1} \\ \frac{\theta_1}{a_2} & -\frac{\theta_1 + 2\theta_2}{2a_2} \end{bmatrix} z + \begin{bmatrix} \frac{1}{a_1} & \frac{\theta_1}{2a_1} \\ 0 & \frac{\theta_2}{a_2} - \frac{\theta_1}{2a_2} \end{bmatrix} u \\ y &= [0 \ 1] z \end{aligned} \quad (2.14)$$

However it does not fit the formalism of (2.12) as it introduces bilinear terms $\theta_1 z_1$ in which z_1 is not measured and this prevents the use of AO. To overcome this problem, (2.14) is turned into its companion form. With this aim in view, the following coordinate transformation is used:

$$x = \begin{bmatrix} \frac{\theta_1}{a_2} & \frac{\theta_1}{a_1} \\ 0 & 1 \end{bmatrix} z \quad (2.15)$$

This leads to:

$$\begin{aligned} \dot{x} &= \begin{bmatrix} 0 & 0 \\ 1 & 0 \end{bmatrix} x \\ &+ \begin{bmatrix} \frac{u_2 - x_2}{a_1 a_2} & \frac{u_1}{a_1 a_2} & 0 \\ 0 & -\frac{x_2}{a_1} - \frac{x_2 + u_2}{2a_2} & \frac{u_2 - x_2}{a_2} \end{bmatrix} \Theta \\ y &= [0 \ 1] x \end{aligned} \quad (2.16)$$

where $\Theta = [\theta_1 \theta_2 \ \theta_1 \ \theta_2]^T$. Therefore (2.16) satisfies the required form (2.12).

Now, to estimate the parameter σ , it is important to note that, by using (2.4) and (2.11):

$$\begin{cases} \theta_1 = (hA)_{ref} \left(\frac{N_{eng}}{\dot{m}_{ref}} \right)^{0.75} \sigma^{0.75} \triangleq f(N_{eng}) \sigma^{0.75} \\ \theta_2 = c_c N_{eng} \sigma \triangleq g(N_{eng}) \sigma \end{cases} \quad (2.17)$$

Thus σ can be directly estimated by including (2.17) in Θ . Therefore (2.16) becomes:

$$\begin{aligned} \dot{x} &= \begin{bmatrix} 0 & 0 \\ 1 & 0 \end{bmatrix} x + \\ &\begin{bmatrix} f(N_{eng})g(N_{eng})\frac{u_2 - x_2}{a_1 a_2} & f(N_{eng})\frac{u_1}{a_1 a_2} & 0 \\ 0 & f(N_{eng})\left(-\frac{x_2}{a_1} - \frac{x_2 + u_2}{2a_2}\right) & g(N_{eng})\frac{u_2 - x_2}{a_2} \end{bmatrix} \theta \\ &\triangleq A(u, y)x + \Phi(u, y)\theta \\ y &= [0 \ 1]x \triangleq Cx \end{aligned} \quad (2.18)$$

with $\theta = [\sigma^{1.75} \ \sigma^{0.75} \ \sigma]^T$.

If persistent exciting conditions (1.63) and (1.64) are verified, Proposition 1.8 can be applied and the AO has the following structure:

$$\begin{aligned} \dot{\hat{x}} &= A(u, y)\hat{x} + \varphi(u, y) + \Phi(u, y)\hat{\theta} \\ &\quad + \{\Lambda S_\theta^{-1} \Lambda^T C^T + S_x^{-1} C^T\} \Sigma (y - C\hat{x}) \\ \dot{\hat{\theta}} &= S_\theta^{-1} \Lambda^T C^T \Sigma (y - C\hat{x}) \\ \dot{\Lambda} &= \{A(u, y) - S_x^{-1} C^T \Sigma C\} \Lambda + \Phi(u, y) \\ \dot{S}_x &= -\rho_x S_x - A(y, u)^T S_x - S_x A(u, y) + C^T \Sigma C \\ \dot{S}_\theta &= -\rho_\theta S_\theta + \Lambda^T C^T \Sigma C \Lambda \end{aligned} \quad (2.19)$$

2.3.3 Extended Kalman filter

For the ease of comparison, a classical EKF presented in [Proposition 1.7](#) is also designed. Since σ is constant, the dynamics $\dot{\sigma} = 0$ is added to the system (2.7) to obtain a third order system described by:

$$\begin{aligned}\dot{x}(t) &= f_{ekf}(x(t), u(t)) \\ y &= Cx(t)\end{aligned}\tag{2.20}$$

with $x = [\sigma \ T_{eb} \ T_{c,o}]^T$; $u = [Q_{g,eb} \ T_{c,i}]^T$ and $C = [0 \ 0 \ 1]$.

Note that assuming σ constant is not restrictive since it also corresponds to the needed assumption in adaptive observer design for parameter estimation.

The EKF to design follows the algorithm:

$$\begin{aligned}\dot{\hat{x}}(t) &= f_{ekf}(\hat{x}(t), u(t)) + K(t)(y(t) - C\hat{x}(t)) \\ \hat{y}(t) &= C\hat{x}(t) \\ K(t) &= P(t)C^T R^{-1} \\ \dot{P}(t) &= F(t)P(t) + P(t)F(t)^T - K(t)CP(t) + Q \\ P(0) &= P_0 = P_0^T \\ F(t) &= \frac{\partial f_{ekf}}{\partial x}(\hat{x}(t), u(t))\end{aligned}\tag{2.21}$$

where the jacobian $F(t)$ are computed with its explicit form.

2.4 Simulation results

To compare the merits of the two methods previously presented, we set them in various contexts on the reference model developed with GT-POWER. The following initial conditions and tuning parameters (chosen to get a trade-off between convergence speed and noise attenuation) have been used in all cases.

Concerning the adaptive observer (2.19):

- $\rho_x = \rho_\theta = 75 \times 10^{-3}$
- $\hat{\theta}(0) = [0.002^{1.75} \ 0.002^{0.75} \ 0.002]^T$,
 $S_x(0) = I_2$, $S_\theta(0) = I_3$, $\Lambda(0) = \mathcal{O}_{2,3}$, $\hat{x}(0) = [29 \ 353.15]^T$

Concerning the EKF (2.21):

- $Q = 100 \times I_3$, $R = 10^8$

- $\hat{x}(0) = [0.002 \ 353.15 \ 353.15]^T$, $P(0) = I_3$

It is worth noting that the initial conditions provided to the two observers are consistent with each other.

2.4.1 Fault scenario

In Section 2.3.1, it has been established that σ is a function of the ratio r defined in (2.9). To simulate a fault on σ let us consider the following evolution of r :

$$r(t) = \begin{cases} 1.4 & \text{for } t < 500 \text{ s} \\ 0.7 & \text{for } t \geq 500 \text{ s} \end{cases} \quad (2.22)$$

The fault is implemented in GT-POWER through the operating point N_{pump} provided to the water pump. Data are then collected to feed the developed observers as depicted in Figure 2.8. Then, following (2.11), the real σ is computed as: $\sigma_{real} = \dot{m}_{c,e}/N_{eng}$. It is depicted with the black dashed plot in the Figure 2.9, 2.11 and 2.12. Note also that the AO estimates a vector of three coherent parameters but only the third term will be plotted in the sequel.

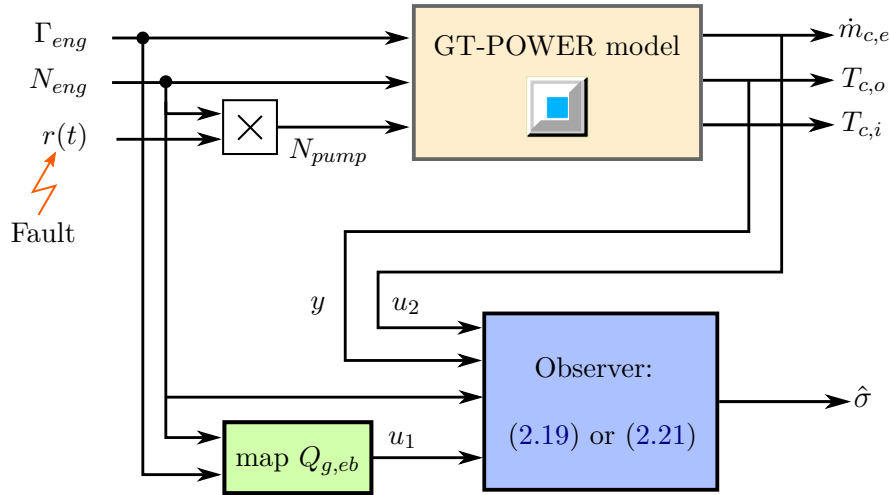


Figure 2.8: Block diagram to evaluate the developed observers

2.4.2 First simulation case: constant engine speed and torque

First, let us consider the simple case of a given constant operating point:

$$N_{eng} = 1600 \text{ rpm}, \quad \Gamma = 816 \text{ N.m}$$

The results corresponding to this case are given in Figure 2.9. One can observe that the EKF estimates the value of the parameter σ with a short settling time. On the other hand, the estimation of σ provided by the AO introduces a bias. This can be explained by the fact that the condition of persistent excitation (1.63) in Proposition 1.8 is not fulfilled. Indeed, if the speed and the torque are constant, it means that the heat flow $Q_{g,eb}$ described by (2.2) is constant. Thus the variable u_1 in (2.16) is not excited and so the observer cannot converge. Consequently, for this scenario, the adaptive observer is not suitable as it suffers from significant limitations.

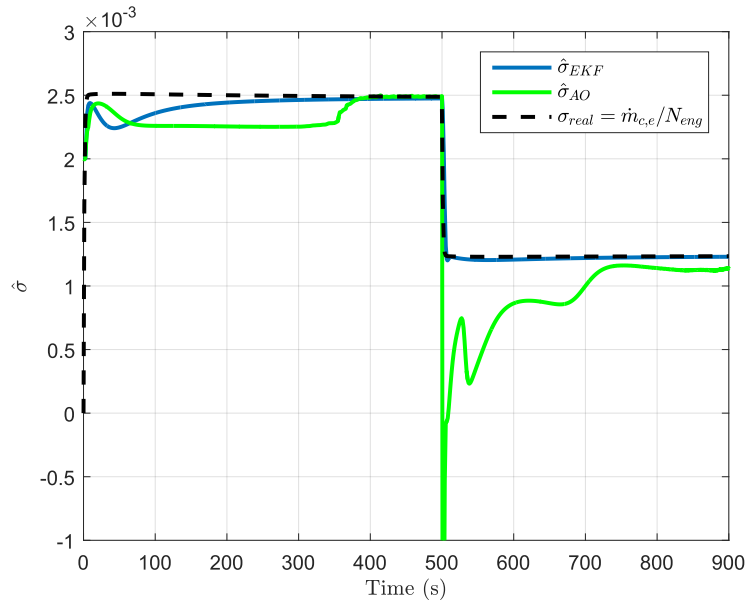


Figure 2.9: Estimation results obtained in the first case

2.4.3 Second simulation case: constant engine speed and time-varying torque

To guarantee the persistent excitation condition (1.63) (this has been done a posteriori), the torque profile is changed into the one depicted in the Figure 2.10. The engine speed is still equal to 1600 rpm.

The obtained results are presented in Figure 2.11. The persistent excitation is now fulfilled, and one can observe that both observers converge and correctly estimate the value of the parameter σ . However, the AO has a significant overshoot which may be unsuitable for fault detection.

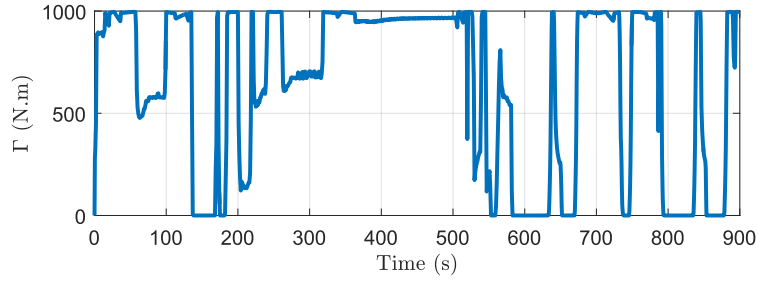


Figure 2.10: Torque profile in the second case

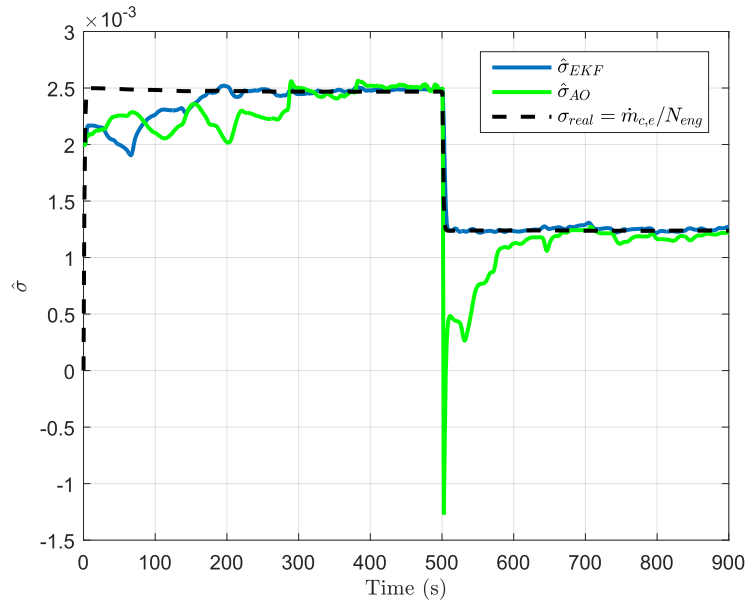


Figure 2.11: Estimation results obtained in the second case

2.4.4 Third simulation case: more realistic profiles

Until now, the engine speed was kept constant in order to respect the assumption that the vector θ is constant. Indeed, if N_{eng} is varying, so are the parameters $f(N_{eng})$ and $g(N_{eng})$ in (2.17). To evaluate the performance of the EKF in a more practically meaningful context, let us consider a third case where torque and speed engine profiles are time-varying. Besides, a white Gaussian noise with a variance of 0.05 is added to the measures $T_{c,o}$ and $T_{c,i}$. The considered profiles are the ones given in Figure 2.6. Corresponding simulations results are depicted in Figure 2.12. One can observe that, even in a noisy realistic case, the estimation capabilities remain similar to the ones obtained in the previous case.

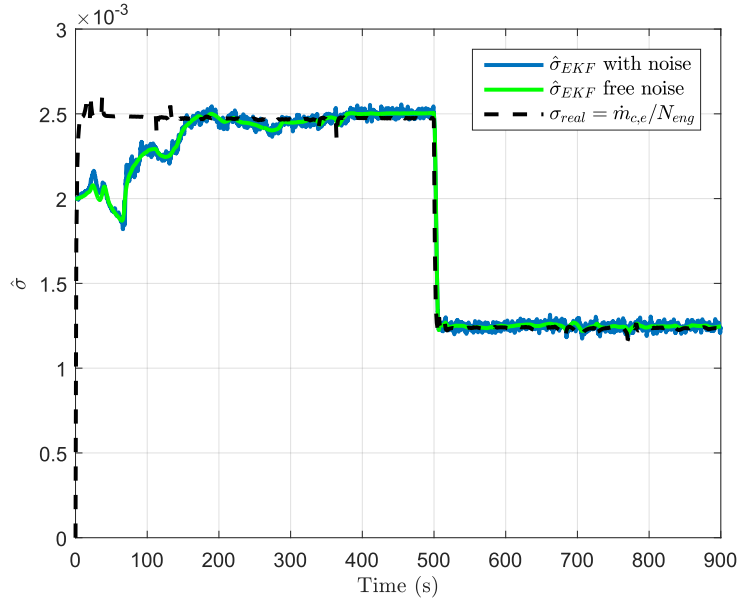


Figure 2.12: Estimation results obtained in the third case

2.5 Conclusion

In this chapter we have proposed a method to estimate the performance degradation of a belt tensioner from the cooling system point of view. A simplified control-oriented model has been developed and validated with a more complex model developed in GT-POWER. The model was then used to design an adaptive observer and an Extended Kalman Filter.

It has been established in [Section 2.4](#) that the EKF has better transient performance than the AO to estimate the parameter σ . Besides, the EKF estimation requires fewer assumptions but it is well known that its convergence is just local and may have numerical instability [[Verhaegen and Van Dooren 1986](#)]. On the other hand, the AO only converges if the engine speed is constant, with sufficient excitation on $Q_{g,eb}$. This condition is, in practice, difficult to obtain, as it implies that the rotation must be constant while providing a variable torque (see [Figure 2.10](#)).

We may also conclude that a single observer is not enough to detect and isolate the fault on the belt tensioner. In fact, as said before, a fault may also occur in other components of the cooling system. For example, a fault on the coolant mass flow rate, as a leak, will affect σ . To overcome this problem, we should monitor all the other systems driven by the belt.

CAC and EGR cooler diagnosis

Contents

3.1	Introduction	49
3.2	Subsystems modeling	51
3.2.1	Gas mixture modeling inside the intake manifold	51
3.2.2	Charge air cooler modeling	52
3.2.3	T_{2A} estimation	53
3.2.4	EGR cooler modeling	54
3.2.5	Summary of the considered model and measurements	55
3.3	Observers design	56
3.3.1	Observer design for k_{cac}	56
3.3.2	LPV observer design for k_{egr}	57
3.3.2.1	LPV modeling	57
3.3.2.2	LPV observer design	58
3.4	Estimation results	59
3.4.1	Heat transfer coefficients expression	59
3.4.1.1	k_{cac} estimation	60
3.4.1.2	k_{egr} estimation	61
3.4.2	k_{cac} observer evaluation	62
3.4.3	k_{egr} observer evaluation	63
3.5	Sensitivity with respect to input uncertainties	64
3.6	Conclusion	67

3.1 Introduction

To meet the legislative standards, the automotive manufacturers have to provide on-board diagnosis (OBD) solutions for the anti-pollution systems [Mohammadpour et al. 2012]. Among them, the Charge Air Cooler (CAC) and the EGR cooler have to be diagnosed. These elements are a part of the systems regulating the soot and NOx emissions (see the engine architecture in Figure 3.1).

Currently, on Volvo's medium duty engines, both diagnoses are achieved with a sensor configuration containing the EGR gas temperature measurement T_{egr} . This sensor is only used for the EGR cooler diagnosis and it is more expensive than the one for the P_2/T_2 measurement (physically the same sensor provides these two variables). The objective is to provide a diagnosis solution of the CAC and the EGR cooler but with a different sensor configuration in which the T_{egr} sensor is removed and replaced by a sensor measuring the temperature T_{2R} . Based on this configuration, two observers will be designed to estimate two characteristic coefficients for the degradation. As in Chapter 2, an Adaptive Observer will be proposed for the CAC diagnosis and an LPV one for the EGR cooler.

This chapter is organized as follows. In Section 3.2, mean value models of the different subsystems are developed. Based on this modeling, in Section 3.3 two observers are designed in order to estimate the characteristic coefficients. Then, in Section 3.4, the performance of the observers are assessed considering real data obtained with a test bench. Next, in Section 3.5, the sensitivity with respect to uncertainties are analyzed. Finally, conclusions are stated in Section 3.6.

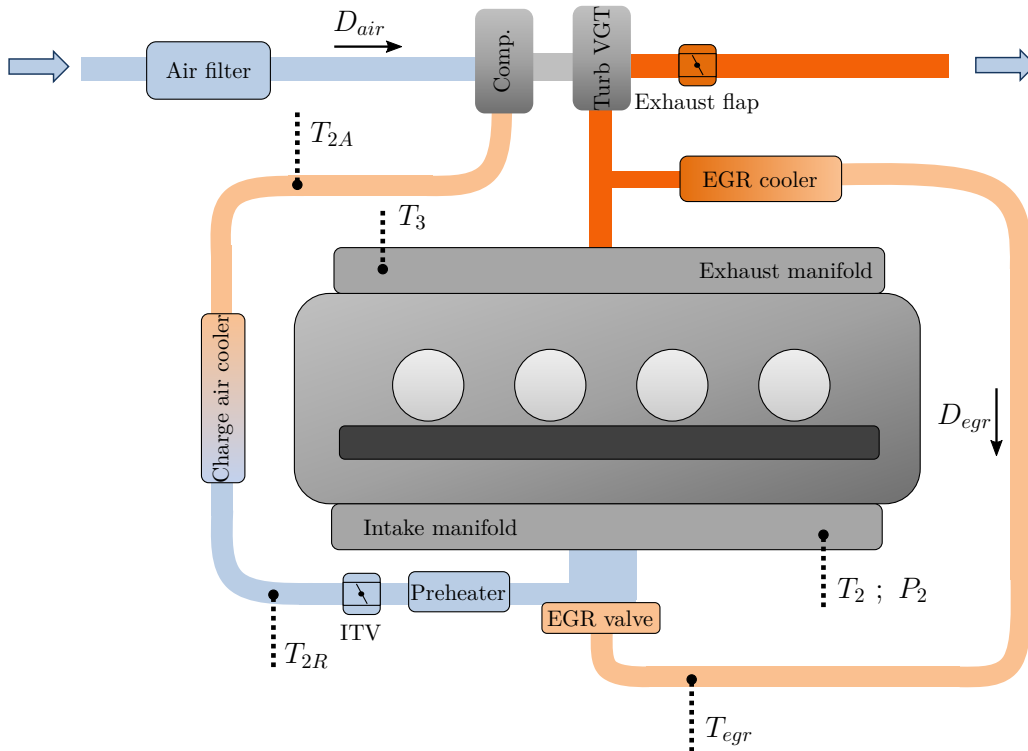


Figure 3.1: Schematic view of the air path in the considered engine

Table 3.1: Nomenclature

Notation	Description	Unit
N_{eng}	Engine speed	r.p.m
T	Temperature of a subsystem	K
P	Pressure of a subsystem	Pa
R	Ideal gas constant for the air	$J.kg^{-1}.K^{-1}$
D	Mass flow rate	$kg.s^{-1}$
γ	Heat ratio	-
c_v	Specific heat capacity at constant volume	$J.kg^{-1}.K^{-1}$
c_p	Specific heat capacity at constant pressure	$J.kg^{-1}.K^{-1}$
Subscript		
2	Inside the intake manifold	
3	Inside the exhaust manifold	
<i>air</i>	Related to the inlet air	
<i>cool</i>	Related to the coolant	
2A	Area located after the compressor	
2R	Area located after the Charge Air Cooler	
<i>egr</i>	Related to the EGR loop	
<i>cac</i>	Related to the Charge Air Cooler	

3.2 Subsystems modeling

The design of observers requires to model the temperature inside the intake manifold and the heat exchanges of the CAC and the EGR cooler. To develop such temperature models for the different subsystems constituting the engine air-path, a control volume approach will be considered as in [Isermann 2014; Castillo 2013].

The notations considered in this chapter follow the nomenclature in Table 3.1 and Figure 3.1 illustrates the location of the different used variables.

3.2.1 Gas mixture modeling inside the intake manifold

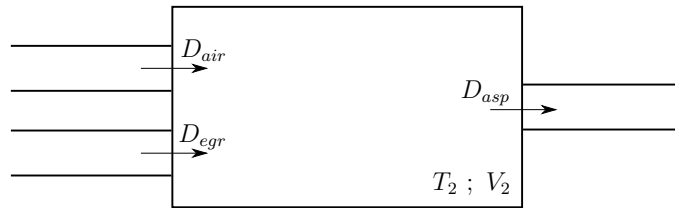


Figure 3.2: Intake manifold volume

According to the first law of thermodynamics, the internal energy U_2 of the gas inside the volume depicted in Figure 3.2 is expressed as:

$$\dot{U}_2 = h_{egr}D_{egr} + h_{air}D_{air} - h_{asp}D_{asp} \quad (3.1)$$

where, the heat transfer to the wall of the storage is neglected and h are the specific enthalpy of the incoming and outgoing flows of the volume.

Based on Joule's second law, the internal energy and the enthalpy are deduced as:

$$\begin{aligned} U_2 &= m_2 c_{v2} T_2 \\ h_{egr} &= c_{p,egr} T_{egr} \\ h_{air} &= c_{p,air} T_{2R} \\ h_{asp} &= c_{p,2} T_2 \end{aligned} \quad (3.2)$$

where m_2 is the gas mass inside the volume. Rigorously, the different heat constants depend on the temperature and the composition of the gas but, as a first-order approximation, they will be considered as constant and equal respectively to c_v and c_p . Taking a time-derivative of (3.1) and using (3.2), one gets:

$$\dot{m}_2 c_v T_2 + m_2 c_v \dot{T}_2 = c_p T_{egr} D_{egr} + c_p T_{2R} D_{air} - c_p T_2 D_{asp} \quad (3.3)$$

Besides, the dynamics of the gas mass inside the volume is given by:

$$\dot{m}_2 = D_{egr} + D_{air} - D_{asp} \quad (3.4)$$

Then, the dynamics of intake manifold temperature is deduced:

$$\dot{T}_2 = \frac{1}{m_2} [((1 - \gamma)D_{asp} - D_{egr} - D_{air})T_2 + \gamma D_{egr} T_{egr} + \gamma D_{air} T_{2R}] \quad (3.5)$$

where $\gamma = \frac{c_p}{c_v}$ stands for the heat ratio considered as a constant.

3.2.2 Charge air cooler modeling

The Charge Air Cooler (CAC) is used to cool the compressed air before the engine to increase its density. This enables to increase the air mass flow rate, and therefore the power density of the engine. Besides, since the temperature is lower, the different components in line are and the combustion can be more efficient (lower fuel consumption for the same pollutants emissions). In Volvo's trucks, the CAC is located in a heat exchangers cluster called "cooling package". This cooling package is composed of the air conditioning condenser, the radiator and the CAC. It is located in front of the truck. Thus the CAC is cooled by the ambient air flow due to the speed and, if needed, a fan.

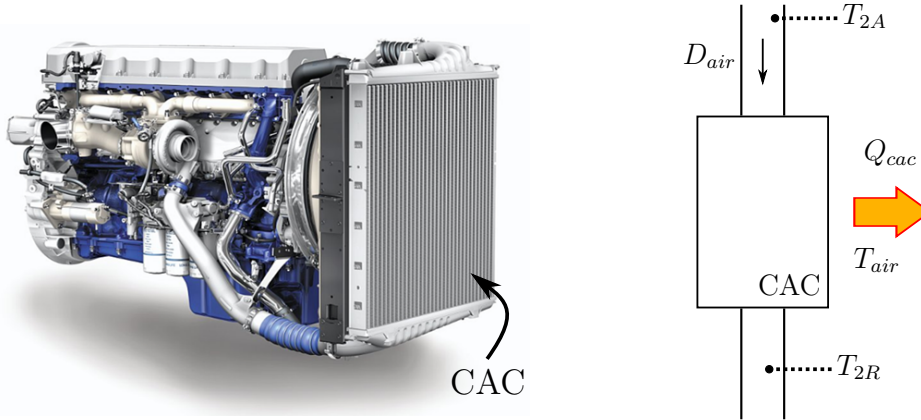


Figure 3.3: Heat exchanges inside the Charge Air Cooler (CAC)

The thermal modeling handled here is similar to the one seen in [Chapter 2](#). Following the scheme in [Figure 3.3](#), a heat balance on the CAC gives the output temperature evolution described by:

$$\dot{T}_{2R} = \frac{D_{air}}{m_{2R}} (T_{2A} - T_{2R}) + \frac{Q_{cac}}{m_{2R}C_{p,air}} \quad (3.6)$$

m_{2R} and Q_{cac} represent, respectively, the gas mass inside the CAC and the heat flow from the CAC to the ambient air. m_{2R} is deduced from the geometrical characteristics given by the manufacturer. Q_{cac} is due to the conduction through the area A_{cac} and can be expressed as:

$$Q_{cac} = h_{cac}A_{cac} \left(T_{air} - \frac{T_{2A} + T_{2R}}{2} \right) \quad (3.7)$$

where h_{cac} is the heat transfer coefficient.

3.2.3 T_{2A} estimation

In practice, T_{2A} is not measured but can be deduced from the definition of the isentropic efficiency of the compressor:

$$\eta_c = \frac{T_{2A,isentropic} - T_{air}}{T_{2A} - T_{air}} = \frac{\left(\frac{P_2}{P_{air}} \right)^{\frac{\gamma-1}{\gamma}} - 1}{\frac{T_{2A}}{T_{air}} - 1} \quad (3.8)$$

Therefore,

$$T_{2A} = T_{air} + \frac{T_{air}}{\eta_c} \left(\left(\frac{P_2}{P_{air}} \right)^{\frac{\gamma-1}{\gamma}} - 1 \right) \quad (3.9)$$

η_c is given by static map experimentally obtained by the manufacturer of the turbocharger. For more details, see [Section 5.2.2.2](#).

To test the accuracy of the T_{2A} modeling (3.9), the needed data have been collected from test bench i.e T_{air} , P_{air} , P_2 and T_{2A} as in Figure 3.4 and for a stationary cycle (the WHTC: see Appendix B). Figure 3.5 shows the evolution of the modeling of T_{2A} and the measurement for a part of the WHTC. One can observe that (3.9) follows all the variations of the real temperature T_{2A} . The observed errors are due to the accuracy of the map giving η_c .

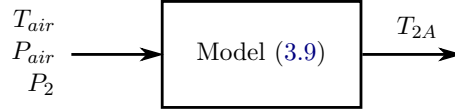


Figure 3.4: Block diagram to evaluate T_{2A} modeling (3.9)

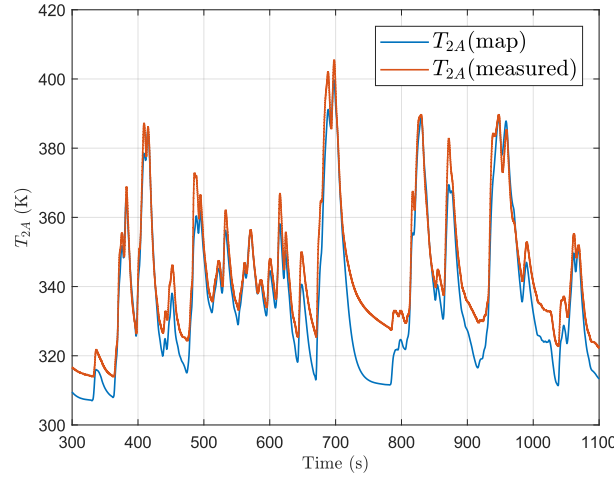


Figure 3.5: Evolution of the temperature after the compressor T_{2A}

3.2.4 EGR cooler modeling

The EGR cooler is used to lower the temperature of the exhaust gases that are recirculated by the EGR system by transferring the heat to the engine coolant. The main objective of the EGR loop is to reduce the NOx emission by changing the gas composition into the cylinders. As a result, it will decrease the maximal temperature reached after the combustion to have lower NOx emissions. However, the gases circulated by the EGR system can be considerably hot because they are taken into the exhaust manifold. In order to not damage the components, preserve fuel consumption and increase the air density, an EGR cooler is added.

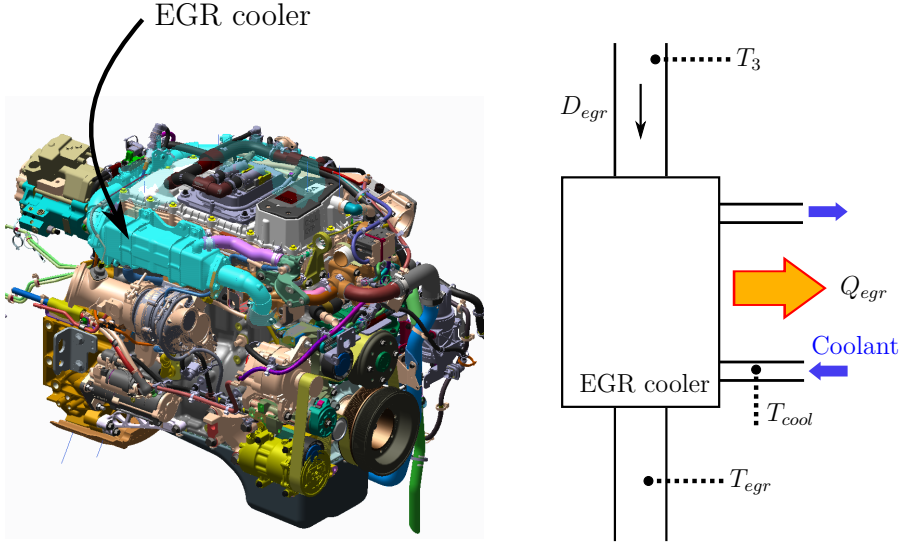


Figure 3.6: Heat exchanges inside the EGR cooler

According to Figure 3.6, a second heat balance on the EGR cooler gives the following EGR temperature dynamics:

$$\dot{T}_{egr} = \frac{D_{egr}c_{p3}}{m_{egr}c_{p,cool}} (T_3 - T_{egr}) + \frac{Q_{egr}}{m_{egr}c_{p,cool}} \quad (3.10)$$

where, m_{egr} stands for the EGR mass gas, Q_{egr} is the heat flow from the EGR cooler to the engine coolant. As in (3.7), the heat flow can be expressed as:

$$Q_{egr} = h_{egr}A_{egr} \left(T_{cool} - \frac{T_3 + T_{egr}}{2} \right) \quad (3.11)$$

where h_{egr} is the heat transfer coefficient.

3.2.5 Summary of the considered model and measurements

In the equations defining the heat flows (3.7) and (3.11), all the variables can be measured except the heat coefficients h_{cac} and h_{egr} . Besides, the surfaces A_{cac} and A_{egr} are not known accurately. To combine these both information in a unique variable, let us define:

$$\begin{aligned} k_{cac} &\triangleq h_{cac}A_{cac} \\ k_{egr} &\triangleq h_{egr}A_{egr} \end{aligned} \quad (3.12)$$

By combining (3.6), (3.7) and (3.12), one can have the following nonlinear system:

$$\dot{T}_{2R} = \frac{D_{air}}{m_{2R}} (T_{2A} - T_{2R}) + \frac{k_{cac}}{m_{2R}c_p} \left(T_{air} - \frac{T_{2A} + T_{2R}}{2} \right) \quad (3.13)$$

where T_{2A} can be given by (3.9).

Then, using (3.5), (3.10), and (3.12), the system hereunder describes the dynamics of T_2 and T_{egr} :

$$\begin{cases} \dot{T}_{egr} = \frac{D_{egr}c_{p3}}{m_{egr}c_{p,cool}}(T_3 - T_{egr}) + \frac{k_{egr}}{m_{egr}c_{p,cool}}\left(T_{cool} - \frac{T_3 + T_{egr}}{2}\right) \\ \dot{T}_2 = \frac{1}{m_2} [((1 - \gamma)D_{asp} - D_{egr} - D_{air})T_2 + \gamma D_{egr}T_{egr} + \gamma D_{air}T_{2R}] \end{cases} \quad (3.14)$$

Based on real engines sensor configuration, we assume that only T_{2R} , T_2 , T_{air} and T_{cool} are perfectly known. The other variables, i.e D_{air} , D_{egr} , D_{asp} , T_{2A} and T_3 are known but subject to uncertainties.

3.3 Observers design

In [Astorga-Zaragoza et al. 2008], the authors showed that the estimation of the heat transfer coefficient can provide a good indicator of a heat exchanger's degradation. Indeed, such a degradation will obviously affect the quality of the heat transfers. This section is devoted to the estimation of k_{cac} and k_{egr} defined in (3.12). An observer-based solution will be used to estimate them based on the two models (3.13) and (3.14).

The methods are explained in this section and the results are shown in Section 3.4.

3.3.1 Observer design for k_{cac}

To estimate the coefficient k_{cac} , one can use for example an adaptive observer like the one defined in Section 1.2.2.2. To fit with the system form described in (1.62), let denote $x = T_{2R}$ and $\theta = k_{cac}$. The following system to observe is obtained:

$$\begin{aligned} \dot{x} &= A(u, y)x + \varphi(u, y) + \Phi(u, y)\theta \\ y &= Cx \end{aligned} \quad (3.15)$$

with, $A(u, y) = -\frac{D_{air}}{m_{2R}}$, $\varphi(u, y) = \frac{D_{air}}{m_{2R}}T_{2A}$, $\Phi(u, y) = \frac{T_{air} - \frac{T_{2A} + T_{2R}}{2}}{m_{2R}c_p}$ and $C = 1$.

Proposition 1.8 can be directly applied on the system (3.15) to get the following

observer:

$$\begin{aligned}
\dot{\hat{x}} &= A(u, y)\hat{x} + \varphi(u, y) + \Phi(u, y)\hat{\theta} \\
&\quad + \{\Lambda S_\theta^{-1} \Lambda^T C^T + S_x^{-1} C^T\} \Sigma(y - C\hat{x}) \\
\dot{\hat{\theta}} &= S_\theta^{-1} \Lambda^T C^T \Sigma(y - C\hat{x}) \\
\dot{\Lambda} &= \{A(u, y) - S_x^{-1} C^T \Sigma C\} \Lambda + \Phi(u, y) \\
\dot{S}_x &= -\rho_x S_x - A(y, u)^T S_x - S_x A(u, y) + C^T \Sigma C \\
\dot{S}_\theta &= -\rho_\theta S_\theta + \Lambda^T C^T \Sigma C \Lambda
\end{aligned} \tag{3.16}$$

To tune the performance of (3.16), the following parameters have been taken:

$$\rho_x = 10, \quad \rho_\theta = 10, \quad \Sigma = 1 \tag{3.17}$$

3.3.2 LPV observer design for k_{egr}

To design an observer for (3.14), the LPV framework has been chosen. First, the LPV modeling is addressed. Then, a synthesis of the observer is proposed.

3.3.2.1 LPV modeling

Adding the dynamics $\dot{k}_{egr} = 0$ to the nonlinear system (3.14), it is possible to turn the extended system into the following quasi-LPV model:

$$\begin{aligned}
\dot{x} &= A(\rho)x + Bu \\
y &= T_2 = Cx
\end{aligned} \tag{3.18}$$

with $x = [T_{egr} \ T_2 \ k_{egr}]^T$, $u = [\frac{D_{egr}c_{p3}}{m_{egr}c_{p,cool}}T_3 \ \frac{D_{air}}{m_2}\gamma T_{2R}]^T$, $\rho = [\rho_1 \ \rho_2 \ \rho_3 \ \rho_4]^T$ and the following state space matrices and parameters,

$$\begin{aligned}
A(\rho) &= \begin{bmatrix} -\frac{D_{egr}c_{p3}}{m_{egr}c_{p,cool}} & 0 & \left(T_{cool} - \frac{T_3 + T_{egr}}{2}\right) \\ \frac{D_{egr}}{m_2}\gamma & \frac{(1-\gamma)D_{asp} - D_{egr} - D_{air}}{m_2} & m_{egr}c_{p,cool} \\ 0 & 0 & 0 \end{bmatrix} \\
&\triangleq \begin{bmatrix} \rho_1 & 0 & \rho_2 \\ \rho_3 & \rho_4 & 0 \\ 0 & 0 & 0 \end{bmatrix} \\
B &= \begin{bmatrix} 1 & 0 \\ 0 & 1 \\ 0 & 0 \end{bmatrix} \\
C &= [0 \ 1 \ 0]
\end{aligned} \tag{3.19}$$

Besides, it is assumed that the varying parameters ρ_i are bounded. Therefore, it can be established that:

$$\rho \in \mathcal{P}_\rho \triangleq \left\{ \rho = [\rho_1 \ \dots \ \rho_4]^T \in \mathbb{R}^4 \text{ and } \rho_i \in [\underline{\rho}_i, \overline{\rho}_i], \text{ for all } i = 1 \dots 4 \right\} \quad (3.20)$$

3.3.2.2 LPV observer design

Since (3.18) is affine in the parameter vector and it belongs to \mathcal{P}_ρ , it can be transformed into a polytopic form:

$$\begin{aligned} \dot{x} &= \sum_{i=1}^{16} \mu_i(\hat{\rho}) (A_i x) + Bu \\ y &= Cx \end{aligned} \quad (3.21)$$

with A_i and μ_i computed with Algorithm 1 and Algorithm 2 respectively.

Since the LPV system has 4 parameters, an interpolation of 16 vertices can lead to a calculation load that is too high such as in an embedded software for a truck. Therefore, to estimate the state vector x containing k_{egr} , we propose an LPV observer where the observer gain is constant:

$$\begin{aligned} \dot{\hat{x}} &= A(\hat{\rho})\hat{x} + L(y - \hat{y}) + Bu \\ \hat{y} &= C\hat{x} \end{aligned} \quad (3.22)$$

The gain L , will be tuned through a pole placement. To obtain a constant gain in the desired pole placement area depicted in Figure 3.7, the LMIs of Proposition 1.2 need to be slightly modified. To meet these specifications, we can combine (1.19) and (1.21) and consider a constant Lyapunov matrix Y . This leads to solve the following LMIs for all $i = 1, \dots, 16$:

$$\begin{aligned} PA_i - YC + A_i^T P - C^T Y^T + 2x_\alpha P &< 0 \\ PA_i - YC + A_i^T P - C^T Y^T + 2x_\beta P &> 0 \\ j(PA_i - YC + A_i^T P - C^T Y^T) + 2y_\alpha P &> 0 \\ j(PA_i - YC + A_i^T P - C^T Y^T) + 2y_\beta P &< 0 \end{aligned} \quad (3.23)$$

L is then deduced as $L = P^{-1}Y$.

Solving (3.23) for:

$$x_\alpha = 1, \quad x_\beta = 50, \quad y_\alpha = 40, \quad y_\beta = -40 \quad (3.24)$$

gives,

$$L = \begin{bmatrix} 262.87 & 17.38 & -29.63 \end{bmatrix}^T \quad (3.25)$$

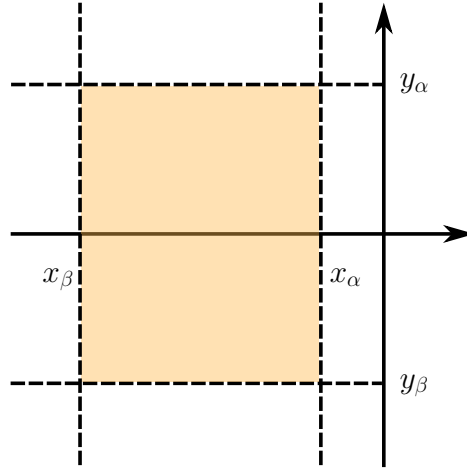


Figure 3.7: Pole placement area

Remark 3.1

It is physically obvious that we cannot have any information on the EGR cooler if there is no mass flow rate in the EGR loop, i.e if $D_{egr} = 0$. In this case, the system to observe (3.18) becomes unobservable. To overcome this problem, when D_{egr} is close to zero, we choose to disable the observer (3.22) and set $k_{egr} = 0$.

3.4 Estimation results

The validation of the two developed observers will be performed using data collected from a stationary and a transient cycles (WHSC/WHTC see Appendix B). These two cycles have been done on a test bench so all the inputs described in Section 3.2.5 are subject to real uncertainties.

As an initial step, based on an experimental sensor configuration, where more variables are measured, we will identify the coefficients k_{cac} and k_{egr} . These identified coefficients will be used as references to evaluate the observers in which less sensors are available. Then, we will test the adaptive observer for the CAC presented in 3.3.1. Finally, the LPV observer for the EGR cooler, described in Section 3.3.2, will be evaluated. The global performances of the tested observers are evaluated with the NRMS index defined Appendix A, and summarized in Table 3.2.

3.4.1 Heat transfer coefficients expression

This section is devoted to the identification and modeling of the unknown variables k_{cac} and k_{egr} . To do so, real data from test bench submitted to a transient cycle (see

Table 3.2: *NRMS* obtained for the different cycles

Cycle	Estimate	
	k_{cac} with (3.16)	k_{egr} with (3.22)
WHSC	2.0%	5.6%
WHTC	2.5%	11.6%

Appendix B) will be used.

3.4.1.1 k_{cac} estimation

With a test bench, it is possible to measure all the variables in (3.13), i.e. D_{air} , T_{2A} , T_{air} and T_{2R} and these variables will be assumed to be perfectly known. Thus, only k_{cac} is unknown. To estimate it, the adaptive observer defined in (3.16) will be used.

In addition, we know that the heat transfer coefficient depends on the air mass flow rate [Bergman and Incropera 2011]. Therefore, to propose a model that can be used whatever the operating point, a relation to deduce k_{cac} is needed. As in Chapter 2, the following phenomenological law is used:

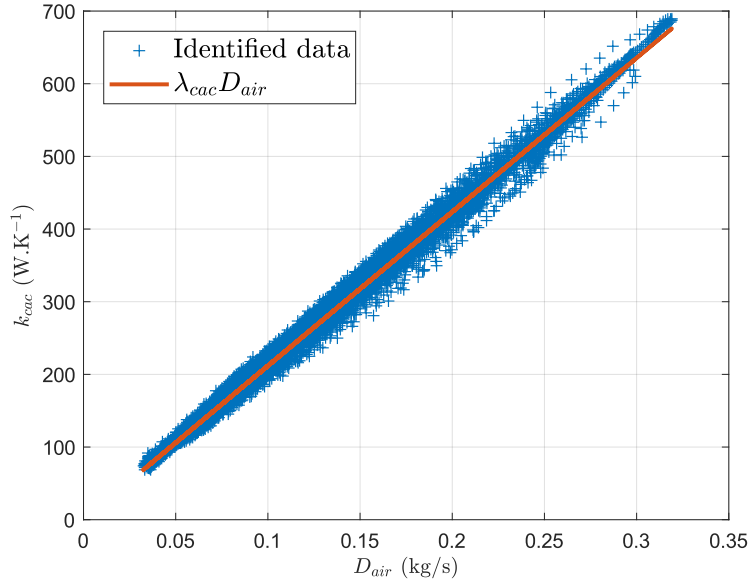
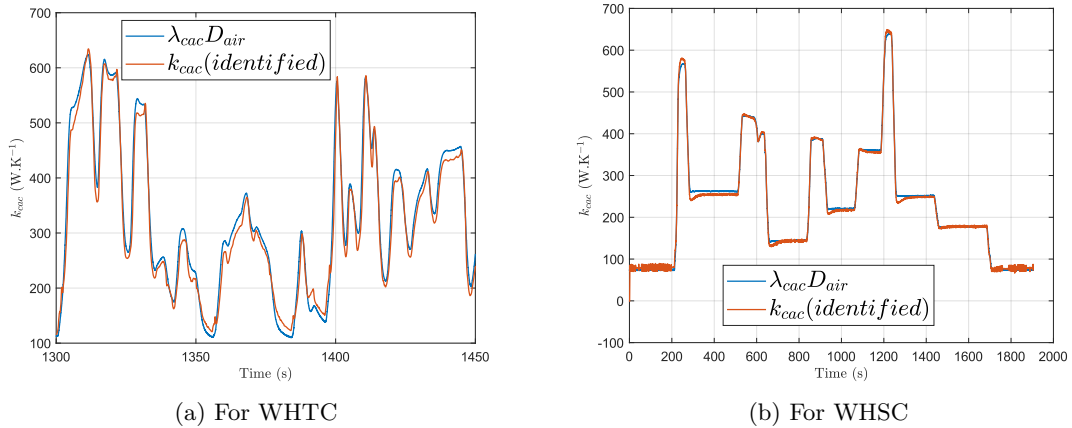
$$k_{cac} = \lambda_{cac} D_{air} \quad (3.26)$$

A linear regression of the identified data obtained with the adaptive observer, gives the constant $\lambda_{cac} = 2118 \text{ J.kg}^{-1}.\text{K}^{-1}$. The results are depicted in Figure 3.8. The value of the coefficient of determination is $R^2 = 0.99$ which is very satisfying.

Remark 3.2

On the test bench, the CAC is replaced by a water heat exchanger. Nevertheless, the phenomenological law (3.26) has also been tested with data from a high-fidelity model that takes into account the full air circulation of the truck.

The identification process has also been done for a stationary cycle to test the relation (3.26) with other operating points. Figure 3.9(a) shows the time-domain results for the WHTC and Figure 3.9(b) depicts the ones obtained for the WHSC. For both cycles, the simple model (3.26) matches very well the identified data. This is confirmed by the values of the FIT index (see Appendix A) which are 94% for the WHTC and 97% for the WHSC.

Figure 3.8: Interpolation of the identified k_{cac} dataFigure 3.9: Time-domain results of the identified data k_{cac}

3.4.1.2 k_{egr} estimation

Combining (3.10), (3.11) and (3.12), one gets the following model for T_{egr} dynamics:

$$\dot{T}_{egr} = \frac{D_{egr}c_{p3}}{m_{egr}c_{p,cool}} (T_3 - T_{egr}) + \frac{k_{egr}}{m_{egr}c_{p,cool}} \left(T_{cool} - \frac{T_3 + T_{egr}}{2} \right) \quad (3.27)$$

In (3.27), the variables T_3 , T_{egr} and T_{cool} are directly measured by the test bench. For D_{egr} , we will use an estimation validated for static conditions. This last point will be detailed in Chapter 4. Using the same procedure in Section 3.4.1.1, k_{egr} is identified

with an adaptive observer. Then the following phenomenological is used to model k_{egr} :

$$k_{egr} = \lambda_{egr} D_{egr} \quad (3.28)$$

The results of the linear regression to determined λ_{egr} are depicted in Figure 3.10. It gives $\lambda = 2353 \text{ J.kg}^{-1}.\text{K}^{-1}$ and a coefficient of determination $R^2 = 0.98$.

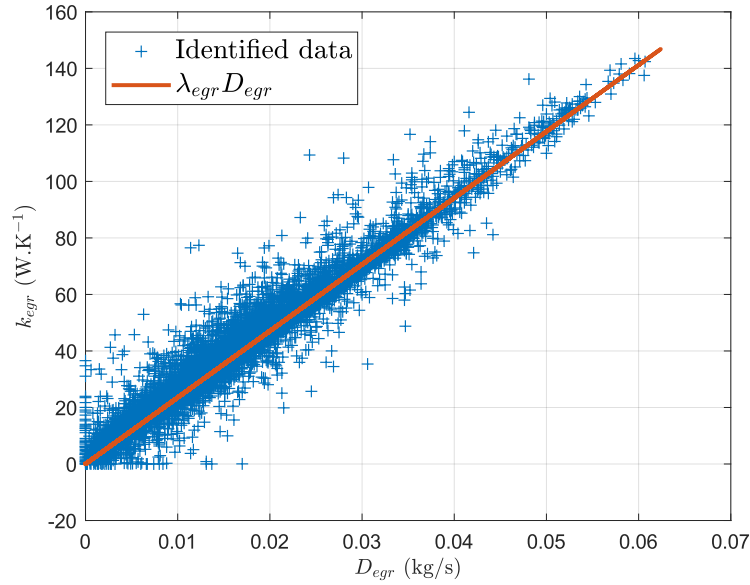
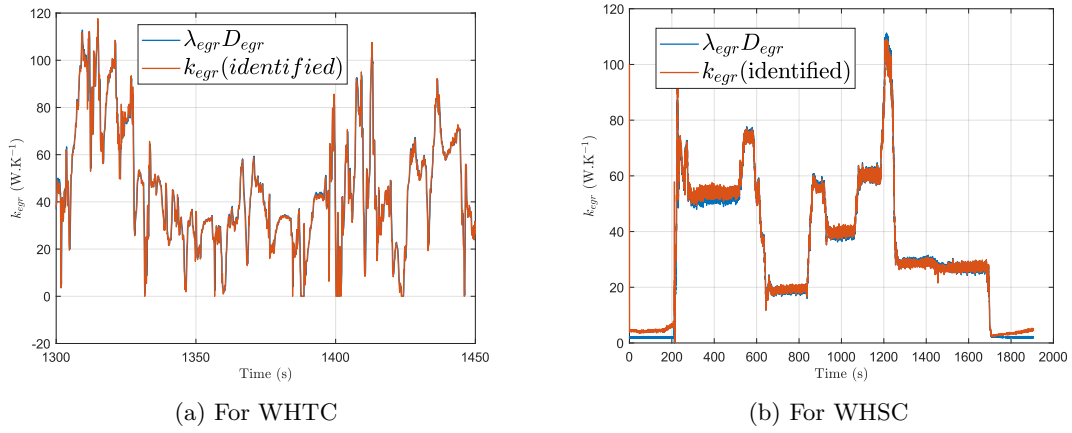
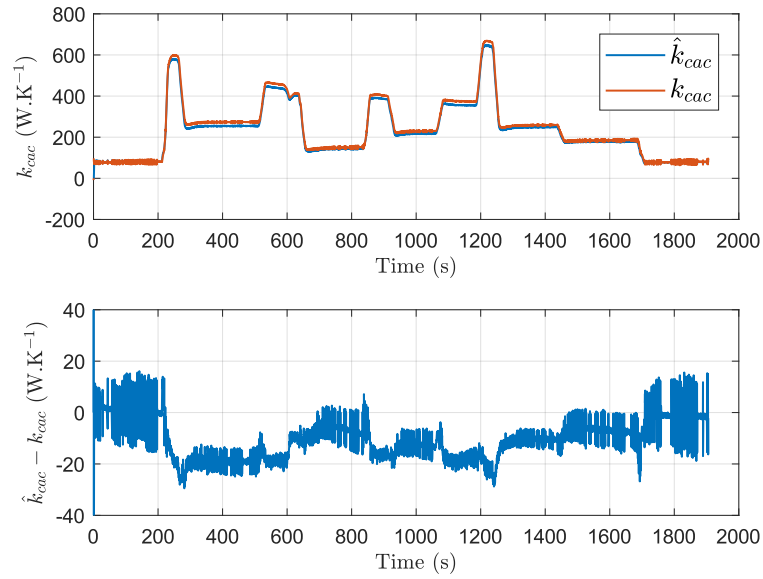


Figure 3.10: Interpolation of the identified k_{egr} data

Figure 3.11(a) and Figure 3.11(b) confirm the good results obtained by the regression. Even with other operating points provided by the WHSC, the model (3.28) manages to follows the identified data. The FIT indexes for both cycles are: 82% and 92% for respectively WHTC and WHSC.

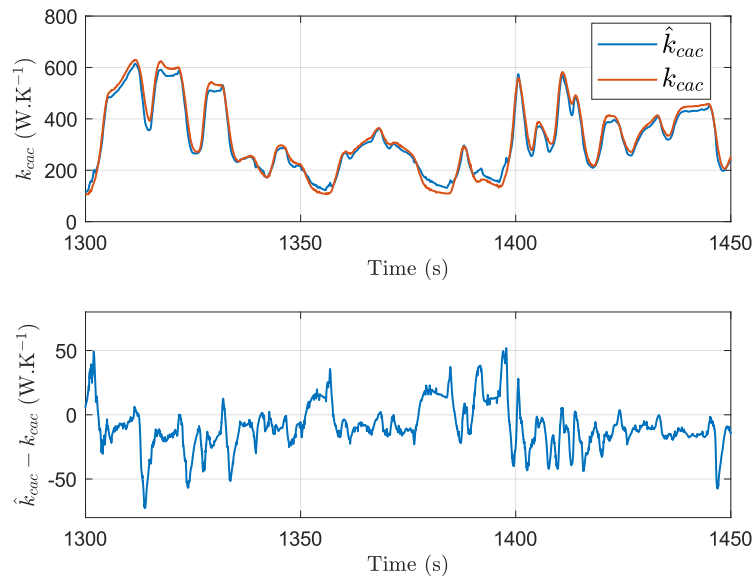
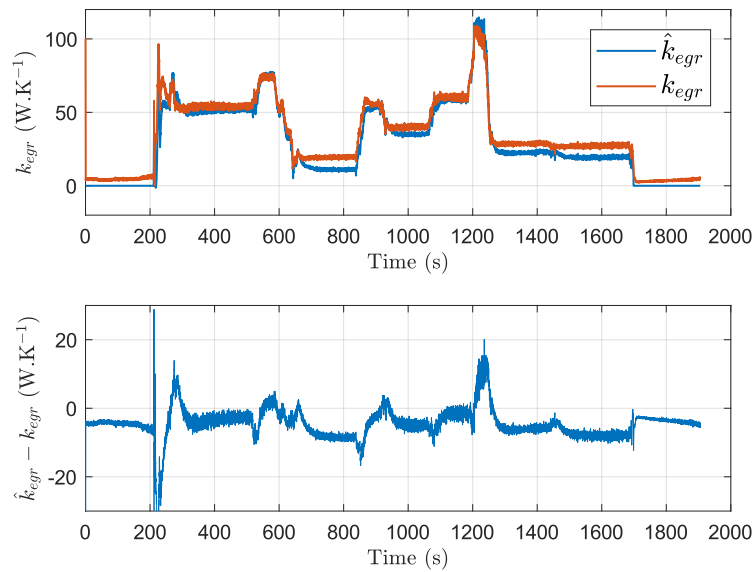
3.4.2 k_{cac} observer evaluation

The estimation of k_{cac} provided by (3.16), obtained for the two scenarios (WHSC/WHTC), are respectively depicted in Figure 3.12 and Figure 3.13. For both cycles, the observer (in blue) manages to follow the reference (in red) previously identified in Section 3.4.1. Most of the time, the absolute error is between $\pm 20 \text{ W.K}^{-1}$ in steady state conditions and can reach more than $\pm 50 \text{ W.K}^{-1}$ in transient conditions. This information is important to determine a threshold for the diagnosis. The NRMS in Table 3.2 for the both cycle is very low, which confirms the good performance of the observer.

Figure 3.11: Time-domain results of the identified data k_{egr} Figure 3.12: k_{cac} estimation for a WHSC

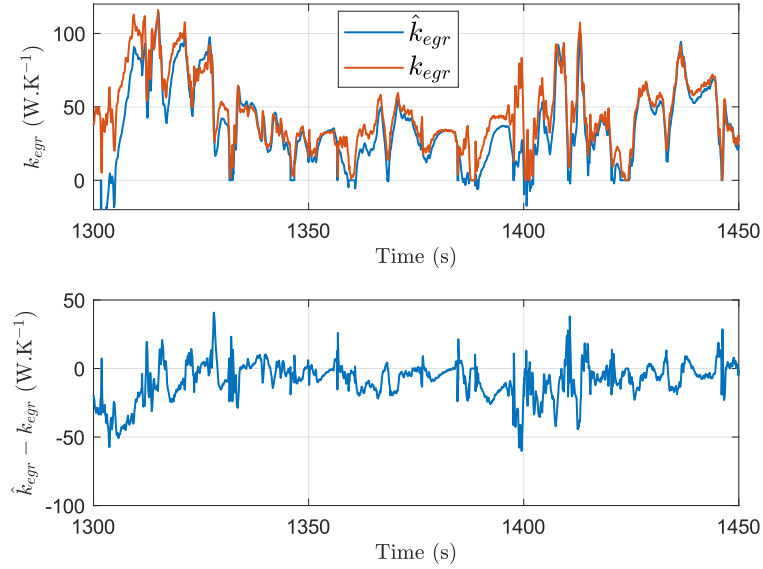
3.4.3 k_{egr} observer evaluation

The results of the observer (3.22) are presented in Figure 3.14 and Figure 3.15. We can see that, even with less sensor available, i.e. T_{egr} measurement, the developed observer provides a good estimation of k_{egr} . The performances are better in stationary conditions than in transient ones. For the WHSC, the absolute error is between ± 20 W.K^{-1} in steady state conditions. With regard to the WHTC, it is between ± 50 W.K^{-1} .

Figure 3.13: k_{cac} estimation for a WHTCFigure 3.14: k_{egr} estimation for a WHSC

3.5 Sensitivity with respect to input uncertainties

We have seen in [Section 3.2.5](#) that the inputs needed for the observers (3.16) and (3.22) are subject to uncertainties. This section aims to determine the influence of each uncertainty on the estimation provided by the two observers. From the error modeling

Figure 3.15: k_{egr} estimation for a WHTC

and distribution summarized in Table 3.3, Monte Carlo methods will be used to know the amplitude error resulting from the uncertainties. This information can be used to calibrate a threshold to diagnose the CAC and the EGR cooler. Note that the variable D_{egr} is not presented in Table 3.3 because it is computed with the mass flow rates D_{air} and D_{asp} . Therefore the errors of these variables will influence D_{egr} as well directly.

Table 3.3: Values of the considered errors on the inputs

Variable	Error modeling	Error distribution	For \hat{k}_{cac} (3.16)	For \hat{k}_{egr} (3.22)
T_{2A}	$T_{2A} + \Delta(T_{2A})$	$\mathcal{N}(0, \frac{20}{3})$	✓	-
D_{air}	$D_{air} \times \Delta(D_{air})$	$\mathcal{N}(1, \frac{0.09}{3})$	✓	✓
D_{asp}	$D_{asp} \times \Delta(D_{asp})$	$\mathcal{N}(1, \frac{0.05}{3})$	-	✓
T_3	$T_3 + \Delta(T_3)$	$\mathcal{N}(0, \frac{20}{3})$	-	✓

500 simulations have been run for each uncertainty and 500 more for all of them together. Therefore, according to in Table 3.3, 7 cases will be considered to test the influence of the uncertainties:

1. $\Delta(T_{2A})$ on adaptive observer (3.16)
2. $\Delta(D_{air})$ on adaptive observer (3.16)
3. $\Delta(T_{2A})$ and $\Delta(D_{air})$ on adaptive observer (3.16)
4. $\Delta(T_3)$ on LPV observer (3.22)

5. $\Delta(D_{air})$ on LPV observer (3.22)
6. $\Delta(D_{asp})$ on LPV observer (3.22)
7. $\Delta(T_3)$, $\Delta(D_{air})$ and $\Delta(D_{asp})$ on LPV observer (3.22)

After one simulation, the mean of the absolute error between free uncertainties data and data corrupted by uncertainties is computed and stored. Then, after the end of the 500 simulations, a box plot is created. Algorithm 3 summarizes the described process for one case. The box plots depicted in Figure 3.16 and Figure 3.17 give the 7 cases (3 for the adaptive observer and 4 for the LPV one). On each box, the central mark indicates the median, and the bottom and top edges of the box indicate the 25th and 75th percentiles, respectively. The whiskers extend to the most extreme data points, and the outliers are plotted individually using the '+' symbol¹.

Algorithm 3: Monte Carlo methods used

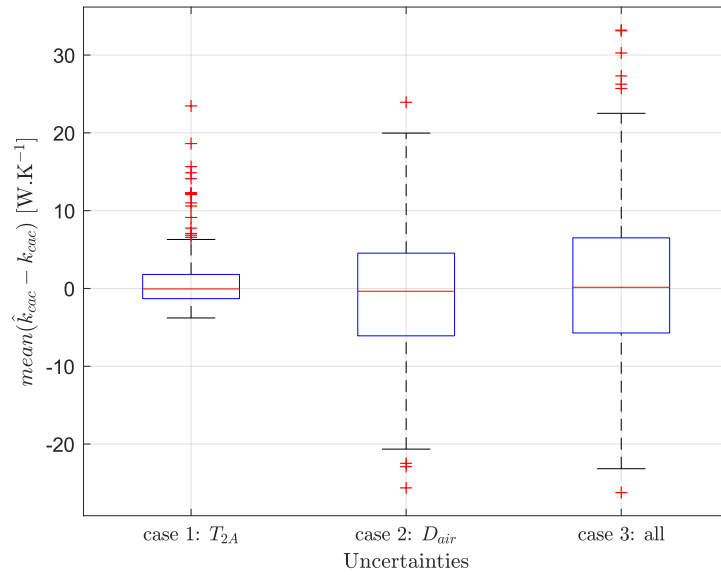
input : Chosen case
output: Plot of the error distribution

for 1 to 500 **do**
 | Compute the stochastic variable(s) Δ according to Table 3.3;
 | Simulate (3.16) or (3.22);
 | Store the value of $\text{mean}(\hat{k}_{cac} - k_{cac})$ or $\text{mean}(\hat{k}_{egr} - k_{egr})$;
end
 Depict the stored values in box plot

Concerning the analysis of the robustness of the observer (3.16) in Figure 3.16, we can see that the most important variable is the mass flow rate D_{air} then, to a lesser degree, T_{2A} . When all the uncertainties are taken into account, 50% of the errors are between -5.7 and 6.5 W.K^{-1} . These errors are very low in comparison with the real values of k_{cac} around 400 W.K^{-1} (cf. Figure 3.12).

Similar remarks may be drawn from the analysis of the robustness of the observer (3.21) in Figure 3.17 about the k_{egr} estimation: the mass flow rates have a big influence on the error estimation and the temperature T_3 uncertainty has almost none. Besides, 50% of the errors are between -7.6 and 9.1 W.K^{-1} . However, from the point of view of relative error, these errors are high because the reference values are around 50 W.K^{-1} (cf. Figure 3.14).

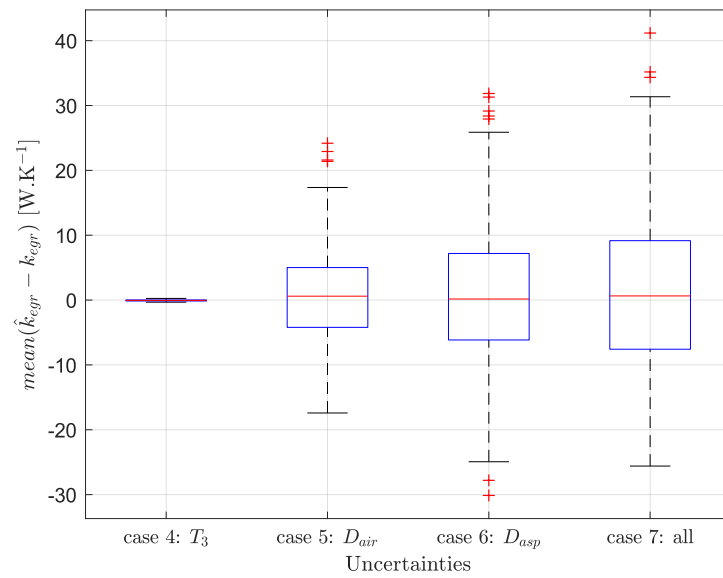
¹Excerpt from Matlab documentation

Figure 3.16: Box plot for k_{cac} estimation

3.6 Conclusion

In this chapter we have provided an observer-based diagnosis solution to monitor the Charge Air Cooler and the EGR cooler. With the considered sensor configuration, without EGR temperature sensor, we have seen that two observers can effectively estimate the image of the heat transfer coefficients. To have an analytical redundancy, the models (3.26) and (3.28) can give us the nominal values of these both coefficients. Then a threshold can be determined to fulfill the legislative standards while taking into account the input uncertainties described in Section 3.5. We have seen in this last section that k_{egr} estimation is more sensitive, in relative errors, to uncertainties than the estimation of k_{cac} . This must be taken into account for the threshold design.

As mentioned in Section 3.4.1.1, the heat exchanger used in the considered test bench is not the real the real component mounted on the commercial trucks. Therefore additional tests have to be done on a running truck.

Figure 3.17: Box plot for k_{egr} estimation

EGR mass flow rate Estimation

Contents

4.1	Introduction	69
4.2	Intake manifold modeling	71
4.3	Observers design	72
4.3.1	Pole placement design	73
4.3.2	FAFE design	75
4.3.3	\mathcal{H}_∞ filter design	77
4.3.4	Kalman filter design	78
4.3.5	Adaptive observer design	79
4.3.6	Sliding mode observer design	80
4.4	Experimental setup	83
4.4.1	ECU implementation	83
4.4.2	Test cell description	84
4.4.3	EGR mass flow rate measurement	85
4.5	Experimental results	85
4.5.1	Medium duty 5L engine	86
4.5.2	Medium duty 8L engine	87
4.5.3	Analysis of the estimation errors	89
4.5.4	Computational performance	91
4.6	Conclusion	92

4.1 Introduction

A common way to reduce NOx emission of diesel engines is to reduce the peak temperature combustion by increasing the CO₂ concentration in the combustion chamber. The automotive manufactures achieve this objective by adding an Exhaust Gas Recirculation (EGR) loop in the engine architecture (as in [Figure 4.1](#)). Therefore, to have a suitable control of the pollutant emissions, it is needed to know the gas composition at the inlet of the engine [[Guzzella and Onder 2010](#)]. Therefore, the quantity of EGR gas, and thus EGR mass flow rate, has to be known as accurately as possible. That's why

most of the manufacturers chooses to directly measure the EGR mass flow rate with a specific sensor.

Recently, Volvo's medium duty engines architecture has evolved and a Venturi effect sensor that measured the EGR mass flow rate has been removed. Therefore, this variable has to be estimated on the new architecture.

This chapter aims to apply several observation approaches presented in Chapter 1 for the estimation of the EGR mass flow rate. In the observer design, this variable will be considered as an additive unknown input. The main idea of the observer is to use the information given by the pressure sensor in the intake manifold as the reference measurement, to estimate this mass flow rate. The final validation consists in implementation on a real truck's embedded computer and comparison of the performance of the different methods.

This chapter is organized as follows. In Section 4.2, the intake manifold pressure is modeled. Based on this model, six different observer structures are proposed to estimate the EGR mass flow rate in Section 4.3. Then, in Section 4.4, the experimental protocol to test the observers on a real engine is described. Next, in Section 4.5, the experimental results are analyzed. Finally, conclusions are stated in Section 4.6.

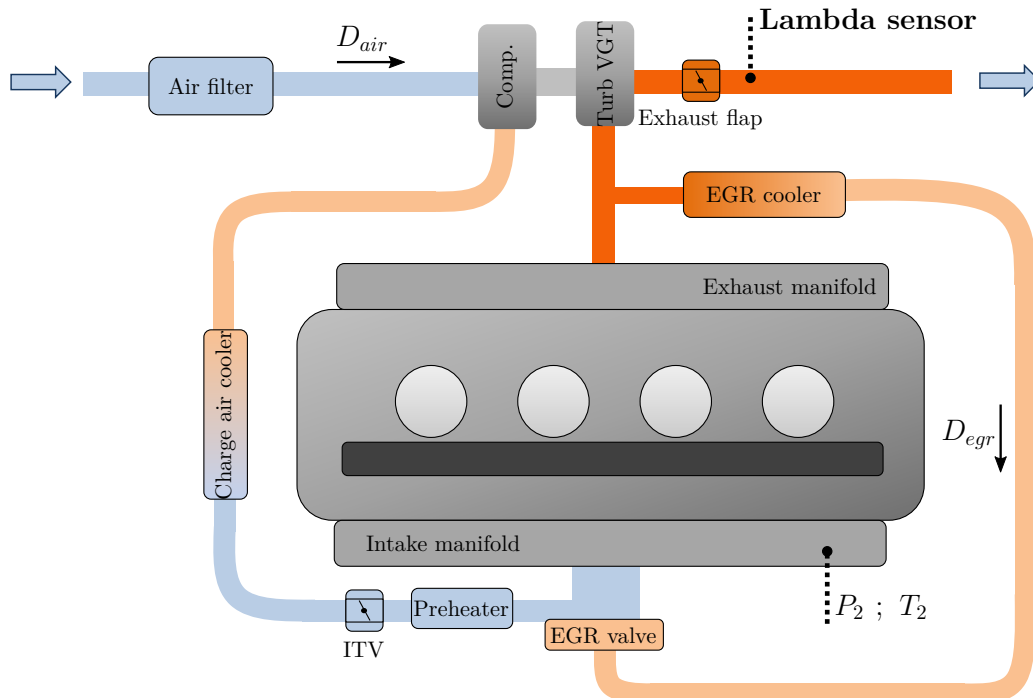


Figure 4.1: Schematic view of the air path in the considered engine

Table 4.1: Nomenclature

Notation	Description	Unit
N_{eng}	Engine speed	r.p.m
Γ_{eng}	Engine torque	N.m
T	Temperature of a subsystem	K
P	Pressure of a subsystem	Pa
R	Ideal gas constant for the air	$\text{J.kg}^{-1}.\text{K}^{-1}$
D	Mass flow rate	kg.s^{-1}
Observer type		
PolP	LPV polytopic observer design through a pole placement area	
FAFE	LPV polytopic FAFE observer	
Hinf	LPV polytopic \mathcal{H}_∞ filter	
KF	Kalman filter for LTV systems	
AO	Adaptive observer	
SM	Sliding mode observer	
Subscript		
2	Inside the intake manifold	
<i>air</i>	Related to the inlet air	
<i>egr</i>	Related to the EGR loop	

4.2 Intake manifold modeling

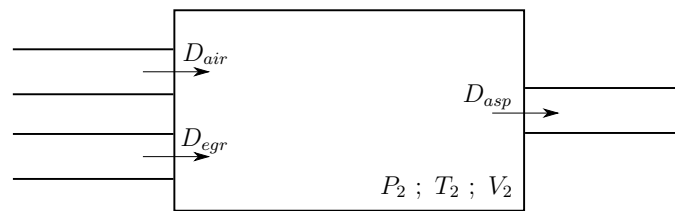


Figure 4.2: Intake manifold volume

Located just before the engine block as depicted in [Figure 4.1](#), this component enables to carry the gas mixture, consisting of inlet air and EGR gas, to each cylinder.

The intake manifold can be represented as an open thermodynamical system, where the quantity of gas can increase or decrease. It is called a "filling and emptying" system. [Figure 4.2](#) synthesized the gas exchanges. Inside this volume, the ideal gas law can be applied and the pressure P_2 can be expressed as:

$$P_2 = \frac{m_2 R T_2}{V_2} \quad (4.1)$$

where m_2 is the total air mass inside the volume V_2 .

Taking the time-derivative of this equation, one obtains:

$$\dot{P}_2 = \frac{\dot{m}_2 RT_2}{V_2} + \frac{m_2 R \dot{T}_2}{V_2} \quad (4.2)$$

where \dot{m}_2 represents the mass rate of gas flowing through the intake manifold and can be expressed, from a balance equation, as: $\dot{m}_2 = D_{air} + D_{egr} - D_{asp}$. Besides, assuming that the temperature varies slowly in comparison to P_2 , we assume $\dot{T}_2 \simeq 0$ and (4.2) becomes:

$$\dot{P}_2 = \frac{RT_2}{V_2} (D_{air} + D_{egr} - D_{asp}) \quad (4.3)$$

In the following, we assume that the mass flow rate D_{air} in (4.3) is a known input variable deduced by a lambda sensor located just after the turbine as we can see in Figure 4.1 (this particular point is more detailed later in chapter 6). According to Appendix C, the air mass flow aspirated by the cylinders can be expressed as:

$$D_{asp} = \frac{\eta_v V_{cyl} N_{eng}}{RT_2 120} P_2 \quad (4.4)$$

where η_v is the volumetric efficiency.

4.3 Observers design

In this section, six observer-based approaches are developed to estimate the EGR mass flow rate D_{egr} . They follow the methods described in Chapter 1 plus another one exposed in [Castillo et al. 2013a]. In brief, we will design three LPV polytopic observers based on:

- (1) Pole placement areas (PolP) cf. Section 1.2.1.1
- (2) Fast Adaptive Fault Estimation (FAFE) algorithm cf. Section 1.2.1.3
- (3) \mathcal{H}_∞ filtering (Hinf) cf. Section 1.2.1.4

and three nonlinear observers based on:

- (4) Kalman filtering for LTV systems (KF) cf. Section 1.2.2.1
- (5) Adaptive Observer (AO) cf. Section 1.2.2.2
- (6) Sliding mode (SM) as in [Castillo et al. 2013a]

Now, the combination of (4.3) and (4.4) gives the following system:

$$\dot{P}_2 = -\frac{\eta_v V_{cyl} N_{eng}}{120V_2} P_2 + \frac{RT_2}{V_2} D_{air} + \frac{RT_2}{V_2} D_{egr} \quad (4.5)$$

which can be rewritten as:

$$\dot{P}_2 = \rho_1 P_2 + u + \rho_2 D_{egr} \quad (4.6)$$

where,

$$\rho_1 = -\frac{\eta_v V_{cyl} N_{eng}}{120V_2}, \quad \rho_2 = \frac{RT_2}{V_2} \quad \text{and} \quad u = \frac{RT_2}{V_2} D_{air} \quad (4.7)$$

Besides, it is practically obvious that the variables ρ_1 and ρ_2 are bounded. Therefore, one can claim that:

$$\rho \in \mathcal{P}_\rho := \left\{ \rho = [\rho_1 \ \rho_2]^T \in \mathbb{R}^2 \text{ s.t } \rho_1 \in [\underline{\rho}_1, \overline{\rho}_1] \text{ and } \rho_2 \in [\underline{\rho}_2, \overline{\rho}_2] \right\} \quad (4.8)$$

where the boundaries are experimentally determined.

All the estimators hereafter shall solve the following problem:

Problem 4.1

Based on the intake pressure manifold pressure P_2 measurement, design an algorithm that provides an estimation of the EGR mass flow rate D_{egr} .

Remark 4.1

The state vector x is not the same for all observers methods thus, for sake of clarity, it will be redefined in the next sections.

4.3.1 Pole placement design

To apply the technique described in Section 1.2.1.1, the dynamic equation $\dot{D}_{egr} = 0$ is added to (4.5). Let denote $[x_1 \ x_2]^T = [P_2 \ D_{egr}]^T$, the following system is obtained:

$$\begin{aligned} \dot{x} &= A(\rho)x + Bu \\ y &= Cx \end{aligned} \quad (4.9)$$

with, $\rho \in \mathcal{P}_\rho$ and u are defined in (4.7),

$$A(\rho) = \begin{bmatrix} \rho_1 & \rho_2 \\ 0 & 0 \end{bmatrix}, \quad B = \begin{bmatrix} 1 \\ 0 \end{bmatrix} \quad \text{and} \quad C = \begin{bmatrix} 1 & 0 \end{bmatrix} \quad (4.10)$$

It appears that $A(\rho)$ is affine in ρ thus (4.9) can be turned into the following LPV polytopic system:

$$\begin{aligned} \dot{x} &= \sum_{i=1}^4 \mu_i(\rho) (A_i x) + Bu \\ y &= Cx \end{aligned} \quad (4.11)$$

with A_i and μ_i are given by [Algorithm 1](#) and [Algorithm 2](#) respectively (see [Section 1.2.1.5](#)):

$$\begin{aligned} A_1 &= \begin{bmatrix} \underline{\rho}_1 & \underline{\rho}_2 \\ 0 & 0 \end{bmatrix}; & A_2 &= \begin{bmatrix} \overline{\rho}_1 & \overline{\rho}_2 \\ 0 & 0 \end{bmatrix} \\ A_3 &= \begin{bmatrix} \underline{\rho}_1 & \overline{\rho}_2 \\ 0 & 0 \end{bmatrix}; & A_4 &= \begin{bmatrix} \overline{\rho}_1 & \underline{\rho}_2 \\ 0 & 0 \end{bmatrix} \end{aligned} \quad (4.12)$$

$$\begin{aligned} \mu_1(\rho) &= \left(\frac{\overline{\rho}_1 - \rho_1}{\overline{\rho}_1 - \underline{\rho}_1} \right) \times \left(\frac{\overline{\rho}_2 - \rho_2}{\overline{\rho}_2 - \underline{\rho}_2} \right) \\ \mu_2(\rho) &= \left(\frac{\overline{\rho}_1 - \rho_1}{\overline{\rho}_1 - \underline{\rho}_1} \right) \times \left(\frac{\rho_2 - \underline{\rho}_2}{\overline{\rho}_2 - \underline{\rho}_2} \right) \\ \mu_3(\rho) &= \left(\frac{\rho_1 - \underline{\rho}_1}{\overline{\rho}_1 - \underline{\rho}_1} \right) \times \left(\frac{\overline{\rho}_2 - \rho_2}{\overline{\rho}_2 - \underline{\rho}_2} \right) \\ \mu_4(\rho) &= \left(\frac{\rho_1 - \underline{\rho}_1}{\overline{\rho}_1 - \underline{\rho}_1} \right) \times \left(\frac{\rho_2 - \underline{\rho}_2}{\overline{\rho}_2 - \underline{\rho}_2} \right) \end{aligned} \quad (4.13)$$

To solve [Problem 4.1](#) the following LPV polytopic observer structure is proposed:

$$\begin{aligned} \dot{\hat{x}} &= \sum_{i=1}^4 \mu_i(\rho) (A_i \hat{x} + L_i (y - \hat{y})) + Bu \\ \hat{y} &= C \hat{x} \end{aligned} \quad (4.14)$$

The desired pole placement area is depicted in [Figure 4.3](#). It is defined as the intersections of a disk with a radius r , a cone with an angle θ , and an open left-half-plane starting from x_α . The application of [Proposition 1.2](#) can give us an LMI formulation of this problem.

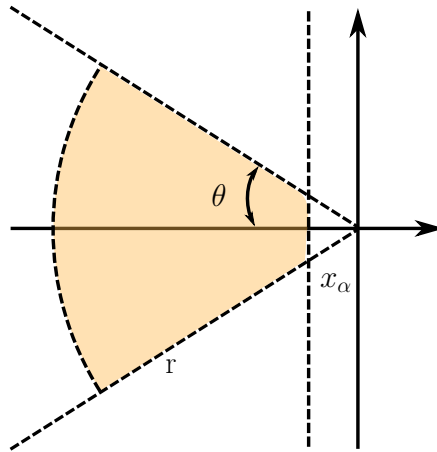


Figure 4.3: Pole placement area

If [Proposition 1.2](#) is applied for $r = 20$, $\theta = \frac{\pi}{6}$ and $x_\alpha = 1$, we can get the observer gains L_i and the eigenvalues of $A_i - L_i C$ given in [Table 4.2](#) are deduced.

Table 4.2: Eigenvalues of $A_i - L_i C$

$\text{eig}(A_1 - L_1 C)$	$\text{eig}(A_2 - L_2 C)$	$\text{eig}(A_3 - L_3 C)$	$\text{eig}(A_4 - L_4 C)$
-10.371	-10.371	-10.348	-10.348
-1.2268	-1.2268	-1.3043	-1.3043

4.3.2 FAFE design

The objective of this section is to design a FAFE observer following the procedure described in Section 1.2.1.3. Let us denote $x = P_2$ and $f = D_{egr}$, therefore (4.5) can be rewritten as:

$$\begin{aligned} \dot{x} &= A(\rho)x + Bu + F(\rho)f \\ y &= Cx \end{aligned} \quad (4.15)$$

with, $\rho \in \mathcal{P}_\rho$ and u are defined in (4.7),

$$A(\rho) = \rho_1, \quad B = 1, \quad F(\rho) = \rho_2 \quad \text{and} \quad C = 1 \quad (4.16)$$

As in the previous section, (4.15) can be turned into the following LPV polytopic system:

$$\begin{aligned} \dot{x} &= \sum_{i=1}^4 \mu_i(\rho) (A_i x + F_i f) + Bu \\ y &= Cx \end{aligned} \quad (4.17)$$

with A_i and F_i are given by Algorithm 1:

$$\begin{aligned} A_1 &= \underline{\rho}_1, \quad A_2 = \overline{\rho}_1, \quad A_3 = \underline{\rho}_1, \quad A_4 = \overline{\rho}_1 \\ F_1 &= \underline{\rho}_2, \quad F_2 = \underline{\rho}_2, \quad F_3 = \overline{\rho}_2, \quad F_4 = \overline{\rho}_2 \end{aligned} \quad (4.18)$$

the interpolation functions μ_i are the same than the ones in (4.13).

The FAFE LPV polytopic observer to design has the following structure:

$$\begin{cases} \dot{\hat{x}} = \sum_{i=1}^4 \mu_i(\rho) (A_i \hat{x} + L_i e_y + F_i \hat{f}) + Bu \\ \dot{\hat{f}} = \Gamma \sum_{i=1}^4 \mu_i(\rho) U_i (\dot{e}_y + \sigma e_y) \\ \hat{y} = C \hat{x} \\ e_y = y - \hat{y} \end{cases} \quad (4.19)$$

Let us mention that the needed assumptions to design (4.19) are fulfilled. Indeed, $\text{rank}(CF_i) = \text{rank}(F_i)$, and the invariant zeros of (A_i, F_i, C) are in the left half plane

for all $i = 1, \dots, 4$. Thus, [Proposition 1.4](#) can be applied for given scalars σ , μ in order to deduce the matrices gains L_i and U_i .

As pointed in [Section 1.2.1.3](#), the parameters σ , μ and Γ are generally arbitrarily chosen without fine tuning. To overcome this problem, we propose to use a Genetic Algorithm to minimize the Root Mean Square (RMS) deviation while tuning σ and Γ . This technique is inspired by [\[Vu et al. 2016; Vu 2017\]](#) and [\[Do 2011\]](#) where the authors used Genetic Algorithms to find optimal weighting functions for an \mathcal{H}_∞ control synthesis. We will not detail how a Genetic Algorithm works and thus for additional information, one can refer to the previous references and [\[Sivanandam and Deepa 2008\]](#) which explains the theory.

Let us first define the Root Mean Square (*RMS*) index as:

$$RMS(\hat{D}_{egr} - D_{egr}) = \sqrt{\frac{1}{N} \sum_{n=1}^N |\hat{D}_{egr}(n) - D_{egr}(n)|^2} \quad (4.20)$$

where D_{egr} contains N observations. The Genetic Algorithm has to solve the following optimization problem:

$$\min_{\sigma, \Gamma} RMS(\hat{D}_{egr} - D_{egr}) \quad (4.21)$$

Note that in (4.21), only σ and Γ are optimized because μ has been set to 1 due to its slight effect on the estimation performance. The implemented procedure is summarized in [Figure 4.4](#). The time domain simulation consists in the implemented FAFE observer (4.19) fed with all the needed data collected from an initial test.

To apply the Genetic Algorithm, an initial test has been done to collect all the needed data.

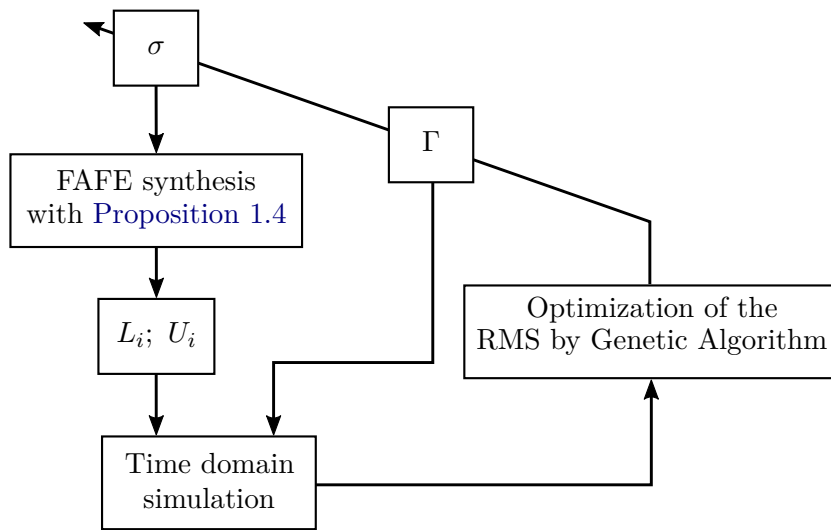


Figure 4.4: FAFE parameters optimization using a Genetic Algorithm

At the end of the optimization process, the following values are obtained:

$$\Gamma = 13.61 \quad \text{and} \quad \sigma = 0.59 \quad (4.22)$$

4.3.3 \mathcal{H}_∞ filter design

The objective of this section is to design an \mathcal{H}_∞ filter following the procedure described in Section 1.2.1.4. Let us denote $x = P_2$ and $f = D_{egr}$, therefore (4.5) can be rewritten as:

$$\begin{aligned} \dot{x} &= A(\rho)x + Bu + F(\rho)f \\ y &= Cx \end{aligned} \quad (4.23)$$

with, $\rho \in \mathcal{P}_\rho$ and u are defined in (4.7),

$$A(\rho) = \rho_1, \quad B = 1, \quad F(\rho) = \rho_2 \quad \text{and} \quad C = 1 \quad (4.24)$$

Let us define a polytopic LPV system $G(\rho)$, which has as inputs u and f and as output y :

$$G(\rho) : \begin{cases} \dot{x} = \sum_{i=1}^4 \mu_i(\rho) (A_i x + F_i f) + Bu \\ y = Cx \end{cases} \quad (4.25)$$

To apply Proposition 1.5 on the above system, the method described in Example 1.3 will be used. Consider the system represented in the block scheme Figure 4.5. It consists of by the polytopic LPV system $G(\rho)$ subject to a fault \tilde{f} filtered by the transfer function \mathcal{W}_f to tune the convergence rate. To solve Problem 4.1, we wish to design a polytopic LPV filter $K_f(\rho)$ defined hereunder:

$$K_f(\rho) : \begin{cases} \dot{x}_f = \sum_{i=1}^4 \mu_i(\rho) \left(A_{fi} x_f + B_{fi} \begin{bmatrix} u \\ y \end{bmatrix} \right) \\ \hat{f} = \sum_{i=1}^4 \mu_i(\rho) \left(C_{fi} x_f + D_{fi} \begin{bmatrix} u \\ y \end{bmatrix} \right) \end{cases} \quad (4.26)$$

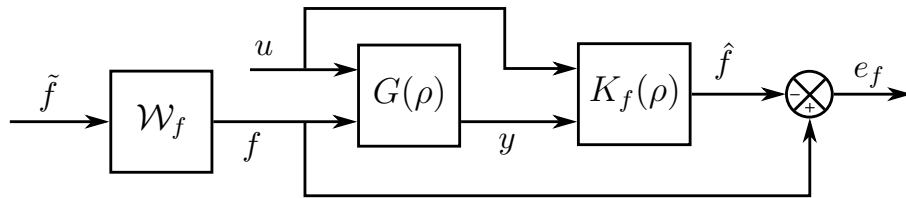
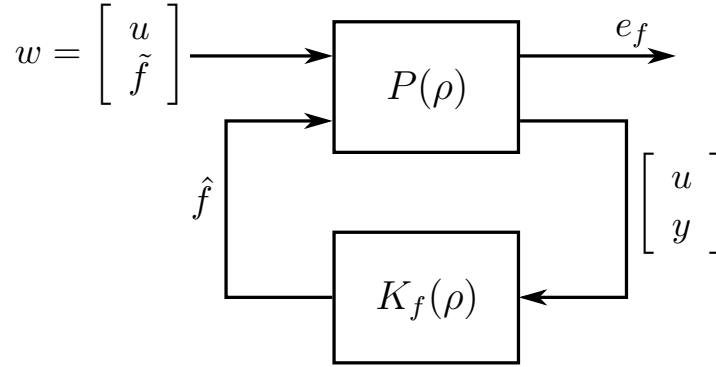


Figure 4.5: Block scheme for \mathcal{H}_∞ filter design

From, the block scheme Figure 4.5, the generalized \mathcal{H}_∞ problem depicted in Figure 4.6 can be obtained. The generalized plant $P(\rho)$ is a polytopic LPV system derived from each vertex of G .

Figure 4.6: Generalized \mathcal{H}_∞ problem

Let us denote the sensitivity function S_{f,e_f} from f to the estimation error e_f . Since [Proposition 1.5](#) minimizes the induced- \mathcal{L}_2 norm from w to e_f by γ_∞ , it is clear that (with a slight abuse of language since the considered system is LPV):

$$\sup_{w \neq 0, w \in \mathcal{L}_2} \frac{\|e_f\|_2}{\|w\|_2} \leq \gamma_\infty \Rightarrow \|S_{f,e_f}\|_\infty \leq \frac{\gamma_\infty}{\|\mathcal{W}_f\|_\infty} \quad (4.27)$$

Therefore, the parameterization of \mathcal{W}_f can tune the rate convergence of the estimation error.

Finally, the synthesis gives the Bode diagram depicted in [Figure 4.7](#), where the inverse of the singular values of \mathcal{W}_f and the ones of S_{f,e_f} at each vertex are depicted. Note that the curves are overlapping. Thus, they cannot be distinguished. At each vertex, the singular values of S_{f,e_f} are under -120 dB at low frequencies, which means that the static error will be very low. Besides, the cutoff frequency is around 1 rad/s.

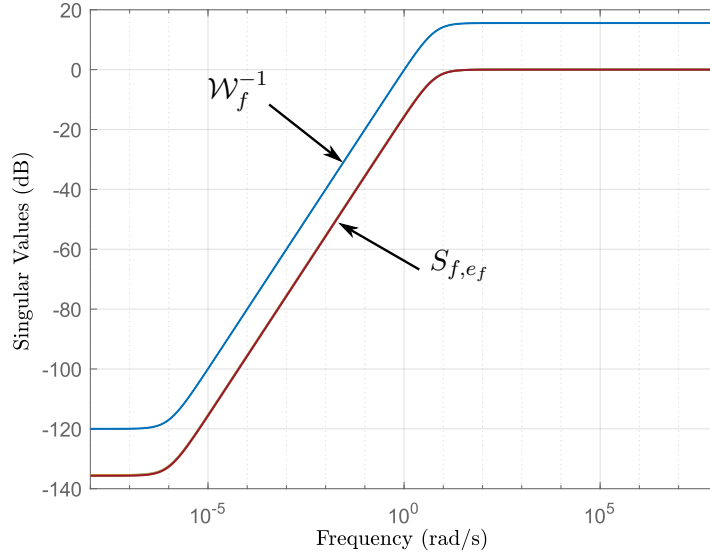
4.3.4 Kalman filter design

This section aims to apply [Proposition 1.6](#) to design a Kalman filter. To do so, the dynamic $\dot{D}_{egr} = 0$ is added to [\(4.6\)](#). Let denote $[x_1 \ x_2]^T = [P_2 \ D_{egr}]^T$, the following system to observe is obtained:

$$\begin{aligned} \dot{x} &= A(t)x + B(t) + q(t) \\ y &= Cx + r(t) \end{aligned} \quad (4.28)$$

where, $q(t)$ and $r(t)$ are white Gaussian noises following the distribution $q(t) \sim \mathcal{N}(0, Q)$ and $r(t) \sim \mathcal{N}(0, R)$, and,

$$A(t) = \begin{bmatrix} \rho_1(t) & \rho_2(t) \\ 0 & 0 \end{bmatrix}, \quad B(t) = \begin{bmatrix} u \\ 0 \end{bmatrix}, \quad C = \begin{bmatrix} 1 & 0 \end{bmatrix} \quad (4.29)$$

Figure 4.7: Bode diagram of $S_{f,ef}$ at each vertex

The Kalman filter to design has the following structure:

$$\begin{aligned}
 \dot{\hat{x}}(t) &= A(t)\hat{x}(t) + B(t) + K(t)(y(t) - \hat{y}(t)) \\
 \hat{y}(t) &= C\hat{x}(t) \\
 K(t) &= P(t)C^T R^{-1} \\
 \dot{P}(t) &= A(t)P(t) + P(t)A(t)^T - K(t)CP(t) + Q
 \end{aligned} \tag{4.30}$$

One can observe that (4.28) can be considered as an LTV system so Proposition 1.6 can be applied. To tune the Kalman filter, the following covariance matrices are chosen:

$$Q = 10^{-3} \quad \text{and} \quad R = 10^8 \tag{4.31}$$

4.3.5 Adaptive observer design

This section is devoted to design an Adaptive observer as described in Section 1.2.2.2. To fit with the system form described in (1.62), let denote $x = P_2$ and $\theta = D_{egr}$. The following system to observe is obtained:

$$\begin{aligned}
 \dot{x} &= A(u, y)x + \varphi(u, y) + \Phi(u, y)\theta \\
 y &= Cx
 \end{aligned} \tag{4.32}$$

with, $A(u, y) = \rho_1$, $\varphi(u, y) = u$, $\Phi(u, y) = \rho_2$ and $C = 1$.

To solve [Problem 4.1](#), the considered Adaptive Observer has the following structure:

$$\begin{aligned}
\dot{\hat{x}} &= A(u, y)\hat{x} + \varphi(u, y) + \Phi(u, y)\hat{\theta} \\
&\quad + \{\Lambda S_{\theta}^{-1}\Lambda^T C^T + S_x^{-1}C^T\}\Sigma(y - C\hat{x}) \\
\dot{\hat{\theta}} &= S_{\theta}^{-1}\Lambda^T C^T \Sigma(y - C\hat{x}) \\
\dot{\Lambda} &= \{A(u, y) - S_x^{-1}C^T \Sigma C\}\Lambda + \Phi(u, y) \\
\dot{S}_x &= -\rho_x S_x - A(y, u)^T S_x - S_x A(u, y) + C^T \Sigma C \\
\dot{S}_{\theta} &= -\rho_{\theta} S_{\theta} + \Lambda^T C^T \Sigma C \Lambda
\end{aligned} \tag{4.33}$$

The system (4.32) is affine in the state and the parameter to estimate. Thus, [Proposition 1.8](#) can be directly applied with the tuning parameters:

$$\rho_x = 12.5, \quad \rho_{\theta} = 8.5, \quad \Sigma = 10^4 \tag{4.34}$$

4.3.6 Sliding mode observer design

Consider the system given by:

$$\dot{P}_2 = \rho_1 P_2 + u + \rho_2 D_{egr} \tag{4.35}$$

Following [[Castillo et al. 2013a](#)], let us define the sliding mode observer to estimate the variable D_{egr} :

$$\begin{aligned}
\dot{\hat{P}}_2 &= \rho_1 \hat{P}_2 + \rho_2 \hat{D}_{egr} + u + \epsilon_1 \\
\dot{\hat{D}}_{egr} &= \epsilon_2
\end{aligned} \tag{4.36}$$

The objective is to find ϵ_1 and ϵ_2 such that [Problem 4.1](#) is solved. These two variables are expressed by the following proposition.

Notation 1

For the sake of clarity, the time dependency of the variables $\epsilon_1(t)$, $\epsilon_2(t)$, $S_1(t)$ and $S_2(t)$ will be omitted hereafter.

Proposition 4.1

The observer (4.36) solves [Problem 4.1](#) if ϵ_1 and ϵ_2 are chosen as follow:

$$\begin{aligned}
\epsilon_1 &= \rho_2 \lambda_1 \text{sign}(S_1) \\
\epsilon_2 &= \lambda_2 \text{sign}(S_2) - \frac{k_4}{k_3} (\hat{D}_{egr} - D_{egr})
\end{aligned} \tag{4.37}$$

with,

$$\begin{aligned}
S_1 &= k_1 (\hat{P}_2 - P_2) + k_2 \int_0^t (\hat{P}_2 - P_2) .ds \\
S_2 &= k_3 (\hat{D}_{egr} - D_{egr}) + k_4 \int_0^t (\hat{D}_{egr} - D_{egr}) .ds
\end{aligned} \tag{4.38}$$

and,

$$k_1 > 0, \quad k_2 = k_1 \rho_1, \quad k_3 > 0, \quad k_4 \in \mathbb{R} \quad (4.39)$$

$$\lambda_1 < 0, \quad \lambda_2 < 0 \quad (4.40)$$

where D_{egr} in (4.37) and (4.38) is calculated as:

$$D_{egr} = -\frac{\rho_1}{\rho_2} (\hat{P}_2 - P_2) + \hat{D}_{egr} + \lambda_1 \text{sign}(S_1) \quad (4.41)$$

Proof: The proof follows the one in [Castillo et al. 2013a]. Let us first define a sliding surface as:

$$S_1 = k_1 (\hat{P}_2 - P_2) + k_2 \int_0^t (\hat{P}_2 - P_2) .ds \quad (4.42)$$

Consider the following Lyapunov function candidate:

$$V_1 = \frac{1}{2} S_1^2 \quad (4.43)$$

Assuming that $\dot{k}_2 = 0$, the time derivative of this function gives:

$$\begin{aligned} \dot{V}_1 &= \dot{S}_1 S_1 \\ &= S_1 k_1 \rho_2 (\hat{D}_{egr} - D_{egr}) + S_1 k_1 \epsilon_1 + S_1 k_1 \rho_1 (\hat{P}_2 - P_2) + S_1 k_2 (\hat{P}_2 - P_2) \end{aligned} \quad (4.44)$$

If ϵ_1 and k_2 are chosen as:

$$\epsilon_1 = \rho_2 \lambda_1 \text{sign}(S_1), \quad k_2 = -k_1 \rho_1 \quad (4.45)$$

this leads to:

$$\dot{V}_1 = S_1 k_1 \rho_2 (\hat{D}_{egr} - D_{egr}) + S_1 k_1 \rho_2 \lambda_1 \text{sign}(S_1) \quad (4.46)$$

one gets:

$$\dot{V}_1 = S_1 k_1 \rho_2 (\hat{D}_{egr} - D_{egr} + \lambda_1 \text{sign}(S_1)) \quad (4.47)$$

In order to ensure $\dot{V}_1 < 0$, λ_1 and k_1 are chosen as:

$$|\hat{D}_{egr} - D_{egr}| < |\lambda_1|, \quad \lambda_1 < 0, \quad k_1 > 0 \quad (4.48)$$

Thus, it can be shown that $S_1 \rightarrow 0$ when $t \rightarrow \infty$ according to Barbalat's Lemma. So, according to (4.42), we have:

$$\lim_{t \rightarrow \infty} \frac{d}{dt} (\hat{P}_2 - P_2) = -\frac{k_2}{k_1} (\hat{P}_2 - P_2) \quad (4.49)$$

since $\frac{k_2}{k_1} > 0$, according to (4.45), we finally have $\hat{P}_2 - P_2 \rightarrow 0$.

Let define a second sliding surface as:

$$S_2 = k_3 (\hat{D}_{egr} - D_{egr}) + k_4 \int_0^t (\hat{D}_{egr} - D_{egr}) .ds \quad (4.50)$$

Due to the variable D_{egr} in (4.50), it is not possible to compute S_2 . However, it can be easily shown that when the estimation error $e = \hat{P}_2 - P_2$ is at steady state (i.e $\dot{e} = 0$), one gets:

$$D_{egr} = -\frac{\rho_1}{\rho_2} (\hat{P}_2 - P_2) + \hat{D}_{egr} + \lambda_1 \text{sign}(S_1) \quad (4.51)$$

Define a second Lyapunov function as:

$$V_2 = \frac{1}{2} S_2^2 \quad (4.52)$$

The time-derivative of the above function is:

$$\dot{V}_2 = S_2 \left(k_3 \epsilon_2 + k_4 \left(\hat{D}_{egr} - D_{egr} \right) \right) \quad (4.53)$$

If ϵ_2 is chosen as:

$$\epsilon_2 = \lambda_2 \text{sign}(S_2) - \frac{k_4}{k_3} \left(\hat{D}_{egr} - D_{egr} \right) \quad (4.54)$$

(4.53) becomes:

$$\dot{V}_2 = S_2 k_3 \lambda_2 \text{sign}(S_2) \quad (4.55)$$

Therefore, to ensure $\dot{V}_2 < 0$ we can chose the following conditions:

$$\lambda_2 < 0 \quad \text{and} \quad k_3 > 0 \quad (4.56)$$

Following the same arguments as before, one can establish that $\hat{D}_{egr} - D_{egr} \rightarrow 0$. ■

As for the FAFE design in [Section 4.3.2](#), we are facing here the problem to chose the different parameters for the sliding mode observer (4.36), i.e k_1 , k_3 , k_4 , λ_1 and λ_2 . Therefore a Genetic Algorithm will be used to deduce them. Due to their slight effects on the estimation performance and for simplification perspectives, k_1 and k_4 have been set to 1. The other parameters, i.e k_3 , λ_1 and λ_2 are obtained by solving the following optimization problem:

$$\min_{k_3, \lambda_1, \lambda_2} RMS \left(\hat{D}_{egr} - D_{egr} \right) \quad (4.57)$$

where RMS is defined in (4.20). The implemented process is summarized in [Figure 4.8](#). The time domain simulation is the same than the one used in [Section 4.3.2](#).

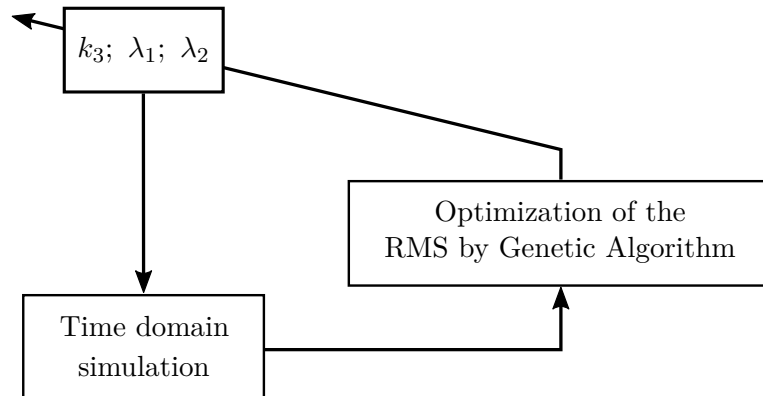


Figure 4.8: Sliding mode observer parameters optimization using a Genetic Algorithm

Finally, the parameters presented in [Table 4.3](#) are chosen for the SM observer.

Table 4.3: Parameters value for the SM observer

Parameter	Value
k_1	1
k_3	0.46
k_4	1
λ_1	$-2.53 \cdot 10^{-5}$
λ_2	$-2.03 \cdot 10^{-4}$

4.4 Experimental setup

This section deals with the experimental protocol to test the observers. First, the implementation of the 6 designed observers in the embedded software is presented. Then, the test cell is described to explain how the data are collected.

4.4.1 ECU implementation

In the Volvo's trucks, the engine control is performed by an embedded system called Electronic Control Unit (ECU), also known as Engine Control Module (ECM). The ECU acquires signals from the sensors or switches and converts them into computational variables in order to apply the engine control strategy. Those variables are treated in programs loaded previously in the ECU memory. Then, the actuator controls are computed and sent to real devices in order to achieve the desired engine operation.

To create the embedded software in the ECU, Volvo uses TargetLink¹, a software developed by the company dSPACE. It enables to generate a C code software from a Simulink model that is suitable for the implementation in the ECU. The scheme presented in Figure 4.9 summarizes the implementation process.

From the embedded software point of view, the 6 designed observers have been setup inside an unique function. It is possible to adjust the scheduling (sampling time) of this function up to 100Hz (0.01s). During the tests bench, the sampling time T_s has been set to 0.01s.

There are different methods available to discretize a continuous-time systems, see for example [Tóth et al. 2010] which deals with the LPV systems or [Roche 2011] which addresses the discretization with a time-varying sampling time. However, for simplification perspectives, we will use the Euler method to discretize the designed

¹see the website of the company: <https://www.dspace.com/en/inc/home/products/sw/pcgs/targetli.cfm>

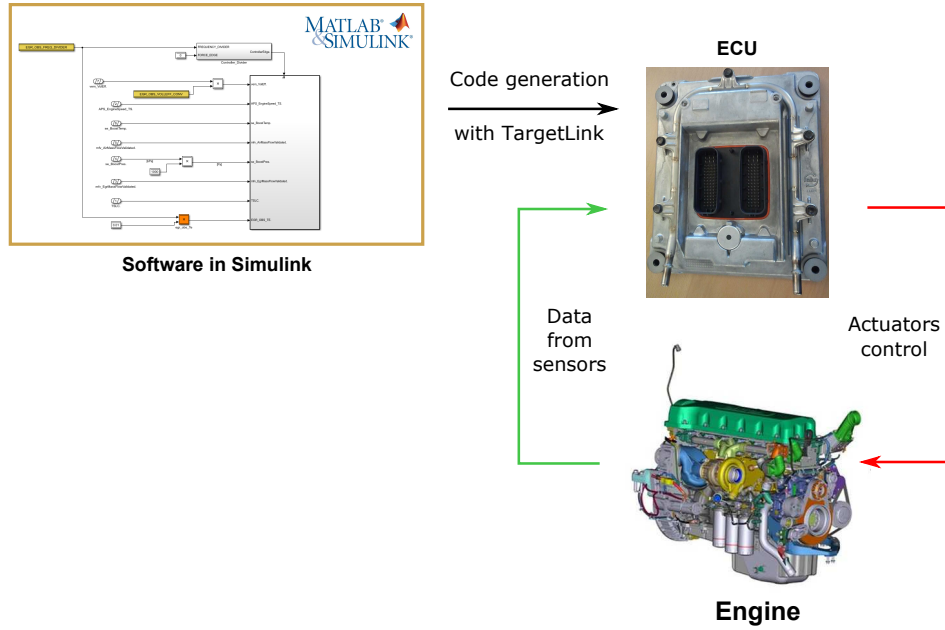


Figure 4.9: Process of the ECU implementation

observers. Even if this method may have instability issues, this choice is justified by both experiments feedback and software simplification. The developed observers (4.14), (4.19), (4.26), (4.30), (4.33) and (4.36) can be represented as:

$$\begin{cases} \dot{X}(t) = F(X(t), u(t), y(t), t) \\ \hat{x}(t) = G(X(t), u(t), y(t), t) \\ \hat{f}(t) = H(X(t), u(t), y(t), t) \end{cases} \quad (4.58)$$

and be turned into the following discrete-time system by the Euler method:

$$\begin{cases} X(k+1) = X(k) + F(X(k), u(k), y(k))T_s \\ \hat{x}(k) = G(X(k), u(k), y(k)) \\ \hat{f}(k) = H(X(k), u(k), y(k)) \end{cases} \quad (4.59)$$

where T_s is the sampling-time.

4.4.2 Test cell description

The test cell operation follows the scheme presented in Figure 4.10. Basically, it consists of an engine to be analyzed, linked to a dynamometer that provides a torque/speed profile for the engine. A computer ensures the control of the test bench and another one analyzes the outputs of the ECU (including the observers estimations). The engine is equipped with standard sensors plus additional ones for test perspectives. Gas sensors allow to know the engine pollutants concentration at different locations. Then, all data are centralized into an XML server.

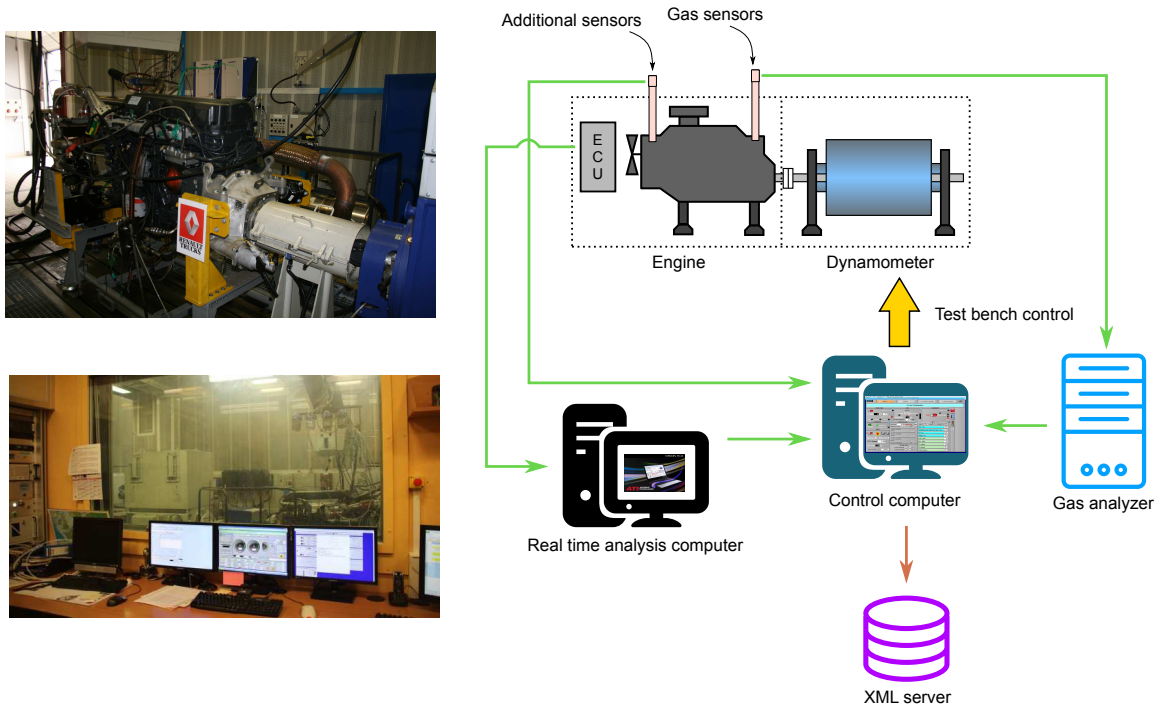


Figure 4.10: Test cell description

4.4.3 EGR mass flow rate measurement

Note that in the schematic view of the engine depicted [Figure 4.1](#), there is no direct measurement of the EGR mass flow rate. In the test bench, this mass flow rate is calculated *a posteriori* from the data provided by the gas analyzer. This calculation is done by the CO_2 concentration measurement inside the exhaust and intake manifolds. Then, knowing exactly the CO_2 that comes from the ambient air and the one produced by the combustion, it is possible to determine the quantity of the EGR gas inside the intake manifold. However, this method does not guarantee an accurate measurement of D_{egr} and may induce some bias in the data. Moreover, this calculation is not reliable in transient conditions. Therefore, in order to validate the real-time estimation \hat{D}_{egr} , only slow varying tests are relevant to compare the performance of the developed observers with the measured D_{egr} .

4.5 Experimental results

The 6 developed observers have been implemented and tested with a unique design on two engine architectures: a medium duty 5L and 8L diesel engine. These choices will allow to test the robustness as the estimation with regard to the calibration software and model uncertainties. Indeed, we have seen in [Section 4.2](#), the variables D_{air} and

D_{asp} are not measured but computed.

As explained in Section 4.4.3, the EGR mass flow rate D_{egr} measurement is not reliable for transient conditions. Therefore, we will only present hereafter, the results for two stationary cycles. The first one is the WHSC (see Appendix B) and the second goes through several operating points of the engine as shown in Figure 4.11. We will call the last cycle, *part load* test.

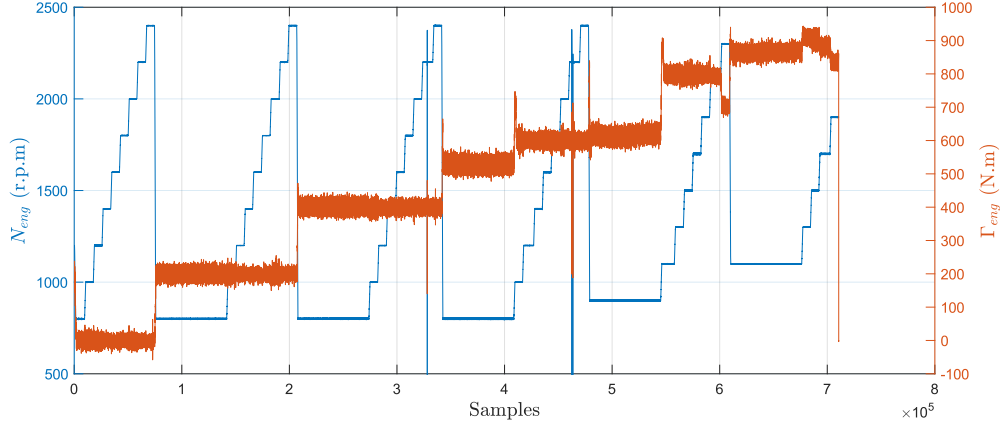


Figure 4.11: Part load profile for the engine speed and torque

Finally, the performance of the designed observers will be compared.

We also remind that the abbreviations of each observers, given in the plot legends, are detailed in Table 4.1.

4.5.1 Medium duty 5L engine

Case 1: WHSC. The estimation results obtained with the 6 observers for this cycle are depicted in Figure 4.12. First, we can see that all the observers have the same performance estimation in terms of speed or accuracy. However, they cannot follow the reference value. Even if the absolute error is low, in comparison with the other mass flow rates values (for example D_{air} can reach 0.2kg/s), the relative error is high for D_{egr} . For the whole cycle, the value of NRMS index (see Appendix A) is 23.6%.

Case 2: Part load. For this cycle, the considered graphs are Figure 4.13 and Figure 4.14. The first one represents a part of the whole cycle, when the torque is set at 600N.m. It appears that, for this torque value, the observers tend to underestimate the reference value and for some points, the error is close to zero. Figure 4.14, on the other hand, provides a representation of the stationary relative error ($\frac{\hat{D}_{egr} - D_{egr}}{D_{egr}}$) on all reached operating points with the part load cycle shown in Figure 4.11. We can observe

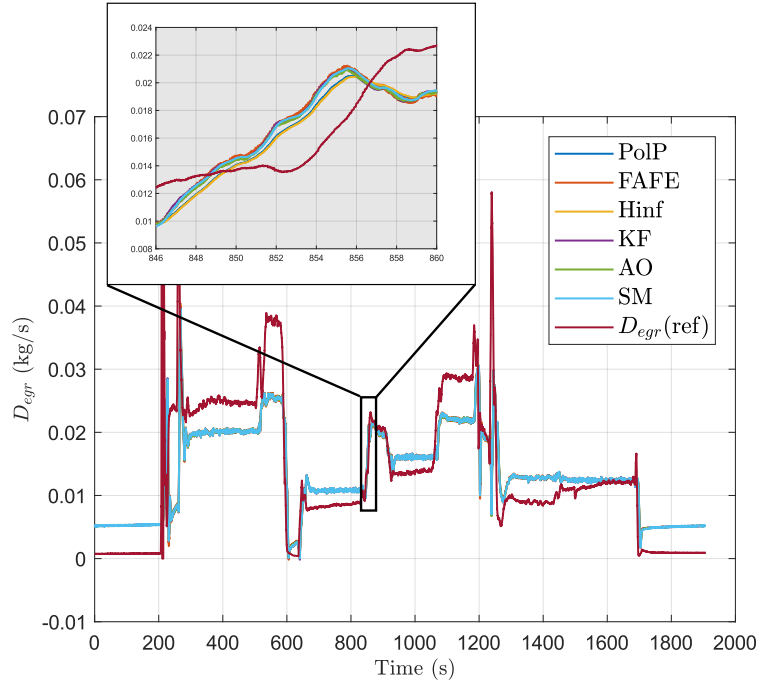


Figure 4.12: WHSC for 5L engine (case 1)

that the relative error is larger than 1 for low engine speeds. This result was expected since, at these speeds, the mass flow rate is very low and therefore the error is more significant. Without taking into account extreme values (at low and high torque), the relative error is between $\pm 20\%$ and the observers tend to underestimate the reference mass flow rate.

4.5.2 Medium duty 8L engine

Case 3: WHSC. The results obtained for the stationary cycle are depicted in [Figure 4.15](#). Again, the estimation performances for all the observers are the same, except for the Kalman filter (KF) which did not converge for all the tested cycles with the 8L engine. From our perspective, the divergence is due to its initialization which may generate instability. For this case, the NRMS is 29.3% which is higher than for the 5L's one. Besides, in the whole cycle, the observers overestimate the reference mass flow rate.

Case 4: Part load. Other time-domain results are given in [Figure 4.16](#) when the torque engine is set at 800N.m. It confirms the overestimation regardless of the engine speed. The [Figure 4.17](#) shows the relative error for the 8L engine for all operating points reached by the part load cycle. For this engine, the error is higher than for the 5L one: for most of the tested points, it is higher than 40%. One can also observe that

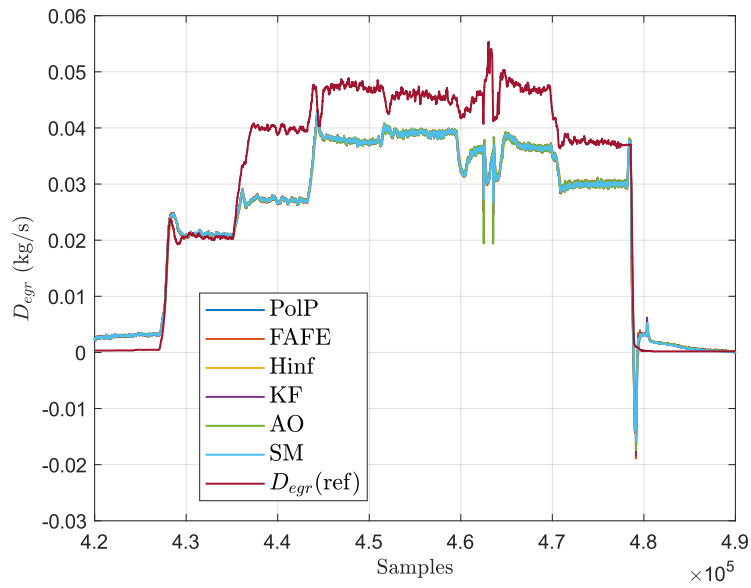


Figure 4.13: Partial results for the part load cycle - 5L (case 2)

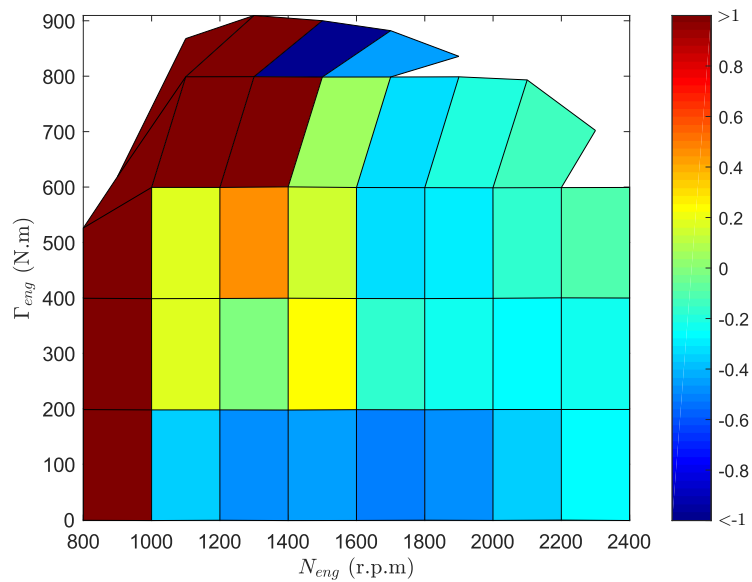


Figure 4.14: Relative error for different operating points - 5L (case 2)

the estimation is always above the reference.

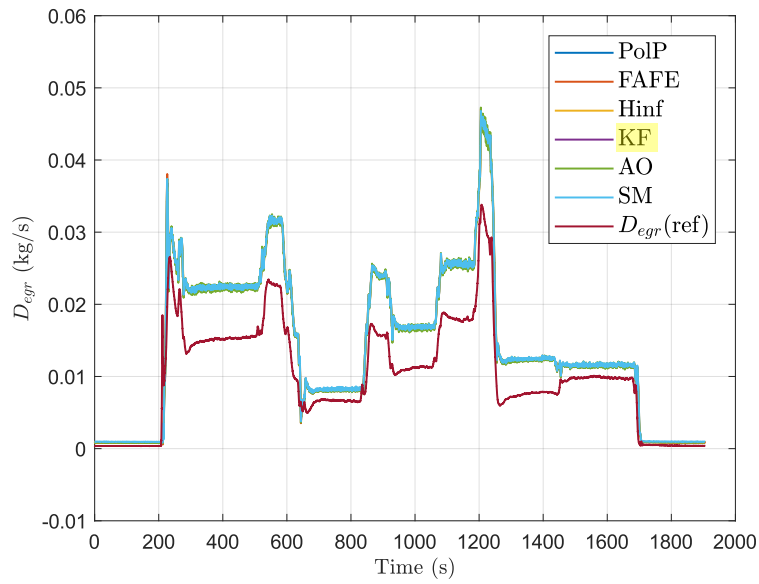


Figure 4.15: WHSC for 8L engine (case 3)

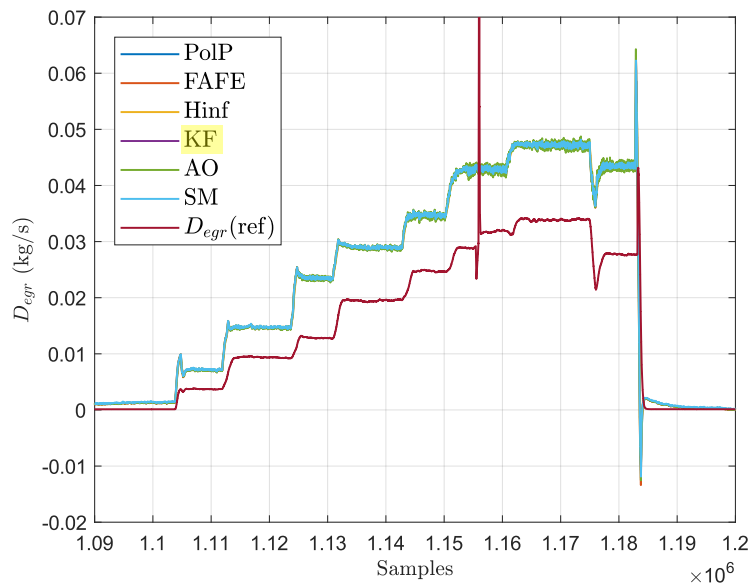


Figure 4.16: Partial results for the part load cycle - 8L (case 4)

4.5.3 Analysis of the estimation errors

In most of the observers model, the estimation of the variable D_{egr} acts as an integral term. Therefore, it compensates for all the modeling uncertainties. We have seen in [Section 4.2](#) that the variable D_{air} is not directly measured but deduced from a lambda sensor located after the exhaust manifold (cf. [Figure 4.1](#)). Thus, D_{air} may be subject

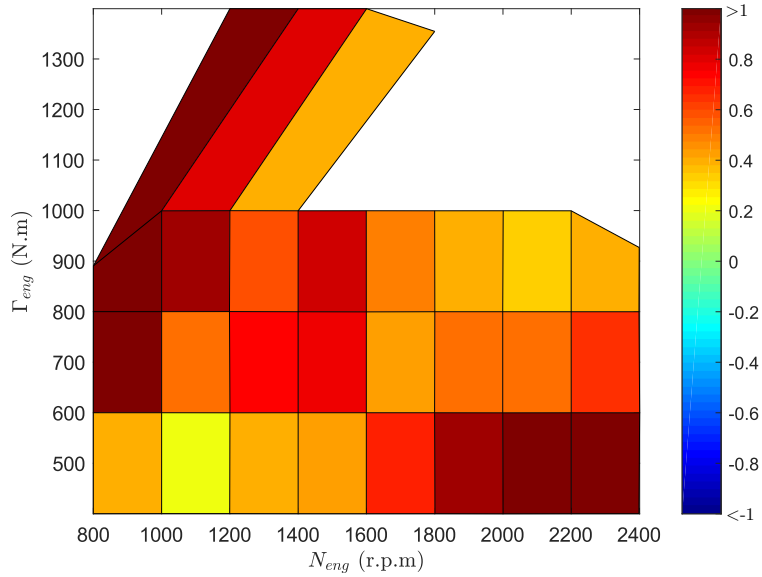


Figure 4.17: Relative error for different operating points - 8L (case 4)

to uncertainties as depicted in Figure 4.18. Even if the relative error is low for this variable, the absolute error directly influences the estimation of D_{egr} which causes high relative error since the considered values are much more lower. Below, we can see in Figure 4.18 that the absolute error of D_{air} explains most of the errors of D_{egr} .

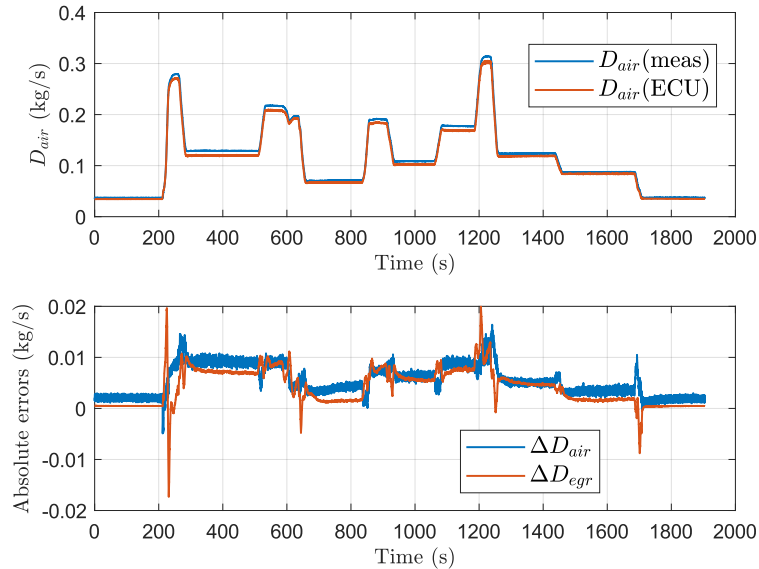


Figure 4.18: Inlet air mass flow rate (top) - Absolute errors of D_{air} and D_{egr} (bottom)

The calibration misstatements of the volumetric efficiency η_v in (4.4) may also ex-

plain the remaining errors of the estimation. But this fact is more difficult to verify because it is not measured. The errors measurement of D_{egr} presented in Section 4.4.3 may also explain the estimation errors.

4.5.4 Computational performance

This section aims to establish which observer has the best computational performance. The criteria used will be the execution time of the function which contains the code of all the observers. During the test, parts of this function have been disabled (i.e not computed), which corresponds to the observers that we do not want to use.

Figure 4.19 shows the time-domain test results. Note that the time accuracy is 1 μs and when all the observers are disabled (in blue in Figure 4.19), the function is executed between 9 and 10 μs . For comparison purpose, the mean of each observer "area" is calculated and displayed in Table 4.4. As can be seen, the values are similar. However the test indicates that the nonlinear observers have the lowest execution time and the polytopic LPV observers have the highest ones. The Adaptive Observer (AO) is the fastest with 10.31 μs and the \mathcal{H}_∞ filter (Hinf) is the slowest with 13.49 μs . In all cases, this is a very low execution time since, in the embedded software, most of the functions have a execution time between 20 and 100 μs . Therefore, the observers have a limited impact on the CPU consumption.

It would be hasty to conclude that the polytopic LPV are less efficient than the nonlinear ones. Indeed, due to implementation limitations of TargetLink (for example the libraries do not include matrix calculations), code simplifications have been implemented for the nonlinear case. For example, the equations with a zero product have been removed. Whereas, for the polytopic case, due to its generic form, we preferred to keep all the matrix coefficients even if they contain zeros. Therefore, some optimization may still be implemented.

Table 4.4: Execution time of the function sorted in ascending order

Observer	Mean of the execution time
AO	10.31 μs
KF	10.45 μs
SM	10.52 μs
FAFE	11.25 μs
PolP	12.52 μs
Hinf	13.49 μs

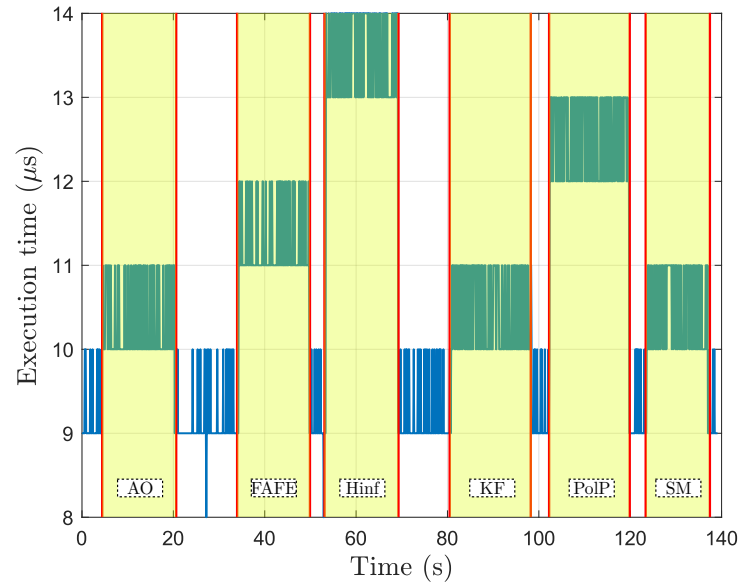


Figure 4.19: Execution time of the function containing the observers

4.6 Conclusion

This chapter provides a comparison of different methods to estimate the EGR mass flow rate of a diesel engine, a key variable for pollutants control. The tests performed on two truck engines have shown that, even if the observer structure is very different, the performance estimation are very similar for all of them. Besides, the CPU consumption appears to be low, which is suitable for an industrial application. The tests also revealed that the inlet air mass flow rate D_{air} has to be known precisely to have a low estimation error. Future works could be done in the model precision to have a commercial implementation.

Exhaust Pressure Estimation

Contents

5.1	Introduction	94
5.2	Mean value model of the engine	95
5.2.1	Exhaust manifold dynamics	96
5.2.2	Turbocharger dynamics	97
5.2.2.1	Rotor speed modeling	97
5.2.2.2	Compressor power	98
5.2.2.3	Turbine power	99
5.2.3	Turbine flow modeling	101
5.2.3.1	Orifice flow equation	101
5.2.3.2	Hammerstein-Wiener model	101
5.2.3.3	Identification results	102
5.2.4	Summary of the nonlinear model of ω_{tc} and P_3	102
5.3	Observer design	103
5.3.1	LPV modeling	104
5.3.2	Problem formulation	105
5.3.3	Synthesis	106
5.4	Simulation results	108
5.4.1	Case 1: D_t defined by the orifice equations (5.13)-(5.15)	109
5.4.2	Case 2: D_t defined by HW model	109
5.5	Some ongoing studies	110
5.5.1	Pressure and EGR mass flow estimation	110
5.5.2	Turbocharger efficiency estimation	111
5.6	Conclusion	112

The results presented in this chapter are based on [Dubuc et al. 2018].

5.1 Introduction

In most automotive engines, the exhaust manifold pressure is directly measured by a sensor. However, some problems have been reported at the Volvo aftermarket concerning the robustness of the sensor. In fact, in addition to its high cost, it must face strong pressure oscillations and high temperature conditions. Indeed, these conditions have caused for example tube clogging problems to the sensor. Therefore it fails to be reliable in all the operating conditions of the engine. Although this pressure information is difficult to get, it is essential for engine control. Among others, it is used to control the exhaust pressure with the exhaust flap in order to control the engine brake power and to estimate the burned fraction to ensure the on-board diagnosis (OBD) for the anti-pollution system. Since it is mandatory to propose an OBD solution [Mohammadpour et al. 2012], its estimation is then of great interest for diagnosis and fault tolerant control objectives.

To overcome such problems, model-based estimation represents an efficient alternative solution to the direct measurement. Therefore, several authors have proposed different methods to estimate the exhaust manifold pressure. One can categorize them in two types: nonlinear observer-based approaches [Fredriksson and Egardt 2002] and inverse model approaches [Castillo et al. 2013b; Olin 2008; Yue-Yun Wang and Haskara 2010]. The latter estimators propose to directly estimate this variable from the information of the exhaust air mass flow through the orifice flow equation or from the turbine's data-maps. In [Fredriksson and Egardt 2002], the authors proposed a generalized Luenberger observer based on mean value models of the intake and exhaust manifolds, the turbocharger and engine dynamics which leads to a fourth order nonlinear observer.

In this chapter, we propose a Linear Parameter Varying (LPV) observer based on mean value models of the turbocharger and the exhaust manifold to estimate the pressure. Since the equipment of the engine under consideration, and thus the available measurement, are different from [Fredriksson and Egardt 2002], the order of the LPV observer is reduced to two. Besides, our method encompasses a systematic calibration procedure, contrary to the previous one where tuning the observer parameters is not an easy task. Moreover, the observer is designed considering two different models for the turbine mass flow rate: a standard orifice equation, and a new identified black-box model. As in Chapter 2, the merits of the developed solution are then validated on a high industrial complex simulator with realistic engine cycles.

The chapter is organized as follows. In Section 5.2, a mean value model is presented. In Section 5.3, based on this model, a LPV polytopic observer is designed to estimate the exhaust pressure. The observer is synthesized in order to minimize an H_∞ criterion associated with a pole placement by Linear Matrix Inequalities (LMIs) regions. In Section 5.4, the performances of this observer are illustrated in a realistic simulator designed with GT-POWER. Then in Section 5.5, perspective works are presented. Finally, conclusions are stated in Section 5.6.

Table 5.1: Nomenclature

Notation	Description	Unit
N_{eng}	Engine speed	rpm
ω_{tc}	Rotor speed of the turbocharger	rad.s ⁻¹
J_{tc}	Shaft moment of inertia of the turbocharger	kg.m ²
\mathcal{P}	Power	W
T	Temperature of a subsystem	K
P	Pressure of a subsystem	Pa
c_p	Specific heat	J.kg ⁻¹ .K ⁻¹
R	Ideal gas constant for the air	J.kg ⁻¹ .K ⁻¹
γ	Specific heat ratio	-
D	Mass flow rate	kg.s ⁻¹
Subscript		
1	Upstream the compressor	
2	Inside the intake manifold	
3	Inside the exhaust manifold	
4	Downstream the turbine	
c	Related to the compressor	
t	Related to the turbine	
egr	Related to the EGR loop	
f	Related to the fuel	

5.2 Mean value model of the engine

The architecture of the diesel engine under consideration is depicted in [Figure 5.1](#). This engine is a medium-duty 4-cylinders 5L diesel one equipped with a Variable Geometry Turbocharger (VGT) and a Exhaust Gas Recirculation (EGR) loop. In this section and in all the chapter, we will use data provided by a high-fidelity simulator designed with GT-POWER. Therefore all the reference data are provided by this simulator.

The measurements considered for this study are: D_c , D_{egr} , P_1 , T_1 , P_2 , T_2 , T_3 , P_4 and ω_{tc} . These variables are typically measured or estimated in the automotive industry. Their nomenclature is given in [Table 5.1](#).

In the following, the exhaust manifold and turbocharger dynamics are modeled using a mean value approach. Then, the problem of estimating the turbine mass flow rate is treated. Finally, the considered system to observer is established.

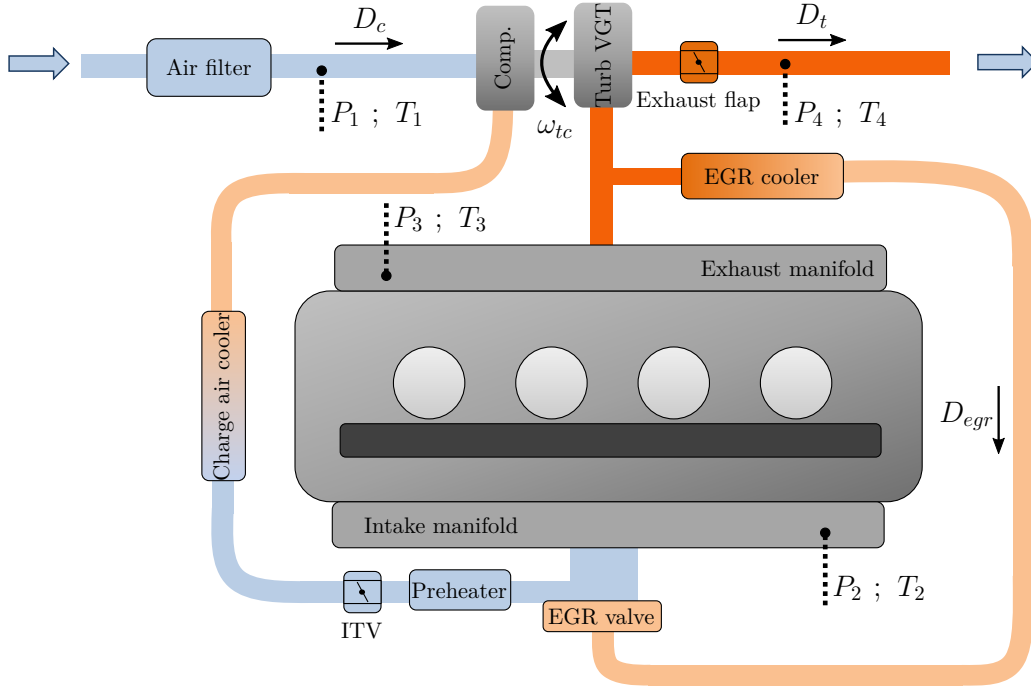


Figure 5.1: Schematic view of the air path in the considered engine

5.2.1 Exhaust manifold dynamics

Located just after the engine block, the exhaust manifold permits to collect all the gases from the cylinders into one pipe which is directly connected to the turbine.

The exhaust manifold can be represented as an open thermodynamical system, where the quantity of gas can increase or decrease. It is called a "filling and emptying" system. Inside this volume, the ideal gas law can be applied and the pressure P_3 can be expressed as:

$$P_3 = \frac{m_3 R T_3}{V_3} \quad (5.1)$$

where m_3 is the total air mass inside the volume V_3 .

By taking a time-derivative of this equation, one obtains:

$$\dot{P}_3 = \frac{\dot{m}_3 R T_3}{V_3} + \frac{m_3 R \dot{T}_3}{V_3} \quad (5.2)$$

where \dot{m}_3 represents the mass rate of gas flowing through the exhaust manifold and can be expressed, from a balance equation, as: $\dot{m}_3 = D_{asp} + D_f - D_{egr} - D_t$. Besides, assuming that the temperature varies slowly in comparison to P_3 , we consider $\dot{T}_3 \simeq 0$ and (5.2) becomes:

$$\dot{P}_3 = \frac{RT_3}{V_3} (D_{asp} + D_f - D_{egr} - D_t) \quad (5.3)$$

In (5.3), we assume that the mass flow rates D_f and D_{egr} are known input variables (in the real engine, they are estimated), and D_{asp} is deduced from the formula in Appendix C. The mass flow rate D_t will be expressed in Section 5.2.3.

5.2.2 Turbocharger dynamics

Located just after the EGR loop and the exhaust manifold, the turbocharger is the combination of a turbine and a compressor (grey parts in Figure 5.1). The role of the compressor is to increase the air mass flow, which goes inside the engine, to increase the quantity of oxygen inside the combustion chamber in order to have the possibility to inject more fuel and thus to have more torque for a given cylinder volume. The turbine is symmetric to the compressor. Its purpose is to convert the energy contained in the exhaust gases into a mechanical energy. This mechanical energy is then transmitted to the compressor by a shaft. Figure 5.2 shows the different components of the turbocharger.

In our case, the turbine has a variable geometry: the orifice section and the flow direction to the turbine wings can be controlled by the position of vanes. Therefore the energy delivered to the compressor can be adjusted depending on the operating point. For example at low engine speeds and torques, the vanes will be almost closed and at high speeds and torques, they will be totally opened. The command u_{vgt} determines the vanes position and it is calculated through the feedback on the boost pressure P_2 . The variable geometry can also be used as back-pressure device for exhaust brake or to drive the EGR flow.

Many studies propose a model of the turbocharger. Some are control-oriented such as [Mohammadpour et al. 2010; Salehi et al. 2013] or modeling-oriented [Jung et al. 2002; Isermann 2014; Moulin 2010; Ceccarelli 2012]. The rotor speed modeling will be exposed according to the study done in [Moulin 2010].

5.2.2.1 Rotor speed modeling

From the mechanical power balance, one can obtain the rotor speed dynamic of the turbocharger:

$$\frac{1}{2} J_{tc} (\dot{\omega}_{tc}^2) = \mathcal{P}_t - \mathcal{P}_c \quad (5.4)$$

where \mathcal{P}_c and \mathcal{P}_t are respectively the compressor and turbine powers.

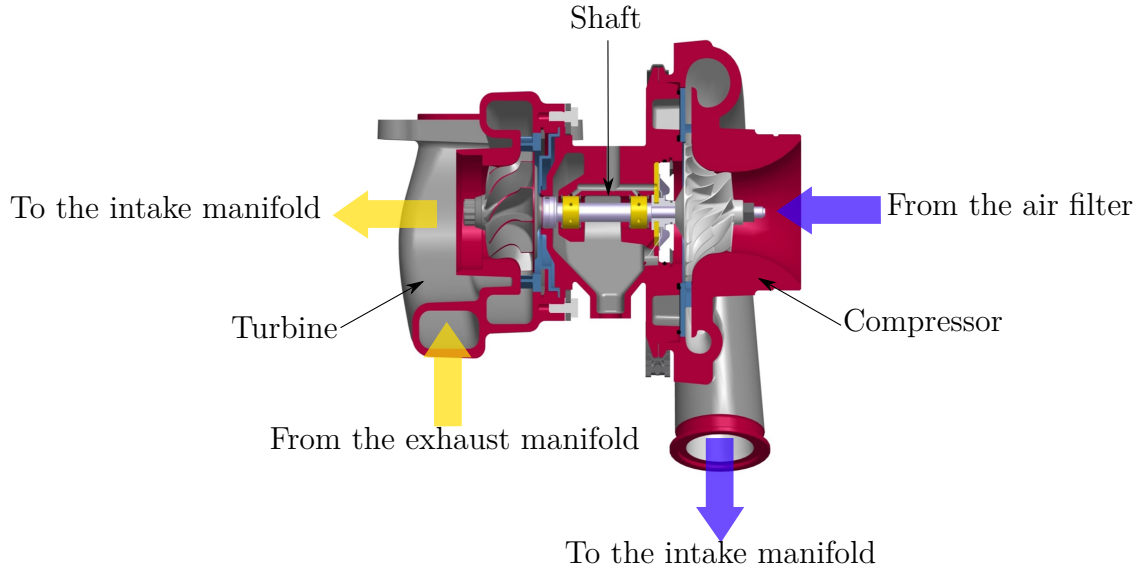


Figure 5.2: Scheme of a turbocharger

Remark 5.1

In this study the mechanical friction is neglected but can be easily added by multiplying \mathcal{P}_t by a constant efficiency as in [Salehi et al. 2013].

5.2.2.2 Compressor power

From the first law of thermodynamics, one can express the compressor power in function of the enthalpy variation as:

$$\mathcal{P}_c = D_c c_{p1} (T_1 - T_{2A}) \quad (5.5)$$

where T_{2A} is the temperature just after the compressor.

In practice, T_{2A} is not measured but it can be deduced from the definition of the isentropic efficiency:

$$\eta_c = \frac{\mathcal{P}_{c,isentropic}}{\mathcal{P}_c} = \frac{T_{2A,isentropic} - T_1}{T_{2A} - T_1} = \frac{\left(\frac{P_2}{P_1}\right)^{\frac{\gamma_1-1}{\gamma_1}} - 1}{\frac{T_{2A}}{T_1} - 1} \quad (5.6)$$

Then, we finally have:

$$\mathcal{P}_c = \frac{1}{\eta_c} T_1 c_{p1} D_c \left(\left(\frac{P_2}{P_1}\right)^{\frac{\gamma_1-1}{\gamma_1}} - 1 \right) \quad (5.7)$$

In order to model the efficiency η_c , a third order polynomial function is used to interpolate the experimental data provided by the manufacturer of the turbocharger. In order to avoid dependency on ambient temperature and pressure, the function inputs are the corrected mass flow rate defined as:

$$D_{c,corr} = D_c \frac{\sqrt{T_1/T_{ref}}}{P_1/P_{ref}}$$

and the pressure ratio:

$$\frac{P_2}{P_1}$$

The map extracted from the interpolated function is depicted in Figure 5.3.

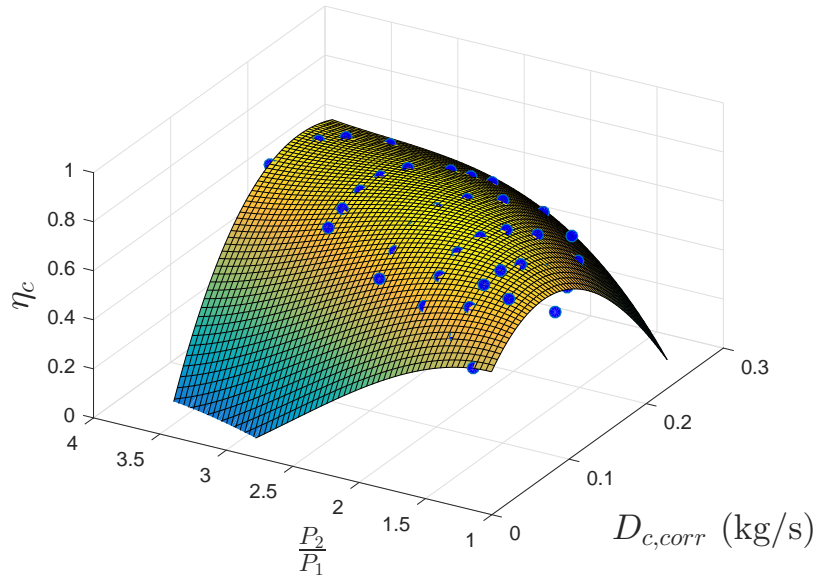


Figure 5.3: Interpolated compressor efficiency map

5.2.2.3 Turbine power

Following the same procedure, the power turbine is expressed as:

$$\mathcal{P}_t = D_t c_{p3} (T_3 - T_4) \quad (5.8)$$

Then T_4 can be expressed from the definition of the isentropic efficiency:

$$\eta_t = \frac{\mathcal{P}_{t,isentropic}}{\mathcal{P}_t} = \frac{\frac{T_4}{T_3} - 1}{\left(\frac{P_4}{P_3}\right)^{\frac{\gamma_3-1}{\gamma_3}} - 1}, \quad (5.9)$$

which leads to:

$$\mathcal{P}_t = \eta_t T_3 c_{p3} D_t \left(1 - \left(\frac{P_4}{P_3} \right)^{\frac{\gamma_3 - 1}{\gamma_3}} \right) \quad (5.10)$$

The difficulty here is how to model the efficiency η_t . Indeed, in addition to the rotor speed and the pressure ratio, it also depends on the vanes position u_{vgt} . Instead of building a four dimensional map, one can use the Blade Speed Ratio (BSR) [Jung et al. 2002], defined as the ratio between the real turbo speed and the ideal peripheral velocity of the exhaust gas, which can be expressed as:

$$BSR = \frac{\frac{D}{2} \omega_{tc}}{\sqrt{2c_{p3} T_3 \left(1 - \left(\frac{P_4}{P_3} \right)^{\frac{\gamma_3 - 1}{\gamma_3}} \right)}} \quad (5.11)$$

where D is the wheel turbine diameter.

As before, a third order polynomial function is used to interpolate the experimental data. The obtained map is shown in Figure 5.4.

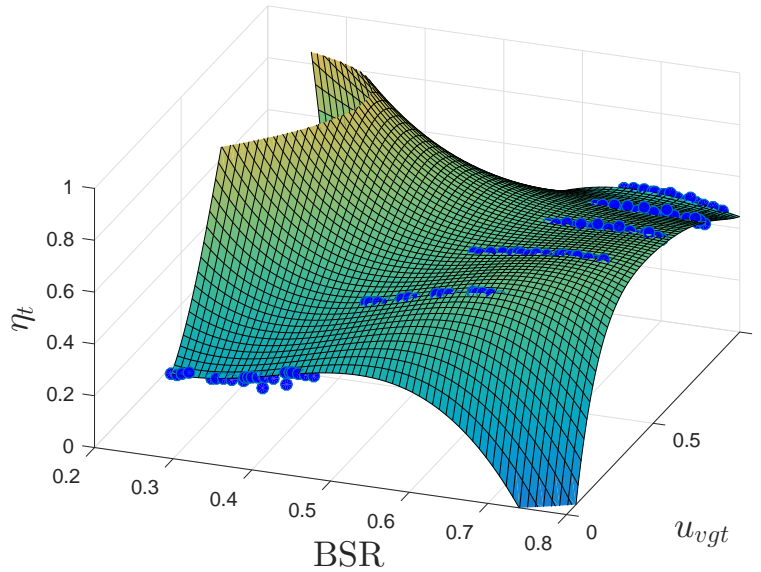


Figure 5.4: Interpolated turbine efficiency map

Remark 5.2

As mentioned in [Isermann 2014], one can consider the parameters γ_1 , γ_3 , c_{p1} , c_{p3} and R as constant. In addition, due to their low dispersion, we assume in the sequel that $\gamma_1 = \gamma_3 = \gamma$.

5.2.3 Turbine flow modeling

Since mass flow rate passing through the turbine D_t is not measured, two different modeling methods are proposed: one based on the orifice flow equation, the other one considering an identified Hammerstein-Wiener one. For comparison purpose, the following fit performance index will be used:

$$FIT = 1 - \frac{\|D_t - D_t(Model)\|_2}{\|D_t - \text{mean}(D_t)\|_2} \quad (5.12)$$

5.2.3.1 Orifice flow equation

Many studies use the standard equations of compressible gas flow through an orifice to model the turbine mass flow rate as in [Olin 2008; Moulin 2010; Ceccarelli 2012; Mohammadpour et al. 2010]. The cited reference propose different formulations depending on the approximation assumptions. Since, we do not have computation limitations, we will use the more detailed one expressed by:

$$D_t = A(u_{vgt}) \frac{P_3}{\sqrt{RT_3}} \Psi \left(\frac{P_4}{P_3} \right) \quad (5.13)$$

$$\Psi \left(\frac{P_4}{P_3} \right) = \sqrt{\frac{2\gamma}{\gamma-1} \left(\Pi^{\frac{2}{\gamma}} - \Pi^{\frac{\gamma+1}{\gamma}} \right)} \quad (5.14)$$

where Π represents the pressure ratio in normal and critical conditions, which is defined by:

$$\Pi = \max \left(\frac{P_4}{P_3}, \left(\frac{2\gamma}{\gamma+1} \right)^{\frac{\gamma}{\gamma-1}} \right) \quad (5.15)$$

In this study, the effective area $A(u_{vgt})$ is identified as a third order polynomial function of the control input u_{vgt} .

5.2.3.2 Hammerstein-Wiener model

In addition to the previous model, which is a knowledge based one, a data-driven model has been calibrated, in the form of a Hammerstein-Wiener (HW) model. A HW model is a combination of three blocks as depicted in Figure 5.5: a static input nonlinearity, a linear dynamic system, and a static output nonlinearity. For more information about this model see for example [Zhu 2002].

In our case, sigmoid networks have been chosen for the input and output nonlinear functions, which can be defined as a sum of weighted sigmoid functions $(e^z + 1)^{-1}$. The linear system is a polynomial model with 1 zero, 2 poles with a delay set to 1.

The functions choice gives tunable parameters vectors to optimize. The identification consists to minimize the prediction error, where the parametric optimization problem is solved by the nonlinear least square method with the trust-region reflective Newton algorithm. For methodology details about this method, see [Nelles 2011]. From an implementation point of view, the identification has been performed with the System Identification Toolbox of MATLAB using the same inputs as the previous model (i.e: P_3 , T_3 , P_4 and u_{vgt} as in Figure 5.5).

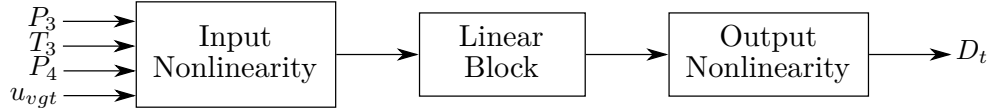


Figure 5.5: Hammerstein-Wiener model block diagram

5.2.3.3 Identification results

The identification of the two models is based on the data obtained with GT-POWER for a transient cycle (see WHTC in Appendix B), i.e P_3, T_3, P_4, u_{vgt} and the reference D_t . The results are depicted in Figure 5.6 associated with their FIT index (5.12) in Table 5.2. Then the models have been fed with the data obtained with a stationary cycle to evaluate their robustness to other operational points. This case is presented in Figure 5.7.

Table 5.2: *FIT* obtained for the different cases

Cycle	Model for D_t	
	Orifice eq.	HW
WHSC	76%	93.1%
WHTC	76.9%	96.4%

First, the FIT obtained for the both cycles and models are higher than 75%. Therefore, both models are valid for the considered operating points. As expected, the HW model significantly improves the FIT and the relative error is close to zero most of the time. However, the model obtained with the orifice equations does not manage to exactly estimate the stationary points but captures the global behavior where, most of the time, the relative error is less than 20%.

5.2.4 Summary of the nonlinear model of ω_{tc} and P_3

Finally, combining equations (5.3)-(5.7) and (5.10), the following nonlinear differential equations represent the dynamic of the turbocharger and the exhaust manifold pressure:

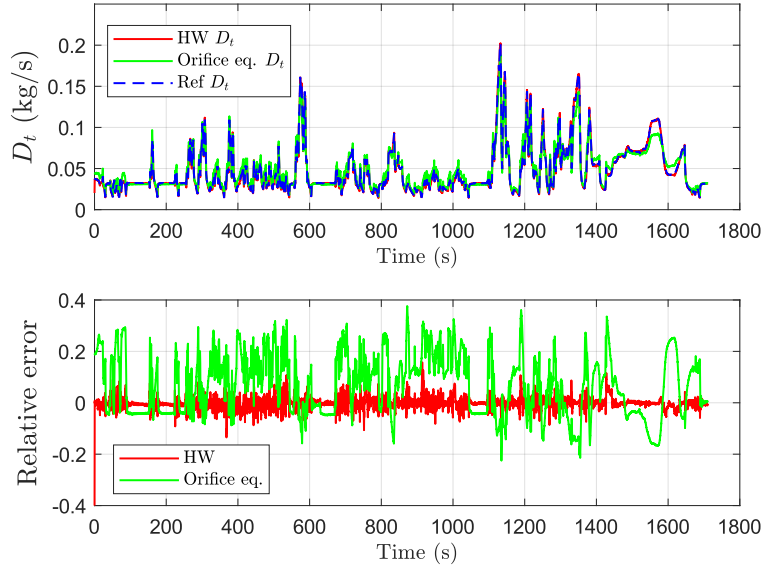


Figure 5.6: Identification results for transient cycle

$$\begin{aligned}
 \dot{\omega}_{tc}^2 &= \frac{2}{J_{tc}} \eta_t T_3 c_{p3} D_t \left(1 - \left(\frac{P_4}{P_3} \right)^{\frac{\gamma_3-1}{\gamma_3}} \right) \\
 &\quad - \frac{2}{J_{tc}} \frac{1}{\eta_c} T_1 c_{p1} D_c \left(\left(\frac{P_2}{P_1} \right)^{\frac{\gamma_1-1}{\gamma_1}} - 1 \right) \\
 \dot{P}_3 &= \frac{RT_3}{V_3} (D_{asp} + D_f - D_{egr} - D_t)
 \end{aligned} \tag{5.16}$$

where D_t , for comparison purpose, will be calculated using the two models defined in the previous Section 5.2.3: the orifice flow equations (5.13)-(5.15) and the identified Hammerstein-Wiener model.

Remark 5.3

Due to their form, the previous model is difficult to validate in open-loop because it has a pure integral behavior. However, this kind of model is common in the literature.

5.3 Observer design

To take into account the nonlinearities of the system described in Section 5.2.4, a quasi-LPV approach is considered to design an observer for the exhaust manifold pressure P_3 .

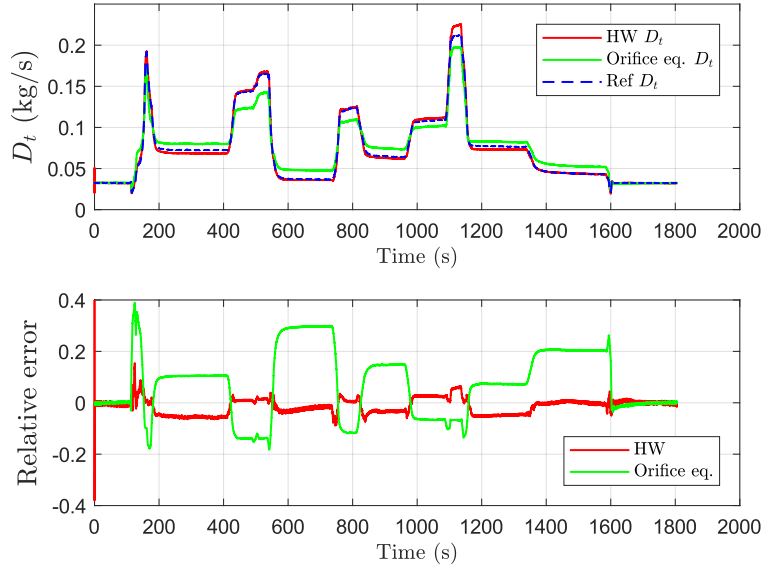


Figure 5.7: Identification results for stationary cycle

5.3.1 LPV modeling

Let denotes $[x_1 \ x_2]^T = [\omega_{tc}^2 \ P_3]^T$ the state vector. We can transform the nonlinear system described by (5.16) into the following quasi-LPV form:

$$\begin{bmatrix} \dot{x}_1 \\ \dot{x}_2 \end{bmatrix} = \begin{bmatrix} 0 & \rho_1 \\ 0 & \rho_2 \end{bmatrix} \begin{bmatrix} x_1 \\ x_2 \end{bmatrix} + \begin{bmatrix} 1 & 0 \\ 0 & 1 \end{bmatrix} \begin{bmatrix} u_1 \\ u_2 \end{bmatrix} \quad (5.17)$$

with, in the case where D_t is given by (5.13)-(5.15),

$$\begin{aligned} \rho_1 &= \eta_t T_3 c_{p3} \left(1 - \left(\frac{P_4}{P_3} \right)^{\frac{\gamma-1}{\gamma}} \right) A(u_{vgt}) \frac{1}{\sqrt{RT_3}} \Psi \left(\frac{P_4}{P_3} \right) \frac{2}{J_{tc}} \\ \rho_2 &= -A(u_{vgt}) \frac{1}{\sqrt{RT_3}} \Psi \left(\frac{P_4}{P_3} \right) \frac{RT_3}{V_3} \end{aligned} \quad (5.18)$$

and

$$\begin{aligned} u_1 &= -\frac{2}{J_{tc}} \mathcal{P}_c \\ u_2 &= \frac{T_3 R}{V_3} (D_{asp} + D_f - D_{egr}) \end{aligned} \quad (5.19)$$

Remark 5.4

This case is convenient for the LPV formulation since (5.13) depends linearly on P_3 . In the case where D_t is obtained by the Hammerstein-Wiener (HW) model, we

choose to divide this nonlinearity by P_3 for the varying parameters. Thus they will be expressed as:

$$\begin{aligned}\rho_1 &= \eta_t T_3 c_{p3} \left(1 - \left(\frac{P_4}{P_3} \right)^{\frac{\gamma-1}{\gamma}} \right) \frac{D_t(HW)}{P_3} \frac{2}{J_{tc}} \\ \rho_2 &= -\frac{RT_3}{V_3} \frac{D_t(HW)}{P_3}\end{aligned}\quad (5.20)$$

It is worth noting that (5.17) is a quasi-LPV model since ρ_1 and ρ_2 depend on $x_2 = P_3$. Therefore, in the LPV observer form, ρ_1 and ρ_2 will be computed on-line using the estimated pressure \hat{P}_3 .

5.3.2 Problem formulation

Like before, let denote $[x_1 \ x_2]^T = [\omega_{tc}^2 \ P_3]^T$ and u as in (5.19), then (5.17) is rewritten as the LPV system:

$$\begin{aligned}\dot{x} &= A(\rho)x + Bu + Ew \\ y &= Cx \\ z &= C_z x\end{aligned}\quad (5.21)$$

where:

$$\begin{aligned}A(\rho) &= \begin{bmatrix} 0 & \rho_1 \\ 0 & \rho_2 \end{bmatrix}; & B &= I_2; & E &= I_2 \\ C &= [1 \ 0]; & C_z &= [0 \ 1]\end{aligned}\quad (5.22)$$

z represents the variable to be estimated, i.e., P_3 , and w is a vector of additive uncertainties that has to be attenuated.

Following the procedure presented in Chapter 1, since the parameter dependence of (5.17) is affine, the matrix $A(\rho)$ can be transformed into a convex polytopic form such that:

$$A(\rho) = \sum_{i=1}^4 \mu_i(\rho) A_i, \quad \mu_i(\rho) \geq 0, \quad \sum_{i=1}^4 \mu_i(\rho) = 1 \quad (5.23)$$

To determine the bounds of ρ_1 and ρ_2 , thus the vertices of the polytope, we used the data obtained for a transient cycle in the formulation (5.18). Its results that $\rho_1 \in [\underline{\rho}_1, \overline{\rho}_1] = [13.42, 1187.08]$ and $\rho_2 \in [\underline{\rho}_2, \overline{\rho}_2] = [-33.44, -3.79]$.

Following Algorithm 1, the vertices A_i of the polytope could be given as:

$$\begin{aligned}A_1 &= \begin{bmatrix} 0 & \underline{\rho}_1 \\ 0 & \underline{\rho}_2 \end{bmatrix}; & A_2 &= \begin{bmatrix} 0 & \overline{\rho}_1 \\ 0 & \underline{\rho}_2 \end{bmatrix} \\ A_3 &= \begin{bmatrix} 0 & \underline{\rho}_1 \\ 0 & \overline{\rho}_2 \end{bmatrix}; & A_4 &= \begin{bmatrix} 0 & \overline{\rho}_1 \\ 0 & \overline{\rho}_2 \end{bmatrix}\end{aligned}\quad (5.24)$$

In the case of two parameters, [Algorithm 2](#) gives the interpolation functions $\mu_i(\rho)$ defined as:

$$\begin{aligned}\mu_1(\rho) &= \left(\frac{\bar{\rho}_1 - \rho_1}{\bar{\rho}_1 - \underline{\rho}_1} \right) \times \left(\frac{\bar{\rho}_2 - \rho_2}{\bar{\rho}_2 - \underline{\rho}_2} \right) \\ \mu_2(\rho) &= \left(\frac{\bar{\rho}_1 - \rho_1}{\bar{\rho}_1 - \underline{\rho}_1} \right) \times \left(\frac{\rho_2 - \underline{\rho}_2}{\bar{\rho}_2 - \underline{\rho}_2} \right) \\ \mu_3(\rho) &= \left(\frac{\rho_1 - \underline{\rho}_1}{\bar{\rho}_1 - \underline{\rho}_1} \right) \times \left(\frac{\bar{\rho}_2 - \rho_2}{\bar{\rho}_2 - \underline{\rho}_2} \right) \\ \mu_4(\rho) &= \left(\frac{\rho_1 - \underline{\rho}_1}{\bar{\rho}_1 - \underline{\rho}_1} \right) \times \left(\frac{\rho_2 - \underline{\rho}_2}{\bar{\rho}_2 - \underline{\rho}_2} \right)\end{aligned}\tag{5.25}$$

The chosen objective is to estimate the state vector x of [\(5.21\)](#) while minimizing a H_∞ criterion with respect to disturbance terms. The proposed polytopic LPV observer has the following structure:

$$\begin{aligned}\dot{\hat{x}} &= \sum_{i=1}^4 (\mu_i(\hat{\rho})(A_i \hat{x} + L_i(y - \hat{y}))) + Bu \\ \hat{y} &= C \hat{x} \\ \hat{z} &= C_z \hat{x}\end{aligned}\tag{5.26}$$

where L_i are unknown matrices to be determined.

Let T_{we_z} denote the transfer from w to the state error estimation $e_z = z - \hat{z}$. The objective here is to design a LPV polytopic observer [\(5.26\)](#) for system [\(5.17\)](#)-[\(5.18\)](#) to solve the following problem:

Problem 5.1

Design an observer [\(5.26\)](#) for system [\(5.17\)](#)-[\(5.18\)](#) such that:

(1) the induced- L_2 norm from for T_{we_z} is bounded by γ_∞ , i.e

$$\sup_{w \neq 0, w \in L_2} \frac{\|e_z\|_2}{\|w\|_2} = \|T_{we_z}\|_\infty \leq \gamma_\infty\tag{5.27}$$

(2) the poles of T_{we_z} at each vertex of the polytope are in a desired region to ensure both convergence performance and stability

5.3.3 Synthesis

First let us notice that, even if the parameter vector is using estimated state variables (due to the quasi-LPV model), we assume here that $\hat{\rho} = \rho$ for the synthesis of the observer [\(5.26\)](#). As presented in [[Heemels et al. 2010](#)], a robustness study with respect

to uncertainty on the scheduling variables is important and could be studied in future works. Following Proposition 1.2 and Proposition 1.3, we can establish the proposition hereunder:

Proposition 5.1

Let consider the LPV system (5.21)-(5.23) and the observer (5.26). If there exists matrices Y_i and a symmetric positive-definite matrix P and for a given α , r and θ , such that:

$$PA_i - Y_i C + A_i^T P - C^T Y_i^T + 2\alpha P < 0 \quad (5.28)$$

$$\begin{bmatrix} -rP & PA_i - Y_i C \\ * & -rP \end{bmatrix} < 0 \quad (5.29)$$

$$\begin{bmatrix} \sin \theta (PA_i - Y_i C + A_i^T P - C^T Y_i^T) & \cos \theta (PA_i - Y_i C - A_i^T P + C^T Y_i^T) \\ * & \sin \theta (PA_i - Y_i C + A_i^T P - C^T Y_i^T) \end{bmatrix} < 0 \quad (5.30)$$

$$\begin{aligned} & \min \quad \gamma_\infty \\ & \text{s.t.} \quad \begin{bmatrix} PA_i - Y_i C + A_i^T P - C^T Y_i^T & E & PC_z^T \\ * & -\gamma_\infty I & 0 \\ * & * & -\gamma_\infty I \end{bmatrix} < 0 \end{aligned} \quad (5.31)$$

for all $i = 1, 2, \dots, 2^N$, then the poles of T_{we_z} at each vertex are in the considered area depicted in Fig. 5.8 and its H_∞ norm is minimized by γ_∞ . Besides, the observer gains L_i are deduced as $L_i = P^{-1}Y_i$.

Proposition 5.1 is now applied to solve Problem 5.1, for a given α , θ and r . There exists a compromise between the area of the pole placement and the disturbance attenuation. Increase θ will reduce the value of γ_∞ but the damping will be more important. After several synthesis, the pole placement parameters are chosen as: $\alpha = 4$, $\theta = \pi/6$, $r = 80$ which gives $\gamma_\infty = 0.8902$ and the following observer gains at the 4 vertices of the polytope:

$$\begin{aligned} L_1 &= [70.60 \quad 1.10]^T, \quad L_2 = [96.79 \quad 2.01]^T \\ L_3 &= [70.60 \quad 1.93]^T, \quad L_4 = [101.91 \quad 2.36]^T \end{aligned}$$

The roots locus of T_{we_z} at each vertex are depicted in Figure 5.8. All the poles have a strictly negative real part and are in the desire cone. One can also observe that two conjugate poles (the cyan ones) are at the limit of the cone due to the optimization.

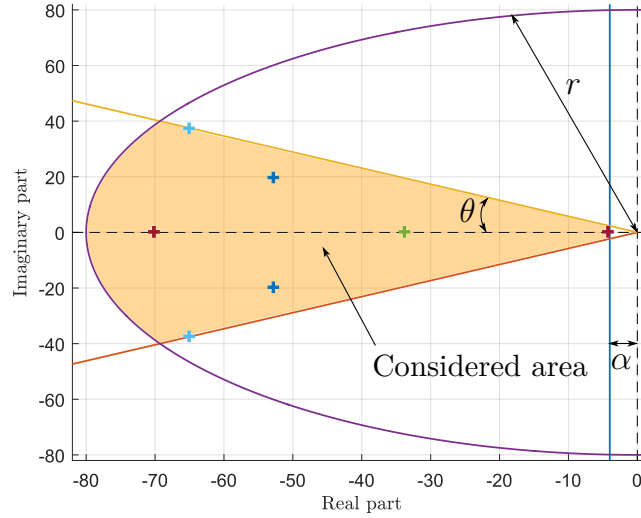
Figure 5.8: Roots locus of T_{wez}

Figure 5.9 shows the frequency response of T_{wez} for different frozen values of the vector ρ . One can observe a good disturbance attenuation in low and high frequencies, without peaks, regardless the value of ρ .

5.4 Simulation results

Like in Section 5.2.3.3, the validation of the observer will be performed on the stationary and the transient cycles (see Appendix B). These two cycles are used as inputs for the GT-POWER simulator, then the needed data are collected to feed the observer (5.26) of the system (5.17). The scheme presented in Figure 5.10, summarizes the considered simulation tests. In addition to both cycles, we will compare the results with the two different models for D_t defined in Section 5.2.3.

The global performance results, evaluated with the NRMS index (see Appendix A), for the different cases and scenarios treated in the following are summarized in Table 5.3.

Table 5.3: NRMS obtained for the different cases

Cycle	Model for D_t	
	Orifice eq.	HW
WHSC	6.1%	2.5%
WHTC	4.9%	1.9%

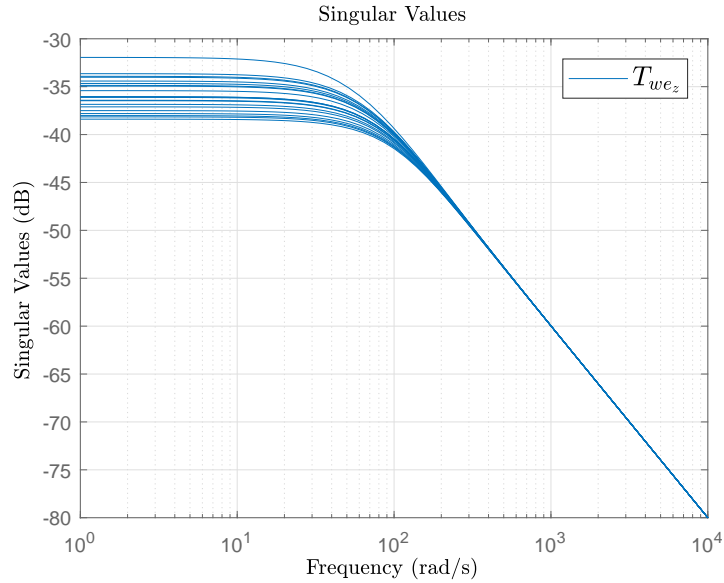


Figure 5.9: Frequency response of $T_{wez}(\rho)$

5.4.1 Case 1: D_t defined by the orifice equations (5.13)-(5.15)

The results obtained for the two scenarios (WHSC/WHTC) in the case where D_t is defined by the orifice flow equations (5.13)-(5.15), are respectively presented in Figure 5.11 and Figure 5.12. The observer manages to follow the variations of the pressure with a reasonable error for both scenarios, since the relative error is less than 10% most of the time for both cycles. However the bias is important for some operating points and highlighted with the stationary cycle in Figure 5.11 around 200s or between 400 and 600s. This is the direct consequence of the modeling error shown in Figure 5.7. Besides, one can see that the observer tends to overestimate P_3 when D_t is underestimated.

5.4.2 Case 2: D_t defined by HW model

In this case D_t is defined by the Hammerstein-Wiener model identified in Section 5.2.3. The results for the WHSC cycle are depicted in Figure 5.13 and for the WHTC in Figure 5.14. One can observe that the estimation is improved and, for some stationary points, the error is close to zero. This is confirmed by the NRMS results shown in Table 5.3.

This significant improvement can only be attributed to the better definition of D_t , since we have seen in Figure 5.6 and Figure 5.7, that the HW model estimates almost perfectly D_t . One can explain the remaining errors by:

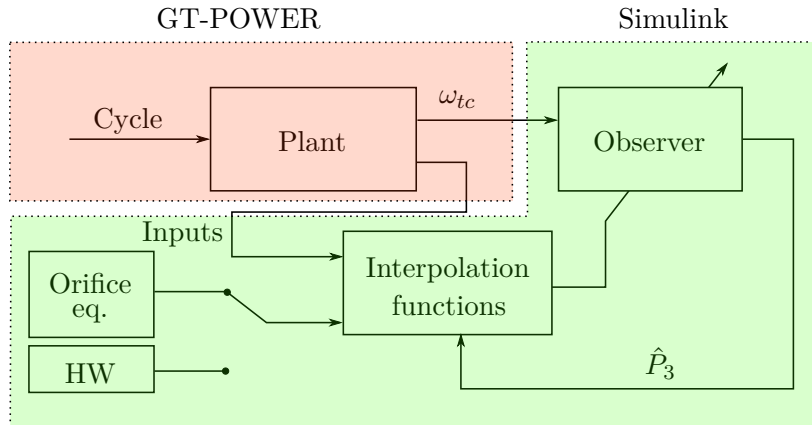


Figure 5.10: Scheme of the simulation tests

- (1) The constant assumption made on the thermal coefficients c_{pi} and γ_i
- (2) The accuracy of the efficiency maps of the turbocharger depicted in [Figure 5.3](#) and [Figure 5.4](#)
- (3) Using the intake manifold pressure to calculate the compressor power (5.7) instead of using the pressure measurement just after the compressor

5.5 Some ongoing studies

During the research work, other topics have been investigated to improve the estimation or the diagnosis of the turbocharger. Due to their similarities with the previous study, only the outline will be presented hereafter.

5.5.1 Pressure and EGR mass flow estimation

One of the weaknesses of the previous observer is that it uses as an input, the EGR mass flow rate D_{egr} . However, as we have underlined, in [Chapter 4](#), this variable is poorly estimated and thus it could be interesting, in practice, to overcome this problem.

In fact, the model established in [Section 5.2.4](#) could be used to also estimate the variable D_{egr} if we assume $\dot{D}_{egr} = 0$ in u_2 . Then, the same procedure as in [Section 5.3.1](#) can be followed and an observer can be designed for the following quasi-LPV system:

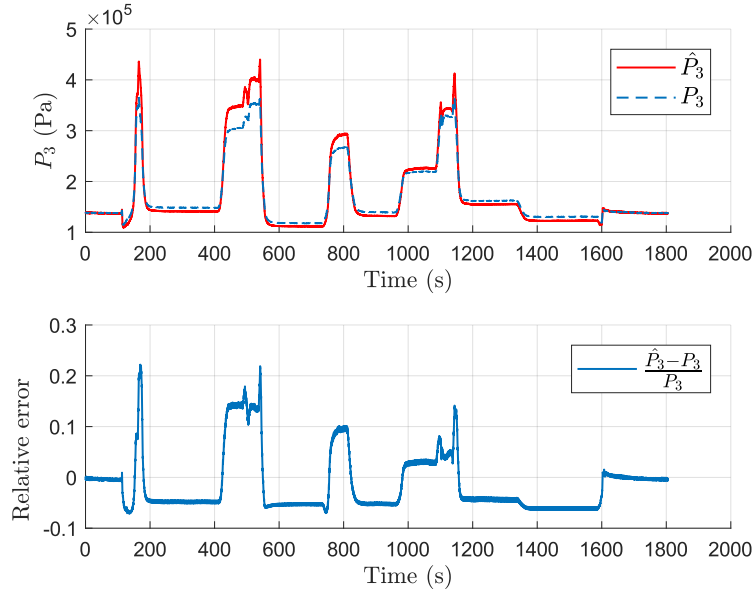


Figure 5.11: Case 1: WHSC cycle with D_t defined by orifice equations (5.13)-(5.15)

$$\begin{bmatrix} \dot{x}_1 \\ \dot{x}_2 \\ \dot{x}_3 \end{bmatrix} = \begin{bmatrix} 0 & \rho_1 & 0 \\ 0 & \rho_2 & \rho_3 \\ 0 & 0 & 0 \end{bmatrix} \begin{bmatrix} x_1 \\ x_2 \\ x_3 \end{bmatrix} + \begin{bmatrix} 1 & 0 \\ 0 & 1 \\ 0 & 0 \end{bmatrix} \begin{bmatrix} u_1 \\ u_2 \end{bmatrix} \quad (5.32)$$

$$y = x_1$$

where, $[x_1 \ x_2 \ x_3]^T = [\omega_{tc}^2 \ P_3 \ D_{egr}]^T$; ρ_1 , ρ_2 and u_1 are given respectively by (5.18) and (5.19). Finally, ρ_3 and u_2 are defined by:

$$\begin{aligned} \rho_3 &= \frac{RT_3}{V_3} \\ u_2 &= \frac{RT_3}{V_3} (D_{asp} + D_f) \end{aligned} \quad (5.33)$$

Then, an observer can be designed with the same procedure described in Section 5.3.3 to both estimate P_3 and D_{egr} .

5.5.2 Turbocharger efficiency estimation

The turbocharger is a key and complex component in the operation of the engine. Its monitoring is very important since any malfunction could damage all the engine and the after treatment system. An interesting indicator of the turbocharger's health could be the efficiencies of the compressor and the turbine like in [Ceccarelli 2012].

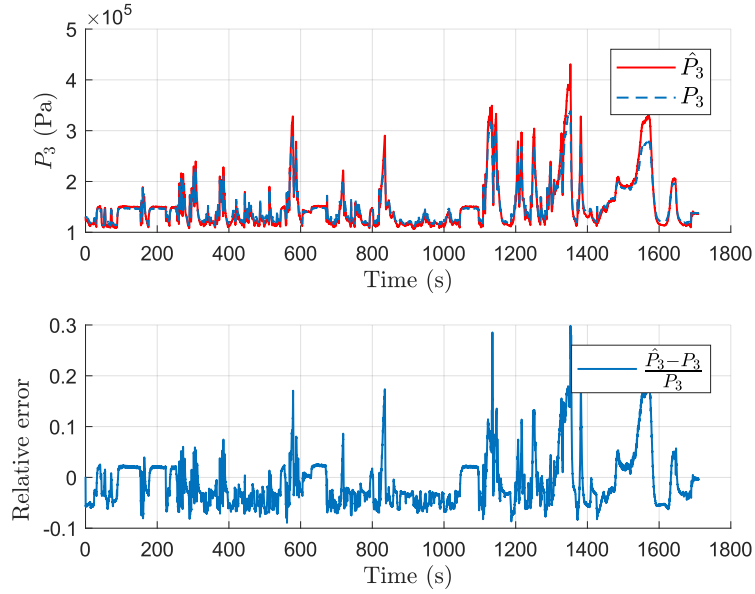


Figure 5.12: Case 1: WHTC cycle with D_t defined by orifice equations (5.13)-(5.15)

Thus, to estimate one of the efficiencies, assuming that the other is known, one can propose to use the model of the turbocharger dynamics:

$$\begin{aligned} \dot{\omega}_{tc}^2 &= \frac{2}{J_{tc}} \eta_t T_3 c_{p3} D_t \left(1 - \left(\frac{P_4}{P_3} \right)^{\frac{\gamma_3 - 1}{\gamma_3}} \right) - \frac{2}{J_{tc}} \frac{1}{\eta_c} T_1 c_{p1} D_c \left(\left(\frac{P_2}{P_1} \right)^{\frac{\gamma_1 - 1}{\gamma_1}} - 1 \right) \\ y &= \omega_{tc}^2 \end{aligned} \quad (5.34)$$

It appears that (5.34) depends linearly on η_t and $\frac{1}{\eta_c}$. Therefore the problem becomes a case already treated in the previous chapters where we need to estimate an unknown input. Thus, the methods seen in Chapter 1 could be used. Alternatively, one could extend the system (5.34) with a null dynamic of η_t or $\frac{1}{\eta_c}$.

5.6 Conclusion

In this chapter, we have proposed a LPV observer-based solution in order to estimate the exhaust manifold pressure of a turbocharged diesel engine. In Section 5.2, a mean value model of the turbocharger and pressure dynamics has been developed. In this section, we also proposed two models of the turbine mass flow rate: a standard physical model from the orifice flow equations and a black-box Hammerstein-Wiener model.

Then, in Section 5.3, thanks to the LPV framework, a polytopic LPV observer has been designed to estimate the state space vector of the system. It is worth mentioning

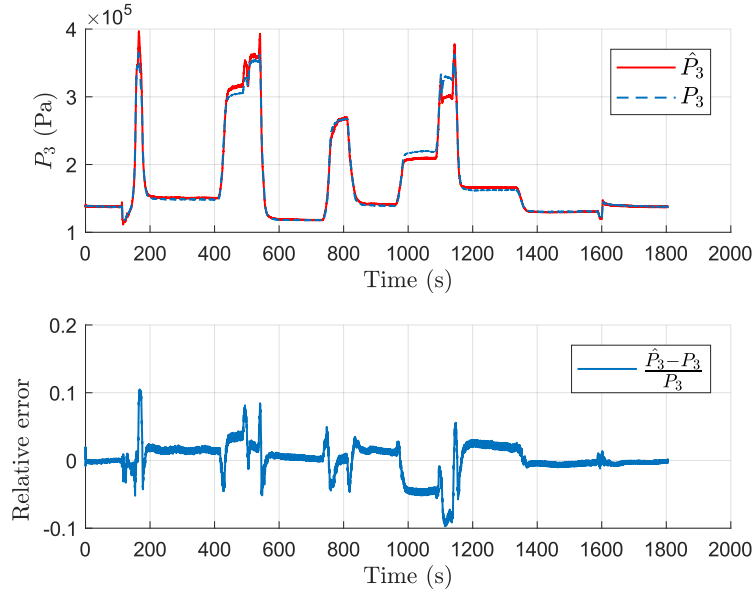


Figure 5.13: Case 2: WHSC cycle with D_t defined by the Hammerstein-Wiener model

that this quasi-LPV observer internally depends on the estimated state variable \hat{x}_2 , and further works must be performed to study the effects of the uncertainties in the parameters due to the estimation of P_3 as investigated in [Heemels et al. 2010].

In Section 5.4, the observer has been tested in a high-fidelity simulator in GT-POWER in different scenarios. It has been shown that the observer has a low estimation error in every tested scenarios. As shown in Table 5.3, the HW model has the best estimation results. This observation could be expected because it has been established in Section 5.2.3 that this model has the best fit. However, this model seems to be too complex for a real-time implementation. Then, in practical implementations, the orifice flow equations may be preferred.

Finally, in Section 5.5 perspectives have been proposed using the same model established in this chapter.

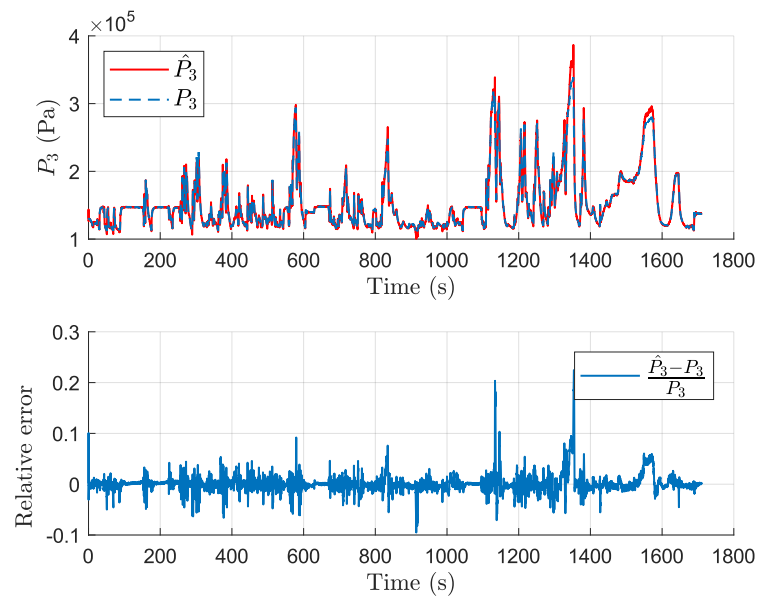


Figure 5.14: Case 2: WHTC cycle with D_t defined by the Hammerstein-Wiener model

Engine mass flow rates estimation submitted to a sensor delay

Contents

6.1	Introduction	115
6.2	Time-delay system modeling	118
6.2.1	O ₂ concentration in the intake manifold	119
6.2.2	O ₂ concentration in the exhaust manifold	119
6.2.2.1	After the DPF	120
6.2.3	Delay modeling	121
6.2.4	Summary of time-delay system modeling	122
6.3	Time-delay observer synthesis	123
6.3.1	Analysis and LPV formulation	123
6.3.2	Design of LPV time-delay observers	127
6.4	Results for EGR and Inlet air mass flow rates estimation	132
6.4.1	Synthesis based on Theorem 6.1	133
6.4.2	Synthesis based on Theorem 6.2	137
6.5	Conclusion	141

6.1 Introduction

To have a suitable control of the pollutants, it is needed to know what is the gas composition at the inlet of the engine [Guzzella and Onder 2010]. Therefore, the quantity of fresh air and recirculated gas, and thus the inlet air mass flow rate and EGR mass flow rate respectively, have to be known as accurately as possible. To estimate both flows, Volvo equipped its medium duty engines with a lambda sensor located just after the turbine of the turbocharger (see Figure 6.1). This sensor enables to measure the oxygen concentration of the exhaust gas mixture and, assuming that the quantity of injected fuel is known, it is possible to reconstruct the EGR and the inlet air mass flow rates.

Nevertheless, the NOx sensor, located after the Diesel Particulate Filter (DPF) in the after-treatment system, can also provide a value of the oxygen concentration. Since there are no additional pipes or reaction which modifies this concentration, its value must be the same than the one measured by the lambda sensor. So why has it been decided to add a redundant sensor? The answer is given by the fact that there are around 2 meters of pipe length between the two considered sensors. Thus, there exists a significant transport delay, in particular at low load, and the pollutants control performances are not acceptable with the estimates based on the NOx sensor. That's why an extra sensor has been added to overcome the delay. It is this sensor configuration that has been used in Chapter 4 to estimate the EGR mass flow rate.

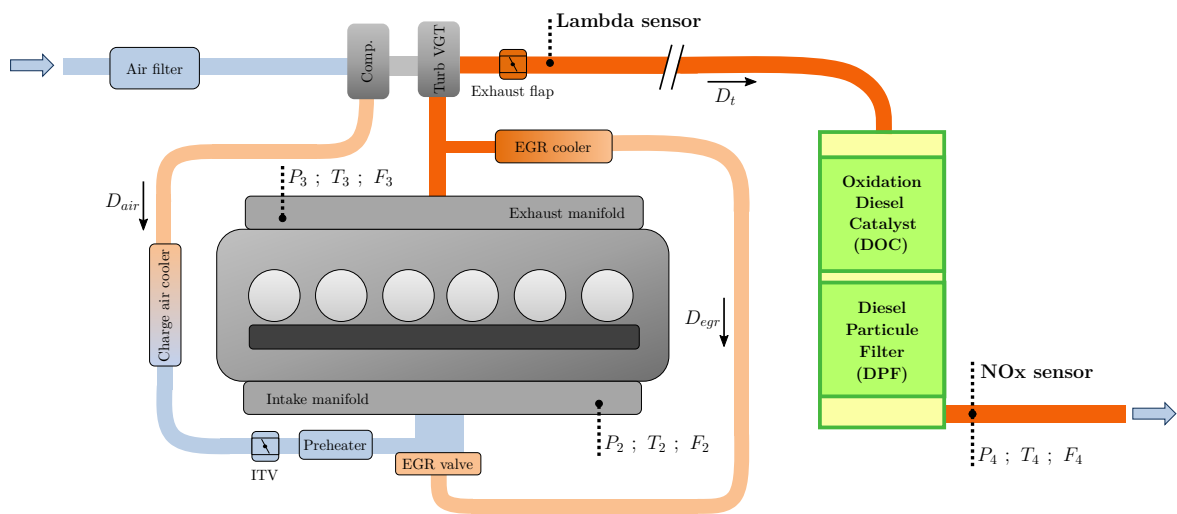


Figure 6.1: Schematic view of the air path and the after treatment system

To illustrate this issue, we will use the data collected from a test-cell equipped with a medium-duty 6-cylinders 8L diesel engine, as presented in Figure 6.1. The data for this case are obtained with a stationary and a transient cycle (WHSC and WHTC respectively, see Appendix B). If the current method (which does not take into account any delay) is applied to estimate the inlet air and EGR mass flow rates, we obtain the results depicted in Figure 6.2. In these Figures, the reference variables D_{air} and D_{egr} are calculated with the lambda sensor, so without delay, and \hat{D}_{air} and \hat{D}_{egr} are calculated with the NOx sensor. For the stationary cycle in Figure 6.2(a) and Figure 6.2(b), there is no particular problem: both estimates follow the reference flows. On the other hand, for the transient cycle in Figure 6.2(c) and Figure 6.2(d), where the delay influence is more significant, the estimates are very deteriorated and not suitable for pollutants control perspective. In this chapter, we aim at improving the flows estimation by taking into account the measurement delay of the NOx sensor.

The transport delay from the exhaust gas to the O₂ sensor (in our case the lambda or NOx sensor) is generally addressed in a control perspective as in [Jankovic and Kolmanovsky 1999] or [Kahveci and Jankovic 2010] where the air-to-fuel ratio control

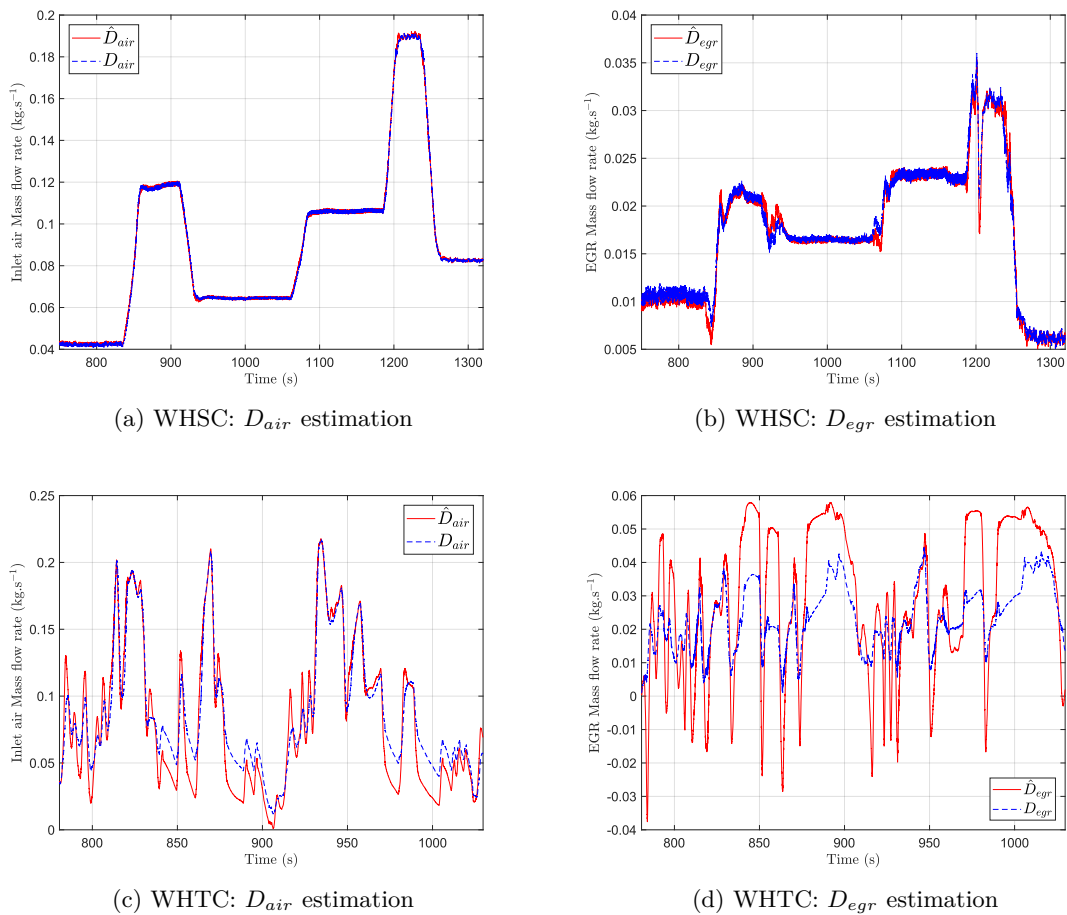


Figure 6.2: Case 0: flows estimation without taking account the delay

in Spark Ignition engines studied. It appears that this problem seems to be specific to the trucks industry because, for private cars, the after-treatment system is not departed far from the engine but located just after, so the pipe length is significantly reduced and the delay as well.

In Chapter 4 an estimation of the EGR mass flow rate has been proposed assuming that the air mass flow rate was known. In this chapter, we propose to design LPV time-delay observers to estimate the inlet air and EGR mass flow rates only based on the information provided by the NO_x sensor in order to physically remove the lambda sensor. To do so, a time-delay model is defined in Section 6.2 based on a volume control approach. Then, in Section 6.3 the theoretical design of an LPV time-delay observer is introduced, and applied in Section 6.4 where the results are presented. Finally, conclusions are stated in Section 6.5.

Table 6.1: Nomenclature

Notation	Description	Unit
N_{eng}	Engine speed	rpm
T	Temperature of a subsystem	K
P	Pressure of a subsystem	Pa
V	Volume of a subsystem	m ³
F	Specie gas concentration	%
R	Ideal gas constant for the air	J.kg ⁻¹ .K ⁻¹
D	Mass flow rate	kg.s ⁻¹
Subscript		
2	Inside the intake manifold	
3	Inside the exhaust manifold	
4	Inside the volume located after the DPF	
<i>air</i>	Related to the inlet air	
<i>t</i>	Related to the turbine	
<i>egr</i>	Related to the EGR loop	
<i>f</i>	Related to the fuel	

6.2 Time-delay system modeling



Figure 6.3: Control volume

To develop a time-delay model of the engine air-path, a control volume approach will be considered as in [Castillo 2013].

Let first define the O₂ concentration in a gas mixture. It is the ratio of its mass between the total gas mass inside the control volume depicted in Figure 6.3:

$$F = \frac{m_{O_2}}{m_{tot}} \quad (6.1)$$

Then, deriving (6.1), one gets:

$$\dot{F} = \frac{RT}{PV} D_{in} (F_{in} - F) \quad (6.2)$$

To describe the O_2 concentration behavior inside different parts of the engine, (6.2) will be applied to three volumes: the volume inside the intake manifold, the exhaust manifold and the volume located just after the DPF.

Notation 2

The notations used in this section and hereafter are defined in Table 6.1 and follow the schematic view of Figure 6.1. Besides, let us mention that the time dependency of the variables T , P , F and D will be reported only if the variable is submitted to a delay.

6.2.1 O_2 concentration in the intake manifold

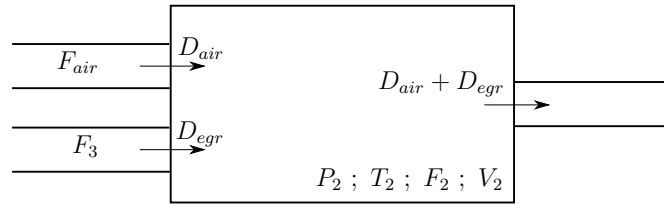


Figure 6.4: Intake manifold volume

The volume depicted in Figure 6.4 is subject to two inlet flows: one from the ambient air, with a concentration F_{air} (which depends mainly on the humidity and altitude) and one from the EGR loop. Therefore, one can model the evolution of O_2 concentration in the intake manifold by:

$$\dot{F}_2 = \frac{RT_2}{P_2V_2} (D_{air}(F_{air} - F_2) + D_{egr}(F_3 - F_2)) \quad (6.3)$$

6.2.2 O_2 concentration in the exhaust manifold

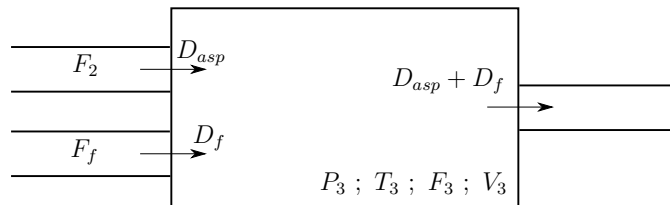


Figure 6.5: Exhaust manifold volume

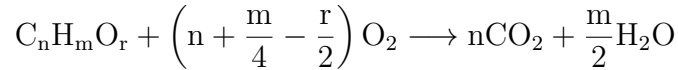
Here, two flows are coming in for this volume (Figure 6.5): one from the intake manifold and the flow induced by the fuel injection. Thus, the dynamics of F_3 can be

described by:

$$\dot{F}_3 = \frac{RT_3}{P_3 V_3} (D_{asp}(F_2 - F_3) + D_f(-F_f - F_3)) \quad (6.4)$$

Note that there is a minus sign before F_f because D_f consumes a F_f concentration of O_2 inside the manifold.

For a diesel engine, the value of F_f is determined by the chemical reaction between a hydrocarbon molecule and some O_2 given by [Flagan and Seinfeld 2012]:



Therefore, $F_f = \left(n + \frac{m}{4} - \frac{r}{2} \right)$ where n , m and r are given by the nature of the fuel used for the combustion.

Remark 6.1

The stoichiometric Air Fuel Ratio (AFR) is often used to find F_f since it is a classical known value in the combustion process. It is defined as:

$$AFR_{stoich} = \frac{m_{air,stoich}}{m_f} \simeq 14.5 \text{ (for diesel)} \quad (6.5)$$

$$\simeq 12.5 \text{ (for biodiesel)}$$

Thus, one can just multiply this value by 20.95% (the O_2 concentration in dry air) to get F_f .

The air mass flow aspirated by the engine will be expressed following the formula in Appendix C.

6.2.2.1 After the DPF

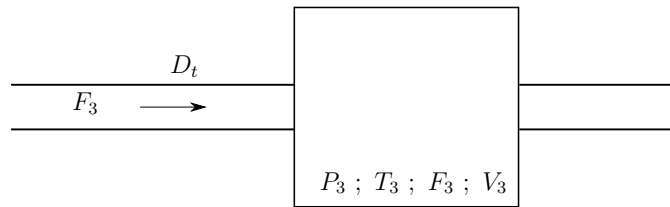


Figure 6.6: Exhaust volume

Contrary to the previous ones, just one flow comes inside this volume (Figure 6.6). Due to the pipe length, the O_2 concentration F_4 is the exhaust concentration one, F_3 , delayed by the transport through the pipe associated with the dynamics of the volume. Thus, one can model the O_2 concentration inside this volume by:

$$\dot{F}_4 = \frac{RT_4}{P_4V_4} D_t (F_3(t - h(t)) - F_4) \quad (6.6)$$

where $h(t)$ is the time transport delay.

Remark 6.2

As exposed in [Chapter 5](#), the turbine mass flow rate D_t can be determined by models as those obtained with the orifice flow equations or with the Hammerstein-Wiener model. In [Chapter 5](#), data obtained from a GT-POWER model have been used to calibrate these models. However, due to the high gas temperature at the exhaust, D_t is not measured at the Volvo test cell. Thus a static approximation of this variable defined as: $D_t = D_{air} + D_f$ will be used in this study to compute D_t offline for performance assessment.

6.2.3 Delay modeling

As explained in [[Bresch-Pietri and Petit 2016](#)], the time propagation $h(t)$ of a fluid with a varying speed $v(t)$ through a pipe of length L , can be defined according to:

$$\int_{t-h(t)}^t v(s).ds = L \quad (6.7)$$

In our case, the gas speed evolution along the pipe is not measured but, it can be related, through the ideal gas law (see for example [[Bresch-Pietri 2012](#)]), to thermodynamic conditions and mass flow rate that are measured or estimated. One can obtain:

$$v(t) = \frac{1}{S} \frac{RT_4}{P_4} D_t \quad (6.8)$$

where S is the pipe area, considered as constant here.

As a first approximation, at steady state conditions, the following relation can be deduced from (6.7), (6.8) and $V_4 = SL$ for:

$$\int_{t-h(t)}^t D_t(s).ds = \frac{V_4 P_4}{RT_4} \Rightarrow h(t) = \frac{V_4 P_4}{RT_4} \frac{1}{D_t} \quad (6.9)$$

Assuming that $\frac{V_4 P_4}{RT_4}$ is constant, or slow varying, the following simple relation can be deduced:

$$h(t) = \frac{K_{delay}}{D_t} \quad (6.10)$$

where $K_{delay} \in \mathbb{R}^+$.

As explained in [Remark 6.2](#), D_t is estimated thus only K_{delay} is unknown in (6.10). K_{delay} will be identified by the nonlinear least square method with a trust-region reflective algorithm, where the sum squared error is minimized. The considered model is (6.6) where F_4 is measured by the NOx sensor, F_3 by the lambda sensor and P_4, T_4 by a pressure and temperature sensors. In short, the following optimization problem is solved:

$$\min_{K_{delay}} \sum (F_4 - F_4(model))^2 \quad \text{subject to} \quad \begin{cases} (6.6) \\ (6.10) \end{cases} \quad (6.11)$$

A transient cycle WHTC (see [Appendix B](#)) done on a test cell will be used to provide the needed data.

The FIT index (defined in [Appendix A](#)) of the whole cycle is 77% when the delay is not taken into account and, when the delay is taken into account, its value is 93%. For sake of clarity, just a partial result is depicted in [Figure 6.7](#). As we can see with the blue curve which does not take into account the delay, the error can be very high in the transient phases and sometimes, the blue and green curves could be in opposition of phase as around 720s. It explains the bad results observed in [Figure 6.2\(d\)](#) and [Figure 6.2\(c\)](#) and the low value of the FIT index. Even if the delay's model (6.10) is simple, the red curve manages to capture all the oscillations and the rising slope of the transients. Moreover the FIT index is high which assesses the performance.

One can also observe in [Figure 6.7](#) that the model does not exactly follow the oscillations of the measure. A justification of this phenomena can be given by the fact that the time constant of the NOx sensor is higher than the lambda one. Thus, the NOx sensor cannot capture all the frequencies and inevitably, the performance of the estimator will be affected.

[Figure 6.8](#) shows the evolution of the modeled delay (6.10) in the whole cycle. At low load, thus when the exhaust flow is low, the delay reaches 1.67s and, at high load, 0.15s, thus $h(t) \in [0.15, 1.67]$.

6.2.4 Summary of time-delay system modeling

Finally, combining equations (6.3), (6.4) and (6.6), the following nonlinear time-delay system describes the O_2 concentration inside the intake and exhaust manifolds and inside the volume after the DPF:

$$\begin{cases} \dot{F}_2 = \frac{RT_2}{P_2V_2} (D_{air}(F_{air} - F_2) + D_{egr}(F_3 - F_2)) \\ \dot{F}_3 = \frac{RT_3}{P_3V_3} (D_{asp}(F_2 - F_3) + D_f(-F_f - F_3)) \\ \dot{F}_4 = \frac{RT_4}{P_4V_4} D_t (F_3(t - h(t)) - F_4) \end{cases} \quad (6.12)$$

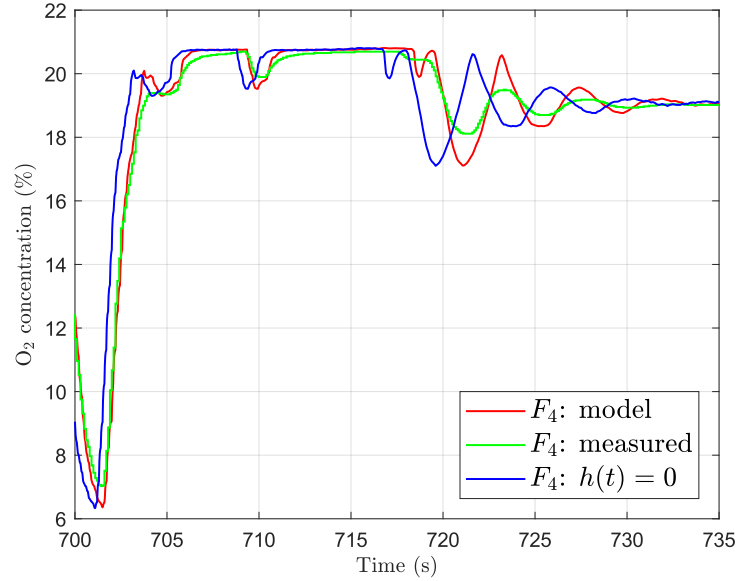


Figure 6.7: Identification results where the measure F_4 is obtained with NOx sensor and the model is (6.6)

where $h(t)$ is given by (6.10).

We assume that the following variables are measured or estimated: $T_2, P_2, T_3, P_3, T_4, P_4, D_f, D_t, D_{asp}$ and F_4 . F_f and F_{air} are constant.

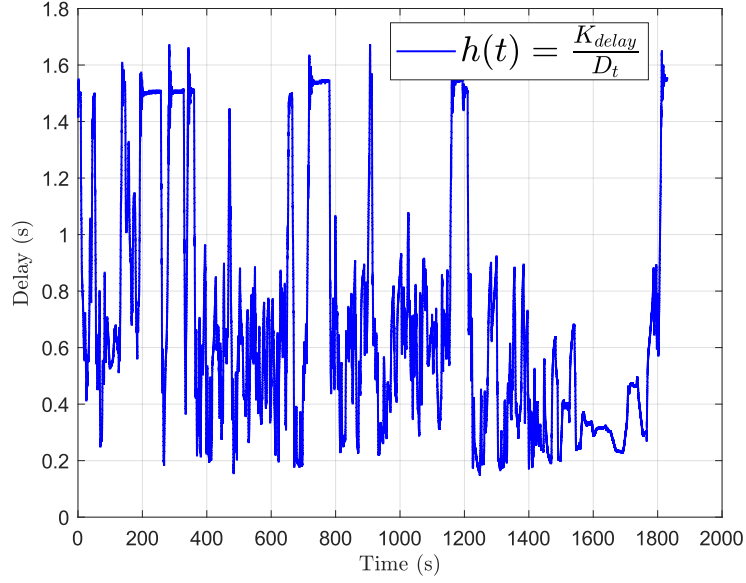
6.3 Time-delay observer synthesis

As a first step, this section is devoted to an LPV formulation and analysis, and in a second phase, some theoretical background is given to design an LPV observer for time-delay system.

6.3.1 Analysis and LPV formulation

The LPV framework is used to design an observer of D_{air} and D_{egr} . Thus, (6.12) can be turned into the following quasi-LPV (qLPV) model:

$$\begin{aligned} \dot{x}(t) &= A(\rho)x(t) + A_h(\rho)x(t - h(t)) + Bu_1(t) + F(\rho)f(t) \\ y(t) &= Cx(t) \end{aligned} \quad (6.13)$$


 Figure 6.8: Evolution of $h(t)$ defined in (6.10)

with, $x(t) = [F_2 \ F_3 \ F_4]^T$, $f(t) = [D_{air} \ D_{egr}]^T$, $u_1(t) = -\frac{RT_3}{P_3V_3}D_f F_f$, $\rho = [\rho_1 \ \rho_2 \ \rho_3 \ \rho_4 \ \rho_5]^T$ and the different matrices and parameters,

$$\begin{aligned}
 A(\rho) &= \begin{bmatrix} 0 & 0 & 0 \\ \frac{RT_3}{P_3V_3}D_{asp} & -\frac{RT_3}{P_3V_3}(D_{asp} + D_f) & 0 \\ 0 & 0 & -\frac{RT_4}{P_4V_4}D_t \end{bmatrix} := \begin{bmatrix} 0 & 0 & 0 \\ \rho_3 & \rho_4 & 0 \\ 0 & 0 & \rho_5 \end{bmatrix} \\
 A_h(\rho) &= \begin{bmatrix} 0 & 0 & 0 \\ 0 & 0 & 0 \\ 0 & \frac{RT_4}{P_4V_4}D_t & 0 \end{bmatrix} := \begin{bmatrix} 0 & 0 & 0 \\ 0 & 0 & 0 \\ 0 & -\rho_5 & 0 \end{bmatrix} \\
 F(\rho) &= \begin{bmatrix} \frac{RT_2}{P_2V_2}(F_{air} - F_2) & \frac{RT_2}{P_2V_2}(F_3 - F_2) \\ 0 & 0 \\ 0 & 0 \end{bmatrix} := \begin{bmatrix} \rho_1 & \rho_2 \\ 0 & 0 \\ 0 & 0 \end{bmatrix} \\
 B &= \begin{bmatrix} 0 \\ 1 \\ 0 \end{bmatrix} \\
 C &= [0 \ 0 \ 1]
 \end{aligned} \tag{6.14}$$

Notation 3

For sake of clarity, the time dependency of the parameters vector is omitted here

and hereafter. Thus $\rho = \rho(t)$.

Remark 6.3

The previous system (6.13) is qLPV because ρ_1 and ρ_2 depend on F_2 and F_3 which are also states of the model. This representation is not unique. For example, in (6.3) there is the term $D_{egr}(F_3 - F_2)$, which can be written as $f_2(t)x_2(t) - f_2(t)x_1(t)$ and thus converted into a qLPV form with two time-varying parameters. The proposed qLPV form (6.13) minimizes the number of varying parameter.

To estimate the desired variables, one can simply extend the states vector of (6.13) with D_{air} and D_{egr} associated with a null dynamics. So we assume:

$$\begin{aligned}\dot{D}_{air} &= 0 \\ \dot{D}_{egr} &= 0\end{aligned}\tag{6.15}$$

Therefore, the following system is derived from (6.13) and (6.15):

$$\begin{aligned}\dot{x}_e(t) &= A_e(\rho)x_e(t) + A_{he}(\rho)x_e(t - h(t)) + B_e u_1(t) \\ y_e(t) &= C_e x_e(t)\end{aligned}\tag{6.16}$$

with, $x_e(t) = [F_2 \ F_3 \ F_4 \ D_{air} \ D_{egr}]^T$ and,

$$\begin{aligned}A_e(\rho) &= \left[\begin{array}{c|c} A(\rho) & F(\rho) \\ \hline 0_{2,5} & \end{array} \right] \\ A_{he}(\rho) &= \left[\begin{array}{c|c} A_h(\rho) & 0_{3,2} \\ \hline 0_{2,5} & \end{array} \right] \\ B_e &= \begin{bmatrix} B \\ 0 \\ 0 \end{bmatrix} \\ C_e &= [0 \ 0 \ 1 \ 0 \ 0]\end{aligned}\tag{6.17}$$

Since the parameter dependence of (6.16) is affine, it can be turned into a polytopic form such as:

$$\begin{aligned}\dot{x}_e(t) &= \sum_{i=1}^{32} \mu_i(\rho)(A_{ei}x_e(t) + A_{hei}x_e(t - h(t))) + B_e(t) \\ y_e(t) &= C_e x_e(t)\end{aligned}\tag{6.18}$$

where the matrices A_{ei} and A_{hei} , correspond to the image of a vertex's polytope and $\mu_i(\rho)$ are the interpolation functions.

Without going into details on the observability conditions of LPV time-delay systems (one can refer to [Sename 2001] and [Briat 2008]), in the case where the stability of the designed observer is determined by a delay dependent condition, the following Proposition can be used to have a necessary condition for the observability of (6.18):

Proposition 6.1

Let denote a system generic LPV polytopic time-delay system as:

$$\begin{aligned} \dot{x}(t) &= \sum_{i=1}^{2^N} \mu_i(\rho)(A_i x(t) + A_{hi} x(t - h(t))) \\ y(t) &= Cx(t) \end{aligned} \quad (6.19)$$

where the matrices A_i and A_{hi} , correspond to the image of a vertex's polytope, $\mu_i(\rho)$ are the interpolation functions and $x \in \mathbb{R}^n$.

(6.19) is observable if the observability is fulfilled for $h(t) = 0$ at each vertex of the polytope, i.e:

$$\text{rank}(\mathcal{O}) = n \quad \text{with} \quad \mathcal{O} = \begin{bmatrix} C \\ C(A_i + A_{hi}) \\ \vdots \\ C(A_i + A_{hi})^{n-1} \end{bmatrix} \quad (6.20)$$

for all $i = 1 \dots 2^N$.

Applying the Proposition 6.1 to the extended system (6.18), gives $\text{rank}(\mathcal{O}) = 4 \neq 5$. A solution to this problem is to add another measurement to reconstruct all the states with an observer. We have two obvious choices:

- (1) Either one can use the exhaust manifold pressure P_3 , with its dynamics defined by:

$$\dot{P}_3 = \frac{RT_3}{V_3}(D_{asp} + D_f - D_{egr} - D_t) \quad (6.21)$$

- (2) Or the intake manifold pressure P_2 dynamics:

$$\dot{P}_2 = \frac{RT_2}{V_2}(D_{air} + D_{egr} - D_{asp}) \quad (6.22)$$

It has been established, in the previous Chapters, that the mass flow rates D_t and D_{asp} are uncertain and the P_3 sensor may be subject to failure. Therefore, the P_2 measurement, which is more reliable, will be preferred to design the observer. Combining (6.22) and the extended system (6.16), the following LPV time-delay system to observe is deduced:

$$\begin{aligned} \dot{x}_o(t) &= A_o(\rho)x_o(t) + A_{ho}(\rho)x_o(t - h(t)) + B_o u(t) \\ y_o(t) &= C_o x_o(t) \end{aligned} \quad (6.23)$$

with, $x_o(t) = [F_2 \ F_3 \ F_4 \ P_2 \ D_{air} \ D_{egr}]^T$, $y_o(t) = [F_4 \ P_2]^T$, $u(t) = [u_1(t) \ u_2(t)]^T$, and,

$$\begin{aligned}
A_o(\rho) &= \left[\begin{array}{cccccc} 0 & 0 & 0 & 0 & \rho_1 & \rho_2 \\ \rho_3 & \rho_4 & 0 & 0 & 0 & 0 \\ 0 & 0 & \rho_5 & 0 & 0 & 0 \\ 0 & 0 & 0 & 0 & \rho_6 & \rho_6 \\ \hline & & & & 0_{2,6} & \end{array} \right] \\
A_{ho}(\rho) &= \left[\begin{array}{cccccc} 0 & 0 & 0 & 0 & 0 & 0 \\ 0 & 0 & 0 & 0 & 0 & 0 \\ 0 & -\rho_5 & 0 & 0 & 0 & 0 \\ \hline & & & & 0_{3,6} & \end{array} \right] \\
B_o &= \begin{bmatrix} 0 \\ 1 \\ 0 \\ 1 \\ 0 \\ 0 \end{bmatrix} \\
C_o &= \begin{bmatrix} 0 & 0 & 1 & 0 & 0 & 0 \\ 0 & 0 & 0 & 1 & 0 & 0 \end{bmatrix}
\end{aligned} \tag{6.24}$$

where, according to (6.22),

$$\begin{aligned}
\rho_6 &= \frac{RT_2}{V_2} \\
u_2(t) &= -\frac{RT_2}{V_2} D_{asp}
\end{aligned} \tag{6.25}$$

$\rho_1, \rho_2, \rho_3, \rho_4, \rho_5$ and u_1 are defined in (6.14).

Again, (6.23) can be put into a polytopic form:

$$\begin{aligned}
\dot{x}_o(t) &= \sum_{i=1}^{64} \mu_i(\rho) (A_{oi}x_o(t) + A_{hoi}x_o(t - h(t))) + B_o u(t) \\
y_o(t) &= C_o x_o(t)
\end{aligned} \tag{6.26}$$

Thus, if Proposition 6.1 is applied to the system (6.26), it gives $\text{rank}(\mathcal{O}) = 6$. We have now enough measurements to estimate all the states and more precisely, D_{air} and D_{egr} .

6.3.2 Design of LPV time-delay observers

This section deals with the design of observers for LPV time-delay systems where two methods are presented. One developed in [Briat et al. 2011], and a new method based on the Finsler's lemma. Before going into details, let's first define some theoretical tools that will be used in the sequel.

The first one, the Jensen's inequality, is very useful to establish the stability of time-delay systems. The following proposition is a particular case of this inequality:

Proposition 6.2 (Jensen's inequality [Gu et al. 2003])

Let $x \in \mathbb{R}^n$ and $P \in \mathbb{R}^n$ with $P = P^T \succ 0$. Then the following inequality holds:

$$\left(\int_{t-h(t)}^t \dot{x}(\theta) d\theta \right)^T P \left(\int_{t-h(t)}^t \dot{x}(\theta) d\theta \right) \leq h(t) \int_{t-h(t)}^t \dot{x}(\theta)^T P \dot{x}(\theta) d\theta \quad (6.27)$$

The second one, the Finsler's lemma, permits to decouple the Lyapunov matrices from the controller or observer gains.

Lemma 6.1 (Finsler's lemma [Oliveira and Skelton 2001])

Let $x \in \mathbb{R}^n$, $Q \in \mathbb{R}^n$ is symmetric and $B \in \mathbb{R}^{m \times n}$ such that $\text{rank}(B) < n$. The following statements are equivalent:

- i) $x^T Q x < 0$, $\forall Bx = 0$, $x \neq 0$.
- ii) $\exists \mathcal{X} \in \mathbb{R}^{n \times m}$: $Q + \mathcal{X}B + B^T \mathcal{X}^T \prec 0$.

The objective is to design an LPV observer of the form:

$$\begin{aligned} \dot{\hat{x}}(t) &= A(\rho)\hat{x}(t) + A_h(\rho)\hat{x}(t-h(t)) + L(\rho)(y(t) - \hat{y}(t)) \\ &\quad + L_h(\rho)(y(t-h(t)) - \hat{y}(t-h(t))) \\ \hat{y}(t) &= C\hat{x}(t) \end{aligned} \quad (6.28)$$

for the class of LPV time-delay systems defined by:

$$\begin{aligned} \dot{x}(t) &= A(\rho)x(t) + A_h(\rho)x(t-h(t)) + Ew(t) \\ y(t) &= Cx(t) \\ z(t) &= C_z x(t) \end{aligned} \quad (6.29)$$

where $x \in \mathbb{R}^{n_x}$ is the state vector, $w \in \mathbb{R}^{n_w}$, \mathcal{L}_2 is the additive noise, $y \in \mathbb{R}^{n_y}$ is the measurement vector, $z \in \mathbb{R}^{n_z}$ is the signal to be estimated. The time-varying parameters ρ and the delay $h(t)$ are assumed to belong to the respective sets:

$$\begin{aligned} \mathcal{P}_\rho &:= \left\{ \rho = [\rho_1 \ \dots \ \rho_N]^T \in \mathbb{R}^N \text{ and } \rho_i \in [\underline{\rho}_i, \bar{\rho}_i], \text{ for all } i = 1 \dots N \right\} \\ \mathcal{H} &:= \{ h : \mathbb{R}_+ \rightarrow [0, h_m], \dot{h}(t) \leq \mu < 1 \} \end{aligned} \quad (6.30)$$

Therefore, the observation error $e(t) = x(t) - \hat{x}(t)$ is governed by the following dynamic equation:

$$\begin{aligned} \dot{e}(t) &= (A(\rho) - L(\rho)C) e(t) + (A_h(\rho) - L_h(\rho)C) e(t-h(t)) + Ew(t) \\ e_z(t) &= C_z e(t) \end{aligned} \quad (6.31)$$

In addition to $\rho \in \mathcal{P}_\rho$, the parameter dependence of the previous systems is affine thus can be turned into a polytopic form. In this case, each matrix M depending on the parameter vector could be written as:

$$M(\rho) = \sum_{i=1}^{2^N} \mu_i(\rho) M_i \quad (6.32)$$

where the matrices M_i , correspond to the image of a vertex's polytope and $\mu_i(\rho)$ are the interpolation functions.

The objective here is to find the gains in the LPV time-delay observer (6.28) for system (6.29) to solve the following problem:

Problem 6.1

Design an observer (6.28) for system (6.29) such that:

- (1) *the estimation error $e = x - \hat{x}$ is asymptotically stable ($e(t) \rightarrow 0$ when $t \rightarrow \infty$) for $w \equiv 0$.*
- (2) *the induced- \mathcal{L}_2 norm from the disturbance w to e_z is bounded by γ_∞ , i.e*

$$\sup_{w \neq 0, w \in \mathcal{L}_2} \frac{\|e_z\|_2}{\|w\|_2} \leq \gamma_\infty \quad (6.33)$$

There are many authors who proposed LMI solutions to solve the stability problem of time-delay systems. A good overview of these methods is presented in [Xu and Lam 2008]. However, in most of cases, if we substitute the corresponding matrices of (6.31) into some existing stability results, there will be multiple induced products between the observer gains and the Lyapunov matrices which are not suitable to design observers. A way to overcome this, is to use the method developed in [Briat 2008] to design (6.28). Adapting the solution to the polytopic case and the observer form (6.28), one can get the following theorem.

Theorem 6.1 (*[Briat 2008]*)

There exists an LPV polytopic time-delay observer (6.28) for (6.29) such that Problem 6.1 is solved if there exist matrices $Y_i, Y_{hi} \in \mathbb{R}^{n_x \times n_y}$, $X \in \mathbb{R}^{n_x \times n_x}$, symmetric positive definite matrices $P, Q, R \in \mathbb{R}^{n_x \times n_x}$ and a positive scalar γ_∞ such that the LMIs hold for all $i = 1, 2, \dots, 2^N$:

$$\begin{bmatrix} -X - X^T & X^T A_i - Y_i C + P & X^T A_{hi} - Y_{hi} C & X^T E & 0_{n_x, n_z} & X^T & h_m R \\ * & -P + Q - R & R & 0_{n_x, n_w} & C_z^T & 0_{n_x} & 0_{n_x} \\ * & * & -(1 - \mu)Q - R & 0_{n_x, n_w} & 0_{n_x, n_z} & 0_{n_x} & 0_{n_x} \\ * & * & * & -\gamma_\infty I_{n_w} & 0_{n_w, n_x} & 0_{n_w, n_x} & 0_{n_w, n_x} \\ * & * & * & * & -\gamma_\infty I_{n_z} & 0_{n_z, n_x} & 0_{n_z, n_x} \\ * & * & * & * & * & -P & -h_m R \\ * & * & * & * & * & * & -R \end{bmatrix} < 0 \quad (6.34)$$

The gains of the observer (6.28) are deduced as $L_i = (X^T)^{-1} Y_i$ and $L_{hi} = (X^T)^{-1} Y_{hi}$.

Proof: The proof is very similar to [Briat 2008] so not detailed too much here. The objective is to solve the Problem 6.1 on the system (6.31). To establish the stability, the following Lyapunov-Krasovskii candidate function is chosen:

$$\begin{aligned} V(t) &= V_1(t) + V_2(t) + V_3(t) \\ V_1(t) &= e(t)^T P e(t) \\ V_2(t) &= \int_{t-h(t)}^t e(\theta)^T Q e(\theta) d\theta \\ V_3(t) &= \int_{-h_m}^0 \int_{t+\theta}^t \dot{e}(\eta)^T h_m R \dot{e}(\eta) d\eta d\theta \end{aligned} \quad (6.35)$$

After having bounded the time-derivative of (6.35), in particular a \dot{V}_3 upper bound with Jensen's inequality 6.2, the projection lemma [Scherer and Weiland 2000] is used to obtain (6.34). ■

Another interesting approach to define LMI constraints isolated from the observer gains is to use the Finsler's lemma 6.1 as in [Nguyen 2016]. It results in a new theorem to design (6.28).

Theorem 6.2

There exists an LPV polytopic time-delay observer (6.28) for (6.29) such that Problem 6.1 is solved if there exist matrices $Y_i, Y_{hi} \in \mathbb{R}^{n_x \times n_y}$, $Z \in \mathbb{R}^{n_x \times n_x}$, symmetric positive definite matrices $P, Q, R \in \mathbb{R}^{n_x \times n_x}$ and two positive scalars γ_∞ and ϵ such that the LMIs hold for all $i = 1, 2, \dots, 2^N$:

$$\begin{bmatrix} -Z^H + h_m^2 R & ZA_i - Y_i C - \epsilon Z^T + P & ZA_{hi} - Y_{hi} C & ZE \\ * & Q - R + C_z^T C_z + \epsilon(ZA_i - Y_i C)^H & R + \epsilon(ZA_{hi} - Y_{hi} C) & \epsilon ZE \\ * & * & -(1 - \mu)Q - R & 0_{n_x, n_w} \\ * & * & * & -\gamma_\infty I_{n_w} \end{bmatrix} < 0 \quad (6.36)$$

The gains of the observer (6.28) are deduced as $L_i = Z^{-1}Y_i$ and $L_{hi} = Z^{-1}Y_{hi}$. Note: $M^H = M + M^T$.

Proof: Consider the same Lyapunov-Krasovskii defined in (6.35), then compute its time-derivative to obtain:

$$\begin{aligned} \dot{V}_1(t) &= \dot{e}(t)^T P e(t) + e(t) P \dot{e}(t) \\ \dot{V}_2(t) &= e(t)^T Q e(t) - (1 - \dot{h}(t)) e(t - h(t))^T Q e(t - h(t)) \\ \dot{V}_3(t) &= h_m^2 \dot{e}(t)^T R \dot{e}(t) - h_m \int_{t-h_m}^t \dot{e}(\theta)^T R \dot{e}(\theta) d\theta \end{aligned} \quad (6.37)$$

Since $h(t) \in \mathcal{H}$, $\dot{h}(t) \leq \mu$ thus the following inequality is deduced:

$$\dot{V}_2(t) \leq e(t)^T Q e(t) - (1 - \mu) e(t - h(t))^T Q e(t - h(t)) \quad (6.38)$$

Note also that $h(t) \leq h_m$, thus the integral term of $\dot{V}_3(t)$ can be bounded, which gives:

$$\dot{V}_3(t) \leq h_m^2 \dot{e}(t)^T R \dot{e}(t) - h_m \int_{t-h(t)}^t \dot{e}(\theta)^T R \dot{e}(\theta) d\theta \quad (6.39)$$

Applying the Jensen's Inequality 6.2 to the right term of (6.39), we obtain:

$$\begin{aligned} \dot{V}_3(t) &\leq h_m^2 \dot{e}(t)^T R \dot{e}(t) - \frac{h_m}{h(t)} (e(t) - e(t - h(t)))^T R (e(t) - e(t - h(t))) \\ &\leq h_m^2 \dot{e}(t)^T R \dot{e}(t) - (e(t) - e(t - h(t)))^T R (e(t) - e(t - h(t))) \end{aligned} \quad (6.40)$$

In addition to the stability requirement, the observer needs also to attenuate the disturbance w on the estimation error e_z . The relation (6.33) is verified if:

$$\dot{V}(t) + e_z(t)^T e_z(t) - \gamma_\infty w(t)^T w(t) < 0 \quad (6.41)$$

To apply the Finsler's lemma 6.1, (6.31) is rewritten in the form of $\mathcal{B}\xi = 0$ with:

$$\mathcal{B} = \begin{bmatrix} -I_{n_x} & A(\rho) - L(\rho)C & A_h(\rho) - L_h(\rho)C & E \end{bmatrix} \quad \text{and} \quad \xi = \begin{bmatrix} \dot{e}(t) \\ e(t) \\ e(t - h(t)) \\ w(t) \end{bmatrix} \quad (6.42)$$

Expanding the relation (6.41), we deduce:

$$\begin{aligned} & \dot{e}(t)^T P e(t) + e(t) P \dot{e}(t) + e(t)^T Q e(t) - (1 - \mu) e(t - h(t))^T Q e(t - h(t)) + h_m^2 \dot{e}(t)^T R \dot{e}(t) \\ & - (e(t) - e(t - h(t)))^T R (e(t) - e(t - h(t))) + e_z(t)^T e_z(t) - \gamma_\infty w(t)^T w(t) < 0 \end{aligned} \quad (6.43)$$

which can be put into the following quadratic form:

$$\begin{aligned} & \xi^T \begin{bmatrix} h_m^2 R & P & 0_{n_x} & 0_{n_x} \\ * & Q - R + C_z^T C_z & R & 0_{n_x} \\ * & * & -(1 - \mu)Q - R & 0_{n_x} \\ * & * & * & -\gamma_\infty^2 I_{n_w} \end{bmatrix} \xi < 0 \\ & \Leftrightarrow \xi^T Q \xi < 0 \end{aligned} \quad (6.44)$$

Thus, according to Finsler's lemma 6.1, one has:

$$Q + \mathcal{X} \mathcal{B} + \mathcal{B}^T \mathcal{X}^T \prec 0 \quad (6.45)$$

In particular, if $\mathcal{X} = \begin{bmatrix} Z \\ \epsilon Z \\ 0_{n_x} \\ 0_{n_x} \end{bmatrix}$ and with the variable changes $Y(\rho) = ZL(\rho)$ and $Y_h(\rho) = ZL_h(\rho)$, one can finally get the LMI (6.36) at each vertex of the polytope. This concludes the proof. ■

6.4 Results for EGR and Inlet air mass flow rates estimation

Some theoretical tools have been exposed in Section 6.3.2 and this section will be devoted to the observer synthesis for the extended system (6.26) and its performance assessment. For comparison purpose, both design methods described in Theorem 6.1 and Theorem 6.2 will be tested in different conditions. In Section 6.4.1, we detail the direct application of Theorem 6.1 (Case 1) with its benefits and some limitations before providing an alternative implementation (Case 2). Similarly, in Section 6.4.2, we present a direct application of Theorem 6.2 (Case 3), before providing variations of it (Cases 4 and 5).

Ideally, one solves (6.34) and (6.36) for all $i = 1, \dots, 64$ while minimizing γ_∞ . However, due to a ill-conditioning problem and a high number of constraints, we did not find a configuration where both conditions are fulfilled. Thus, in the following, the constant γ_∞ has been fixed to complete the optimization program implemented with the parser YALMIP [Löfberg 2004] and solved with SDPT3 [Tütüncü et al. 2003].

To apply both theorems, the following parameters have to be chosen:

- For Theorem 6.1: E and γ_∞ .
- For Theorem 6.2: E , γ_∞ and ϵ .

The two remaining parameters h_m and μ are experimentally determined using the formula (6.10).

For the sake of clarity, the figures in the sequel represent a part of the transient cycle WHTC. Actually, the time-domain range is the same than the one presented in Figure 6.2(c) and Figure 6.2(d). A global performance index, the *NRMS* Appendix A, summarized in Table 6.2, will evaluate the estimation on the whole cycle for different cases presented hereafter.

Table 6.2: NRMS for the different cases

Estimation method	Case	NRMS	
		D_{air} estimation	D_{egr} estimation
Initial	0	5.5%	22.5%
Theorem 6.1	1	2.5%	7.2%
	2	3.5%	9.1%
Theorem 6.2	3	3.1%	10.8%
	4	3.8%	15%
	5	3.8%	15%

6.4.1 Synthesis based on Theorem 6.1

Case 1. In this first case, consider a full parameter dependent observer for the system (6.26). Therefore, synthesis has to deduce the gains L_i and L_{hi} in the following observer:

$$\begin{aligned} \dot{\hat{x}}_o(t) &= \sum_{i=1}^{64} \mu_i(\rho) [A_{oi}\hat{x}_o(t) + A_{hoi}\hat{x}_o(t-h(t)) + L_i(y_o(t) - \hat{y}_o(t)) \\ &\quad + L_{hi}(y(t-h(t)) - \hat{y}_o(t-h(t)))] + B_o u(t) \\ \hat{y}_o(t) &= C\hat{x}_o(t) \end{aligned} \quad (6.46)$$

Let apply Theorem 6.1 to design (6.46). For the following tuning parameters:

$$E = [1 \ 1 \ 1 \ 1 \ 1 \ 1]^T \times 10^{-5} \quad \text{and} \quad \gamma_\infty = 10^7 \quad (6.47)$$

one can obtain the estimation results depicted in Figure 6.9(a) and Figure 6.9(b) for D_{air} and D_{egr} respectively.

In comparison with the initial method (Case 0) that does not take into account the delay, the designed observer significantly improves the estimation of D_{air} and D_{egr} . The results for D_{air} in Figure 6.9(a) are very accurate. Despite the presence of the delay,

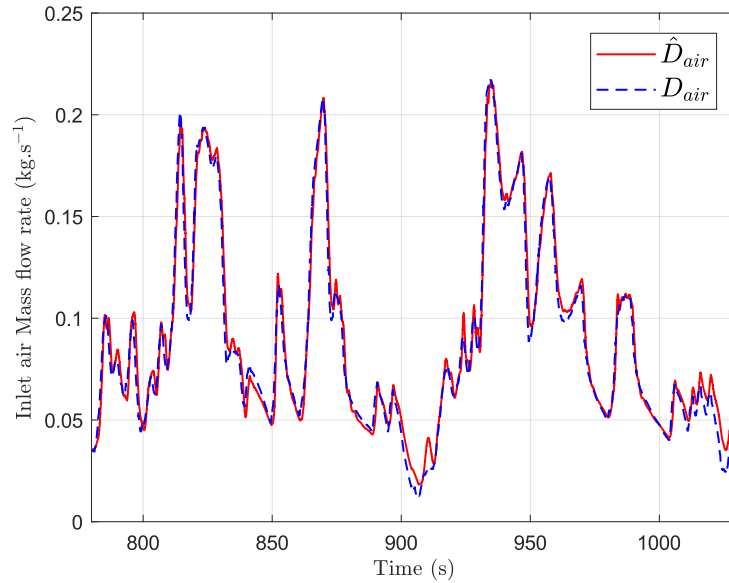
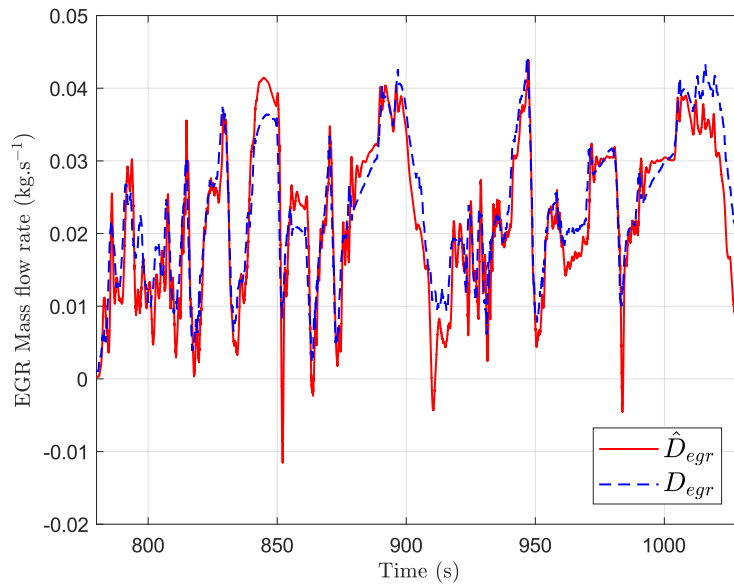
(a) Case 1: D_{air} estimation(b) Case 1: D_{egr} estimation

Figure 6.9: Results for case 1

the observer manages to follow the reference provided by an undelayed sensor (which is the lambda sensor located after the turbine measuring F_3). Regarding the estimation of D_{egr} , the estimation error is larger. One can explain the observed differences by, of course, the modeling uncertainties which are indeed directly compensated by \hat{D}_{air} and \hat{D}_{egr} since they represent integral terms in (6.23). But, one can also explain the errors

by the technical characteristics of the NOx sensor. Indeed, as explained in [Section 6.2.3](#), the NOx sensor is slower than the lambda one thus, during transient phenomena, its value is not the same than the one provided by the lambda sensor and so is the estimate. In addition, we noticed that, during stationary state, there exists a bias between the two sensors due to the calibration. To compensate this bias, a constant offset has been added to the NOx sensor values without guarantee that it is always constant.

Case 2. A big disadvantage of the previous design is its high computational demanding to determine the gains for the observer (6.26) since an interpolation of 64 vertices is needed to have $L(\rho)$ and $L_h(\rho)$ which could be not suitable for a real-time application. Therefore, instead of a parameter dependent gains matrices, we are now looking for constant ones such that:

$$\begin{aligned}\dot{\hat{x}}_o(t) &= A_o(\rho)\hat{x}_o(t) + A_{ho}(\rho)\hat{x}_o(t - h(t)) + L(y_o(t) - \hat{y}_o(t)) \\ &\quad + L_h(y(t - h(t)) - \hat{y}_o(t - h(t))) + B_o u(t) \\ \hat{y}_o(t) &= C_o \hat{x}_o(t)\end{aligned}\tag{6.48}$$

Thus the LMIs in [Theorem 6.1](#) are transformed into:

$$\begin{bmatrix} -X - X^T & X^T A_i - YC + P & X^T A_{hi} - Y_h C & X^T E & 0_{n_x, n_z} & X^T & h_m R \\ * & -P + Q - R & R & 0_{n_x, n_w} & C_z^T & 0_{n_x} & 0_{n_x} \\ * & * & -(1 - \mu)Q - R & 0_{n_x, n_w} & 0_{n_x, n_z} & 0_{n_x} & 0_{n_x} \\ * & * & * & -\gamma_\infty I_{n_w} & 0_{n_w, n_x} & 0_{n_w, n_x} & 0_{n_w, n_x} \\ * & * & * & * & -\gamma_\infty I_{n_z} & 0_{n_z, n_x} & 0_{n_z, n_x} \\ * & * & * & * & * & -P & -h_m R \\ * & * & * & * & * & * & -R \end{bmatrix} \prec 0 \tag{6.49}$$

for all $i = 1, 2, \dots, 2^N$. The new gains are deduced as $L = (X^T)^{-1}Y$ and $L_h = (X^T)^{-1}Y_h$.

If we apply [Theorem 6.1](#) with the LMIs (6.49) for:

$$E = \begin{bmatrix} 1 & 1 & 1 & 1 & 1 & 1 \end{bmatrix}^T \times 10^{-5} \quad \text{and} \quad \gamma_\infty = 10^7 \tag{6.50}$$

the results presented in [Figure 6.10\(a\)](#) and [Figure 6.10\(b\)](#) are obtained.

First, we can see that the time-domain results are less accurate than the previous ones, especially for D_{egr} estimation. The \hat{D}_{air} follows all the variations of the reference D_{air} accurately for high values and less for low values. Theses partial observations are confirmed by the *NRMS* index in [Table 6.2](#). This index is still low for D_{air} estimation but increases for the D_{egr} one. However, both *NRMS* values for this case are lower than the initial ones obtained without taking account the delay.

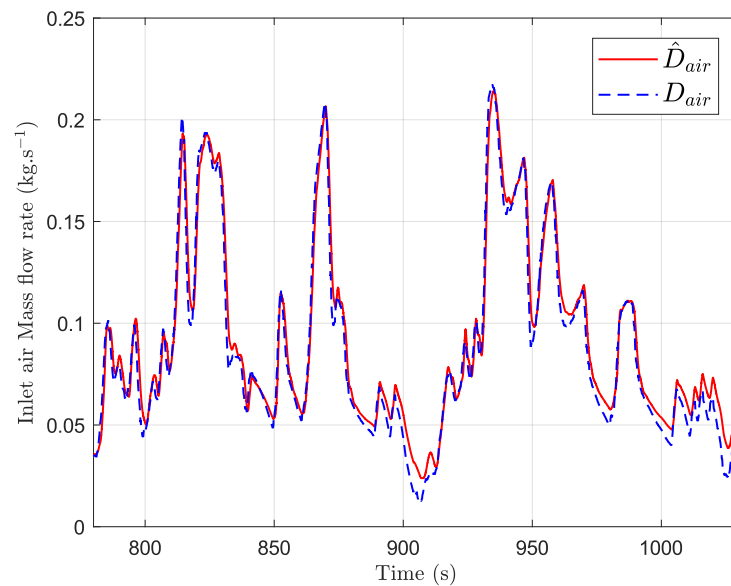
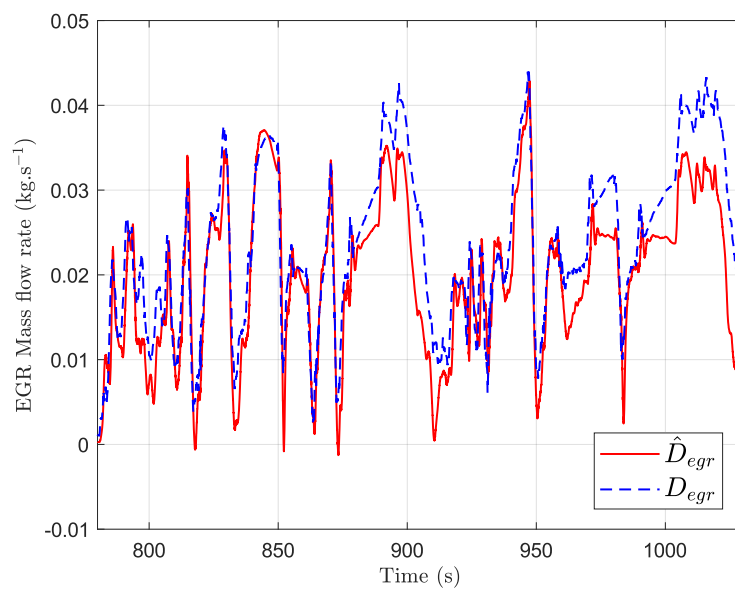
(a) Case 2: D_{air} estimation(b) Case 2: D_{egr} estimation

Figure 6.10: Results for case 2

It appears that the reduction of the observer's complexity, which leads to greater conservatism, is done at the expense of the estimation quality. The observer seems to be not fast enough over the full range parameters variation to follow D_{air} and D_{egr} .

6.4.2 Synthesis based on Theorem 6.2

Case 3. As a first step, let apply Theorem 6.2 to design (6.46). For the following tuning parameters:

$$E = \begin{bmatrix} 1 & 1 & 1 & 1 & 1 & 1 \end{bmatrix}^T \times 10^{-5} \quad \text{and} \quad \epsilon = 10^5 \quad \gamma_\infty = 10^8 \quad (6.51)$$

the deduced estimated flows are depicted in Figure 6.11(a) and Figure 6.11(b).

Remark 6.4

Due to the ill-conditioning previously mentioned, it was not an easy task to obtain a good design with Theorem 6.2. To have a better conditioning, we scaled the system matrices by considering the variable change $\bar{x}(\tau) = x(\lambda\tau)$, with $\lambda > 0$. Indeed, consider the following time-delay system:

$$\dot{x}(t) = Ax(t) + A_h x(t - h(t)) + Bu(t) \quad (6.52)$$

Then,

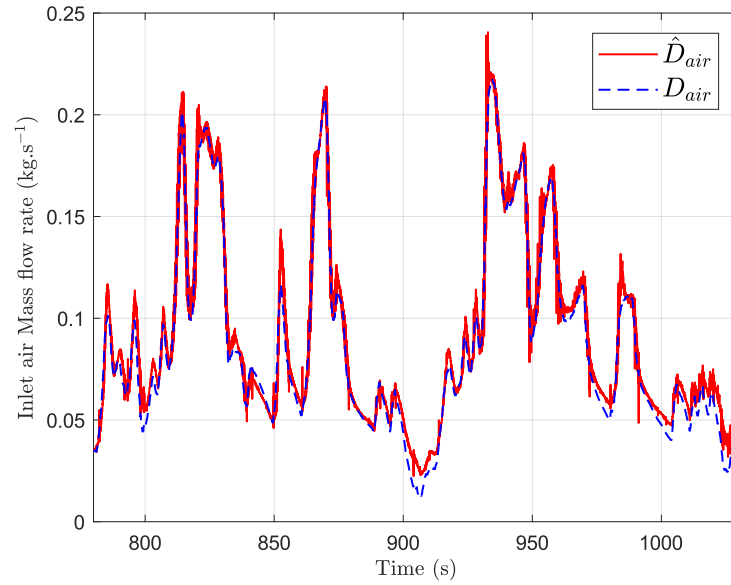
$$\begin{aligned} \frac{d\bar{x}(\tau)}{d\tau} &= \lambda \frac{dx}{dt}(\lambda\tau) \\ &= \lambda \left[Ax(\lambda\tau) + A_h x\left(\lambda\left(\tau - \frac{1}{\lambda}h(\lambda\tau)\right)\right) + Bu(\lambda\tau) \right] \\ &= \lambda A \bar{x}(\tau) + \lambda A_h \bar{x}\left(\tau - \frac{1}{\lambda}\bar{h}(\tau)\right) + \lambda B \bar{u}(\tau) \end{aligned} \quad (6.53)$$

We noticed that for $\lambda = 0.01$ the synthesis is improved. To reconstruct the gains L_i and L_{hi} of (6.46), only a division of the designed gains by λ is needed.

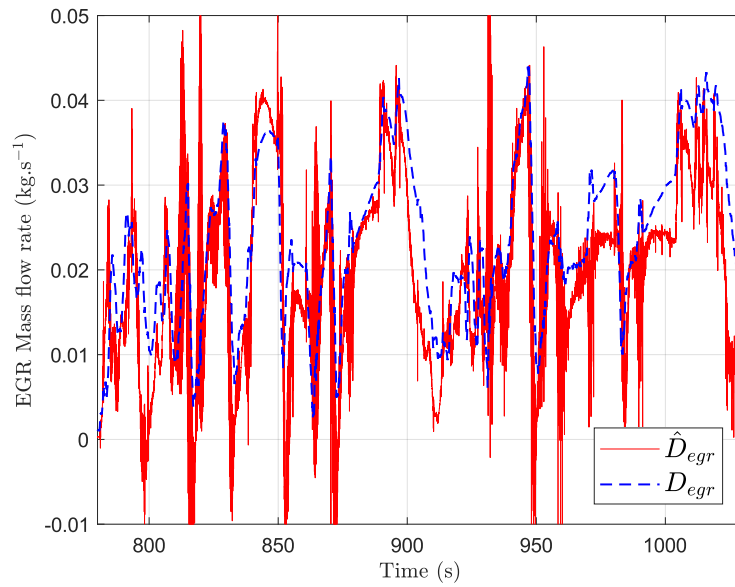
With observer gains depending on the 6 parameters (so a polytope of 64 vertices), we can have a good estimation of D_{air} and D_{egr} . The *NRMS* in Table 6.2 is low, at the same level as in the previous cases, but it appears that the estimations are noisy, especially for \hat{D}_{egr} .

Case 4. Similarly to the Case 2, where the parameter dependency has been removed in the observer gains, the aim is to lighten the computation load by designing the observer (6.48). Following the same idea which leads to (6.49), Theorem 6.2 is adapted by taking two constant matrices $Y, Y_h \in \mathbb{R}^{n_x \times n_y}$ in (6.36). With the same parameters in (6.51), the results when L and L_h are constant are presented in Figure 6.12(a) and Figure 6.12(b).

The observations are similar to the ones performed in Case 2. The estimation of D_{air} is accurate for high flow values and less for low values. On the other hand, \hat{D}_{egr} follows the variations of the reference but a significant relative error could exist for some time intervals. In Table 6.2, the corresponding *NRMS* is the highest but still lower than the initial method.



(a) Case 3: D_{air} estimation



(b) Case 3: D_{egr} estimation

Figure 6.11: Results for case 3

Case 5. A final case is presented here where we are looking for an observer with the following structure:

$$\begin{aligned} \dot{\hat{x}}_o(t) &= A_o(\rho)\hat{x}_o(t) + A_{ho}(\rho)\hat{x}_o(t - h(t)) + L(y_o(t) - \hat{y}_o(t)) + B_o u(t) \\ \hat{y}_o(t) &= C\hat{x}_o(t) \end{aligned} \quad (6.54)$$

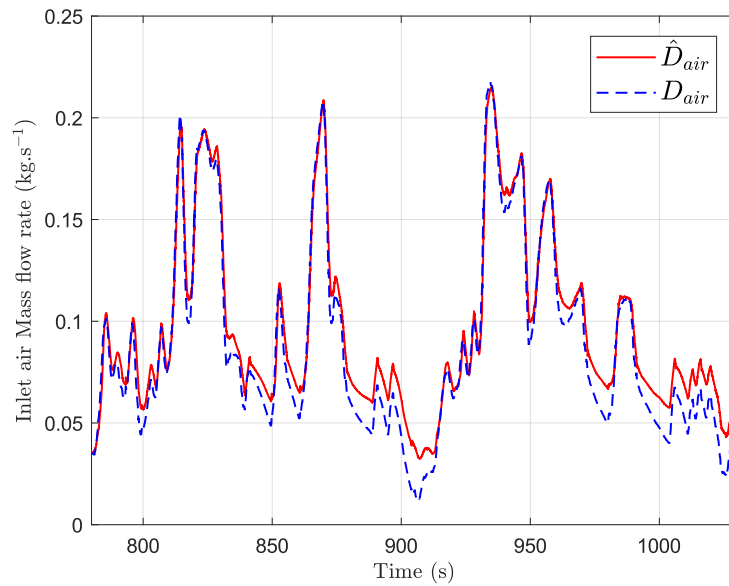
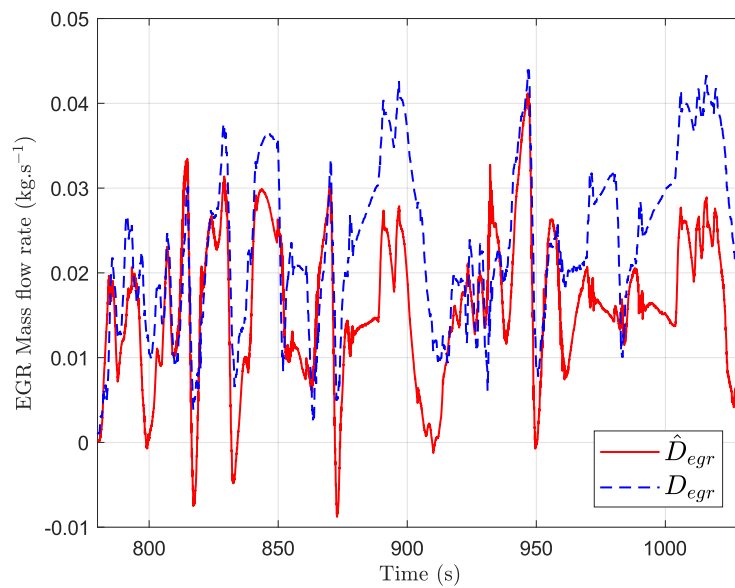
(a) Case 4: D_{air} estimation(b) Case 4: D_{egr} estimation

Figure 6.12: Results for case 4

(6.54) has a constant gain matrix L and L_h is equal to zero.

Such an observer structure enables to mitigate the computational burden by avoiding to use and thus store past values of the output over the time interval $[0, h_m]$. This substantially moderates the memory requirements as, in the case of a sample time of 10ms, one would otherwise need to store approximately 170 values, a number which is

far from being negligible. To deduce L in (6.54) the LMIs of Theorem 6.2 is adapted with $Y \in \mathbb{R}^{n_x \times n_y}$ and Y_h is considered null. In this case, we can obtain the results depicted in Figure 6.13(a) and Figure 6.13(b).

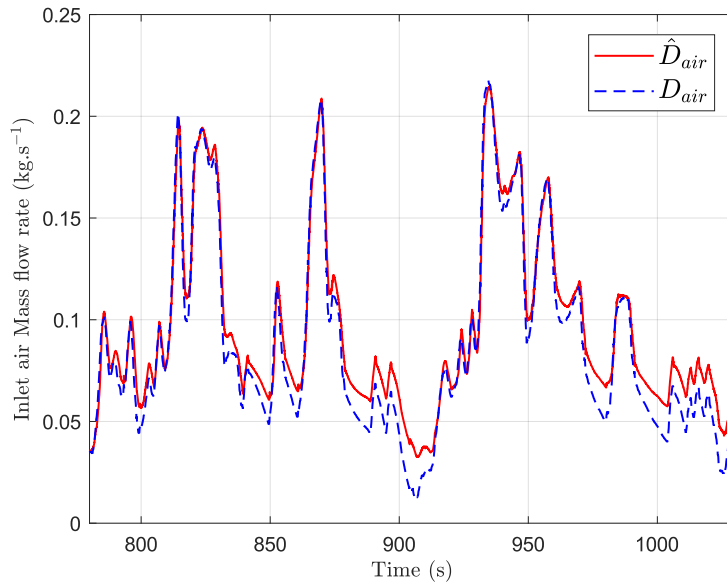
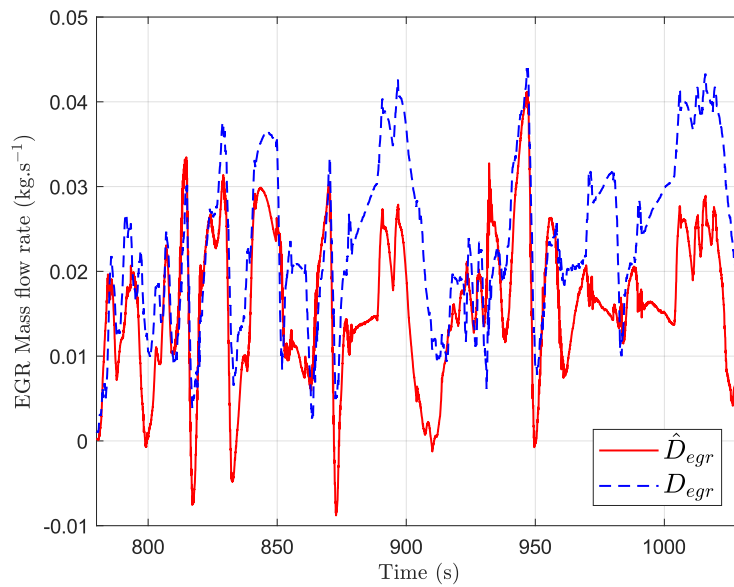
(a) Case 5: D_{air} estimation(b) Case 5: D_{egr} estimation

Figure 6.13: Results for case 5

The performance are similar to the ones obtained in case 4. In addition the $NRMS$ is also the same. So, it appears that a constant gain L can be enough to deduce a

correct estimation for D_{air} and D_{egr} .

6.5 Conclusion

In this chapter we have proposed several LPV time-delay observers to estimate the inlet air and EGR mass flow rates by using a delayed measurement provided by the NOx sensor instead of the lambda sensor. In [Section 6.4](#), based on [Theorem 6.1](#) and [Theorem 6.2](#), we exposed different designs more or less computationally demanding and it has been established that a time-delay observer can provide estimation performance quite similar to the one obtained with a strategy requiring an additional sensor, not subject to delay. We have also observed that the more complex the observer is, the more the estimations are accurate.

One of the encountered difficulties is the ill-conditioning of the system which leads to a high conservatism in the synthesis. Indeed, we did not succeed to minimize the γ_∞ while stabilizing the system and it must be set to a huge value to have a correct synthesis. In addition, a change of variable has been used to have a proper optimization with [Theorem 6.2](#). During the tests, [Theorem 6.1](#) appears to be more effective and less conservative than [Theorem 6.2](#). However it is done at the price of greater complexity in the LMIs. In fact, the solvertime is 56.3s for the case 1 and only 9.5s for the case 3. To improve the synthesis, one could consider a parameter-dependent Lyapunov function to reduce the conservatism then use gridding techniques to solve the LMIs like in [[Briat et al. 2011](#)]. However, given the large number of parameters, the number of LMIs may be very high. Indeed, as pointed in [[Hoffmann and Werner 2015](#)], the required memory grows with $\mathcal{O}(n_g^N)$, where n_g is the size of the grid. One may also investigate nonlinear time-delay observers as in [[Germani et al. 2002](#)].

One may also investigate the model improvement and especially the delay modeling. As explained in [Remark 6.2](#), we did not use a real measurement for the variable D_t in [\(6.10\)](#) but an approximation. In further works, real experiments on test bench could be done to see if real data can improve the quality of the estimation.

Conclusion and Perspectives

General conclusions

The thesis dealt with the development of observers for various systems in the truck. The objectives were:

- (1) Diagnose a component to prevent engines failure.
- (2) Diagnose anti-pollution systems to meet legislation.
- (3) Estimate variables needed for the engine control.
- (4) Replace a sensor by an observer to reduce the production cost.

In summary, the works of the thesis were presented in 6 chapters as follows:

- [Chapter 1](#) provided some theoretical background on control theory with a particular focus on observer design. It presented the different observer structures that have been used along the thesis. Two types of observers have been considered in there: LPV systems, written into a polytopic form, and nonlinear systems.
- [Chapter 2](#) dealt with the monitoring of a serpentine belt tensioner performance, a critical automotive engine component guaranteeing the cooling system efficiency. A belt tensioner fault will affect the transmission, deteriorate the water pump efficiency, and eventually, lead the engine to stall. Monitoring this component is thus a key to design predictive or corrective maintenance. In this chapter, we proposed to estimate a parameter which is shown to be characteristic of this component's health by using an Adaptive Observer or an Extended Kalman Filter. Respective merits of these solutions have been compared using simulations performed with GT-POWER on a high-fidelity model. Even if the Adaptive Observer has guaranteed convergence properties, it has been shown that the Extended Kalman Filter had better performance for this topic.
- [Chapter 3](#) gave an on-board diagnosis (OBD) solution for the charge air cooler (CAC) and EGR cooler; that need to be diagnosed to meet the legislation. Although these diagnoses are already achieved at Volvo, for cost saving, another sensor configuration has been considered. Two observers have been designed to estimate the heat transfer quality of the charge air cooler and the EGR cooler. Then, they have been evaluated on real data from test bench. It has been established that the proposed solutions could efficiently diagnose the CAC and the EGR cooler.

- [Chapter 4](#) compared different observer approaches to estimate an important variable for the pollutant emissions control: the EGR mass flow rate. This chapter aimed to apply 5 observation approaches presented in [Chapter 1](#) for the estimation of the EGR mass flow rate plus one already developed in the literature. In the observer design, this variable has been considered as an additive unknown input. The main idea of the observer was to use the information given by the pressure sensor in the intake manifold as the reference measurement, to estimate this mass flow rate. The final validation consisted in implementing on a real truck's embedded computer and comparing the performance of the different methods. The tests performed on two truck engines have shown that, even if the observer structure was very different, the performance estimation were very similar for all of them. Besides, the CPU consumption appeared to be low, so it can be used in a commercial context.
- [Chapter 5](#) proposed a method for estimating the exhaust manifold pressure. The knowledge of this variable is essential in order to fulfill functions such as the exhaust brake control. However, while in most cases the pressure is directly measured, the sensor may encounter failures in some specific operating conditions. Its estimation is then of great interest for diagnosis and fault tolerant control objectives. Based on mean value models of the turbocharger and the exhaust manifold, a Linear Parameter Varying (LPV) polytopic observer has been designed to provide an estimation of the pressure. The merits of this solution were illustrated with the high-fidelity professional simulator GT-POWER. The results showed that the developed method is a promising way to estimate the pressure with a small relative error.
- [Chapter 6](#) dealt with the estimation of the EGR and inlet air mass flow rates with the NOx sensor located in the after treatment system. The problem was, there exists a significant transport delay between the NOx and lambda sensor currently used to estimate the both mass flow rates. To take into account the delay, LPV time-delay observers have been designed based on an existing method and a new one deduced from Finsler's lemma. The validation and the comparison of the different methods have been done with real data from a test-bench. Even with the delay, the developed observers succeeded to well estimate the flows, particularly for the inlet air mass flow rate.

Perspectives

Here, we will just establish general perspectives and draw the future work direction. For shorter perspectives, we refer the reader to the conclusions in the associated chapters.

In this study, some topics are more advanced as depicted in [Figure 6.15](#) through the analysis of the TRL (Technology Readiness Level). As shown in [Figure 6.14](#), this scale

describes the maturity of a technology and is based on a scale from 1 to 9 with 9 being the most mature technology [Héder 2017]. The observers developed in Chapter 4 are the most advanced because they have been implemented on a real truck's embedded computer. Even if real data have been used to validate the methods in Chapter 3 and Chapter 6, additional tests need to be performed to evaluate the calculation time and to improve the modeling. The methods of Chapter 2 and Chapter 5 have been only validated on a high-fidelity model which explains the TRL 3 for these topics.

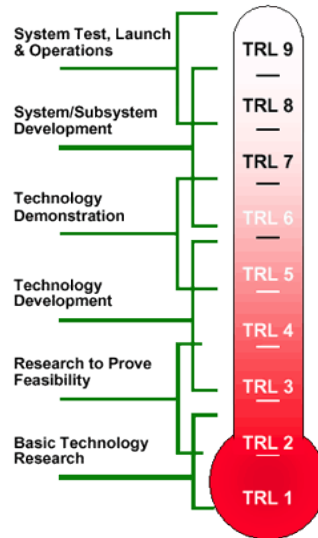


Figure 6.14: TRL scale. Source: wikipedia

For future projects, we have identified several needs in terms of diagnosis and estimation. It consists in:

- *Estimate the exhaust manifold temperature* (the variable T_3 in Figure 5.1). Due to high temperature and strong pressure oscillations conditions, measure this variable is too costly for the manufacturer. Therefore, currently, a open loop model estimates the temperature. However, its inaccuracies cause control problems. Indeed, when T_3 is too high, the control strategy imposes to reduce the amount of fuel injected and thus the torque produced by the engine. It is therefore necessary to know the temperature as accurately as possible, otherwise the engine will be unnecessarily restricted. Following the same modeling as in Chapter 3, an observer could be designed to estimate the temperature.
- *Provide a diagnosis solution for the starter motor*. The starter is an electrical device used to rotate the crankshaft in the engine in order to reach the required rotational speed for the ignition to occur. It has been identified this system encounters premature wear. Thus an observer-based solution could be designed to monitor a too large deviation. The starter is basically a DC motor thus, for

example, the works in [Christophe 2001] (which deals with the nonlinear systems diagnosis applied to electrical machines) could be applied.

- *Detect an urea fault injection.* To reduce the NOx emissions, the after-treatment system injects urea to trigger a chemical reaction. Legislation requires an OBD solution to certify that this system is working properly. For this reason, manufacturers must ensure that the injected solution is urea. Model-based solutions could be studied to address this problem.
- *Estimate wall temperatures inside the after-treatment system.* In order to ensure that the different chemical reactions within the post-treatment system to take place, a certain temperature must be reached. Even if the system is equipped with many temperature sensors, due to the distributed nature of the flow temperature, the optimal point is not reached. First, some work should be devoted to modeling and then, depending on the available sensors, observers could be considered.

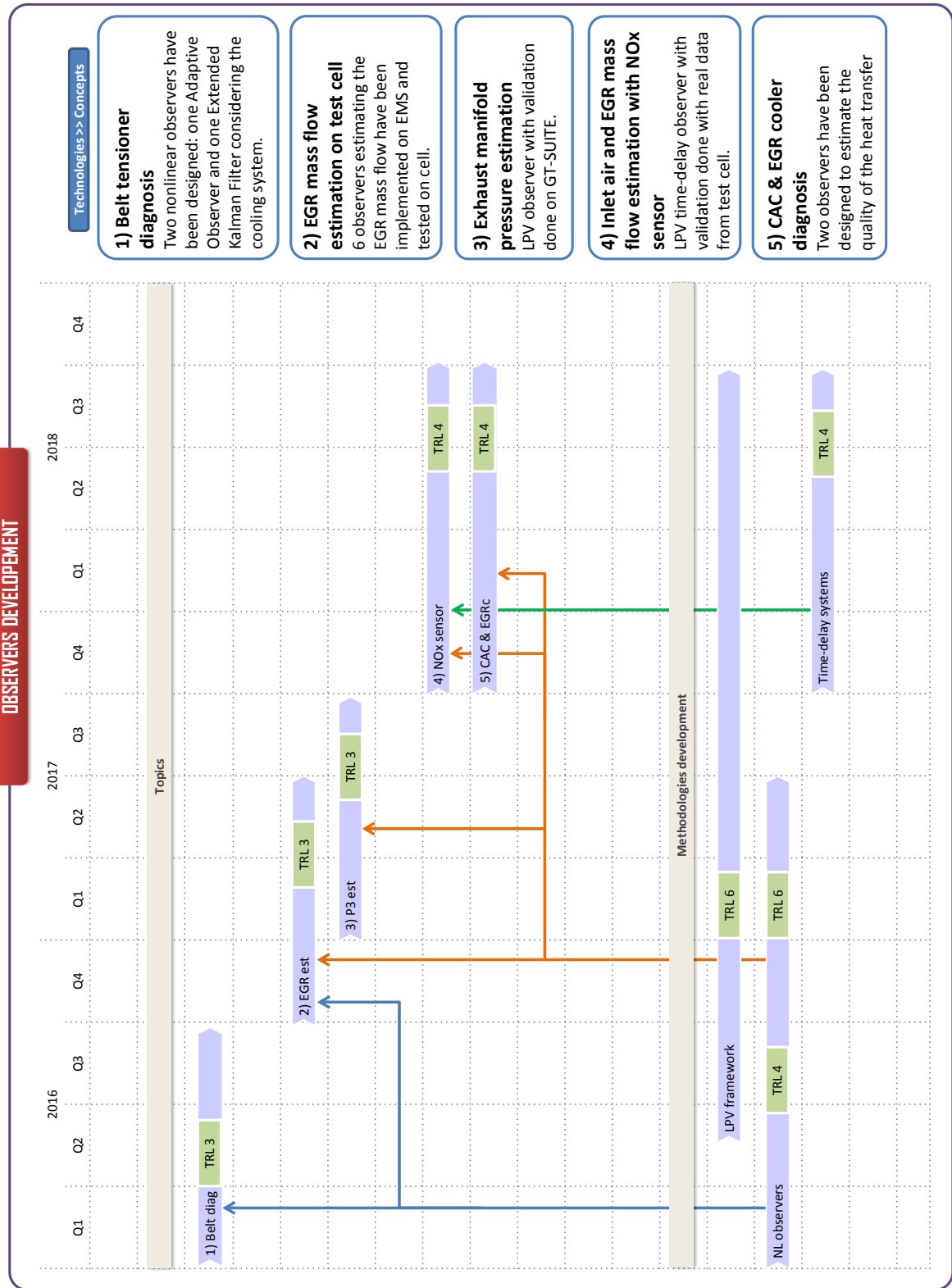


Figure 6.15: Development and readiness of the topics addressed in this thesis

Performance index

Definition A.1

Given, a vector data x which contains N observations, and its estimate \hat{x} , the Normalized Root Mean Square (NRMS) is defined as:

$$NRMS = \frac{\sqrt{\frac{1}{N} \sum_{n=1}^N |\hat{x}(n) - x(n)|^2}}{\max_{n=1,N} x(n) - \min_{n=1,N} x(n)} \quad (\text{A.1})$$

The NRMS is very useful to evaluate the performance of the different observers.

Definition A.2

Given, a observation vector data x , and its estimate \hat{x} , the fit index is defined as:

$$FIT = 1 - \frac{\|x - \hat{x}\|_2}{\|x - \text{mean}(x)\|_2} \quad (\text{A.2})$$

This index is classically used for identification process.

World harmonized cycles

The World Forum for Harmonization of Vehicle Regulations, which is part of the United Nations Economic Commission for Europe, itself part of the United Nations, has established a harmonized global technical regulation (GTR) covering the type-approval procedure for heavy-duty engine exhaust emissions. In the GTR No.4 [UNECE 2007], two representative test cycles are described to cover typical driving conditions in the European Union, the United States of America, Japan and Australia. These two cycles are:

- The World Harmonized Stationary Cycle (WHSC), which is a succession of stationary points in the engine speed and torque (cf. Figure B.1(a)).
- The World Harmonized Transient Cycle (WHTC), which is a transient test based on the pattern of heavy duty commercial vehicles (cf. Figure B.1(b)).

Thus, all along the study, we will refer to these two cycles to provide realistic engine conditions to validate our methods.

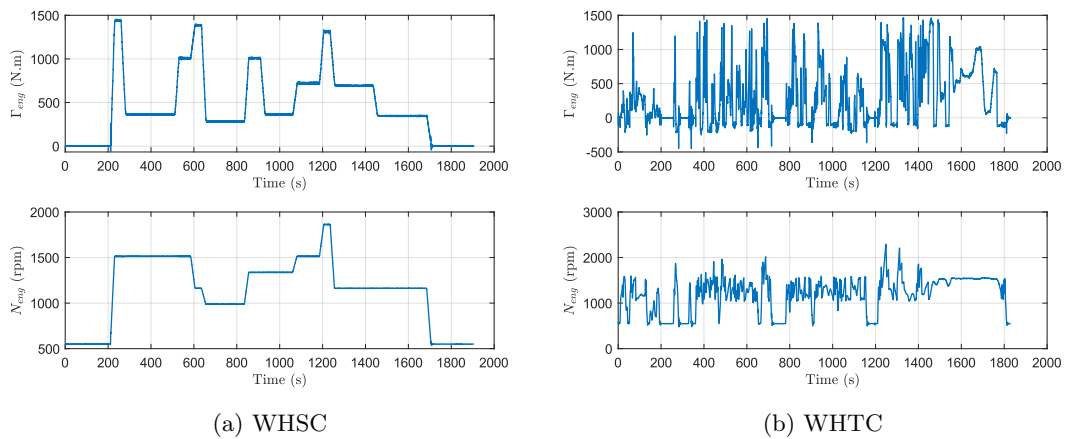


Figure B.1: The two standard cycles used

Air mass flow aspirated by the cylinders

The air mass flow aspirated by the cylinders can be expressed as:

$$D_{asp} = \frac{\eta_v V_{cyl} N_{eng}}{RT_2 120} P_2 \quad (\text{C.1})$$

where V_{cyl} is the cylinder volume, T_2 is the intake manifold temperature, P_2 is the intake manifold pressure and η_v is the volumetric efficiency defined as the ratio between the actual volume flow rate of gases entering the cylinders and the theoretical volume flow rate of gases displaced by the pistons. It is experimentally determined by a map in function of the engine speed and the intake manifold pressure: $\eta_v(N_{eng}, P_2)$. See [Isermann 2014] for a more detailed model and about the efficiency protocol measurement.

Bibliography

- Apkarian, Pierre, Pascal Gahinet, and Greg Becker (Sept. 1995). “Self-scheduled H_∞ control of linear parameter-varying systems: a design example.” In: *Automatica* 31.9, pp. 1251–1261 (cit. on p. 12).
- Astorga-Zaragoza, Carlos-Manuel et al. (Jan. 2008). “Observer-based monitoring of heat exchangers.” In: *ISA Transactions* 47.1, pp. 15–24 (cit. on pp. 35, 56).
- Bara, G. Iulia et al. (Jan. 2001). “Parameter-dependent state observer design for affine LPV systems.” In: *International Journal of Control* 74.16, pp. 1601–1611 (cit. on p. 26).
- Bergman, T. L. and Frank P. Incropera, eds. (2011). *Fundamentals of heat and mass transfer*. 7th ed. Hoboken, NJ: Wiley (cit. on pp. 36, 60).
- Besançon, Gildas (2000). “Remarks on nonlinear adaptive observer design.” In: *Systems & control letters* 41.4, pp. 271–280 (cit. on p. 30).
- (2007). *Nonlinear observers and applications*. Vol. 363. Springer (cit. on pp. 9, 29, 30).
- Besançon, G., J. De León-Morales, and O. Huerta-Guevara (June 2006). “On adaptive observers for state affine systems.” In: *International Journal of Control* 79.6, pp. 581–591 (cit. on pp. 30, 41).
- Borges, Renato A and Pedro LD Peres (2006). “ H_∞ LPV filtering for linear systems with arbitrarily time-varying parameters in polytopic domains.” In: *Decision and Control, 2006 45th IEEE Conference on*. IEEE, pp. 1692–1697 (cit. on p. 24).
- Boussak, M. (Nov. 2005). “Implementation and Experimental Investigation of Sensorless Speed Control With Initial Rotor Position Estimation for Interior Permanent Magnet Synchronous Motor Drive.” In: *IEEE Transactions on Power Electronics* 20.6, pp. 1413–1422 (cit. on p. 30).
- Boyd, Stephen et al. (1994). *Linear matrix inequalities in system and control theory*. Vol. 15. Siam (cit. on p. 15).
- Bresch-Pietri, Delphine (Dec. 2012). “Robust control of variable time-delay systems : Theoretical contributions and applications to engine control.” Theses. Ecole Nationale Supérieure des Mines de Paris (cit. on p. 121).
- Bresch-Pietri, Delphine and Nicolas Petit (2016). “Implicit integral equations for modeling systems with a transport delay.” In: *Recent Results on Time-Delay Systems*. Springer, pp. 3–21 (cit. on p. 121).
- Briat, C., O. Sename, and J.-F. Lafay (Sept. 2011). “Design of LPV observers for LPV time-delay systems: an algebraic approach.” In: *International Journal of Control* 84.9, pp. 1533–1542 (cit. on pp. 127, 141).
- Briat, Corentin (2008). “Commande et Observation Robustes des Systemes LPV Retardés.” PhD thesis. Grenoble INP (cit. on pp. 12, 125, 129, 130).
- Castillo, F. et al. (2013a). “Simultaneous Air Fraction and Low-Pressure EGR Mass Flow Rate Estimation for Diesel Engines.” In: *IFAC Proceedings Volumes* 46.2, pp. 731–736 (cit. on pp. 72, 80, 81).
- Castillo, Felipe (2013). “Modeling and Control of the Air-Path of Diesel Engines for the EURO 7.” PhD thesis. Université de Grenoble (cit. on pp. 51, 118).

- Castillo, Felipe et al. (Apr. 2013b). “Exhaust Manifold Pressure Estimation Diesel Equipped with a VGT Turbocharger.” In: SAE Technical Paper (cit. on p. 94).
- Ceccarelli, Riccardo (2012). “Model-based fault detection in Diesel engines air-path.” PhD thesis. Grenoble INP (cit. on pp. 97, 101, 111).
- Chen, Jie and Ron J Patton (1999). *Robust Model-Based Fault Diagnosis for Dynamic Systems*. Boston, MA: Springer US (cit. on p. 4).
- Chilali, M. and P. Gahinet (1996). “ H_∞ design with pole placement constraints: an LMI approach.” In: *IEEE Transactions on Automatic Control* 41.3, pp. 358–367 (cit. on p. 16).
- Christophe, Cyrille (2001). “Surveillance des systèmes non linéaires: Application aux machines électriques.” PhD thesis. Université des Sciences et Technologie de Lille (cit. on pp. xx, 146).
- Chui, C. K. and G. Chen (2009). *Kalman filtering: with real-time applications*. 4th ed. Berlin: Springer (cit. on p. 29).
- Cortona, E, C H Onder, and L Guzzella (Jan. 2002). “Engine thermomanagement with electrical components for fuel consumption reduction.” In: *International Journal of Engine Research* 3.3, pp. 157–170 (cit. on p. 35).
- Ding, Steven X. (2008). *Model-based fault diagnosis techniques: design schemes, algorithms, and tools*. Berlin: Springer (cit. on p. 4).
- Do, Anh Lam (2011). “Robust LPV Control of vehicle dynamics for comfort and safety improvements.” PhD thesis. Université Grenoble Alpes (cit. on p. 76).
- Dubuc, Donatien et al. (2017). “Observer-based fault diagnosis for trucks belt tensioner.” In: *20th IFAC World Congress* (cit. on pp. 7, 33).
- Dubuc, Donatien et al. (2018). “Exhaust pressure LPV observer for turbocharged diesel engine on-board diagnosis.” In: *10th IFAC Symposium on Fault Detection, Supervision and Safety for Technical Processes, SAFEPROCESS 2018* (cit. on pp. 7, 93).
- Flagan, Richard C. and John H. Seinfeld (2012). *Fundamentals of air pollution engineering*. Mineola, N.Y: Dover. 562 pp. (cit. on p. 120).
- Fredriksson, J. and B. Egardt (2002). “Estimating exhaust manifold pressure in a turbocharged diesel engine.” In: *Conference on Control Applications*. Vol. 2, pp. 701–706 (cit. on p. 94).
- Germani, Alfredo, Costanzo Manes, and Pierdomenico Pepe (2002). “A new approach to state observation of nonlinear systems with delayed output.” In: *IEEE Transactions on Automatic Control* 47.1, pp. 96–101 (cit. on p. 141).
- Gu, Keqin, Vladimir L Kharitonov, and Jie Chen (2003). *Stability of Time-Delay Systems*. Birkhäuser (cit. on p. 128).
- Guzzella, L. and Christopher H. Onder (2010). *Introduction to modeling and control of internal combustion engine systems*. 2nd ed. Berlin: Springer. 354 pp. (cit. on pp. 69, 115).
- Hammouri, Hassan and Jesus De Leon Morales (1990). “Observer synthesis for state-affine systems.” In: *Decision and Control, 1990., Proceedings of the 29th IEEE Conference on. IEEE*, pp. 784–785 (cit. on p. 29).
- Héder, Mihály (2017). “From NASA to EU: the evolution of the TRL scale in Public Sector Innovation.” In: *The Innovation Journal* 22.2, pp. 1–23 (cit. on p. 145).
- Heemels, WP Maurice H, Jamal Daafouz, and Gilles Millerioux (Sept. 2010). “Observer-Based Control of Discrete-Time LPV Systems With Uncertain Parameters.” In: *IEEE Transactions on Automatic Control* 55.9, pp. 2130–2135 (cit. on pp. 106, 113).

- Hjartarson, Arnar et al. (2013). “LPV aeroservoelastic control using the LPVTools toolbox.” In: *AIAA Atmospheric Flight Mechanics (AFM) Conference*, p. 4742 (cit. on p. 14).
- Hoffmann, Christian and Herbert Werner (2015). “A survey of linear parameter-varying control applications validated by experiments or high-fidelity simulations.” In: *IEEE Transactions on Control Systems Technology* 23.2, pp. 416–433 (cit. on p. 141).
- Hwang, Inseok et al. (May 2010). “A Survey of Fault Detection, Isolation, and Reconfiguration Methods.” In: *IEEE Transactions on Control Systems Technology* 18.3, pp. 636–653 (cit. on p. 4).
- Isermann, Rolf (2014). *Engine modeling and control: modeling and electronic management of internal combustion engines*. Springer (cit. on pp. 35, 38, 51, 97, 100, 153).
- Janiszewski, Dariusz (Nov. 2006). “Extended Kalman Filter Based Speed Sensorless PMSM Control with Load Reconstruction.” In: IEEE, pp. 1465–1468 (cit. on p. 30).
- Jankovic, Mrdjan J and I Kolmanovsky (1999). “Controlling nonlinear systems through time-delays: an automotive perspective.” In: *European Control Conference (ECC)*. Karlsruhe: IEEE, pp. 3715–3719 (cit. on p. 116).
- Jung, Merten et al. (Oct. 2002). “Parameterization and Transient Validation of a Variable Geometry Turbocharger for Mean-Value Modeling at Low and Medium Speed-Load Points.” In: SAE Technical Paper (cit. on pp. 97, 100).
- Kahveci, Nazli E and Mrdjan J Jankovic (June 2010). “Adaptive controller with delay compensation for Air-Fuel Ratio regulation in SI engines.” In: *American Control Conference (ACC)*. Baltimore: IEEE, pp. 2236–2241 (cit. on p. 116).
- Kalman, Rudolph E and Richard S Bucy (1961). “New results in linear filtering and prediction theory.” In: *Journal of basic engineering* 83.1, pp. 95–108 (cit. on p. 29).
- Khalil, Hassan K. (1996). *Nonlinear systems*. 2nd ed. Prentice Hall. 734 pp. (cit. on p. 29).
- Künzli, Nino et al. (2000). “Public-health impact of outdoor and traffic-related air pollution: a European assessment.” In: *The Lancet* 356.9232, pp. 795–801 (cit. on p. 3).
- Li, Xiuliang, Qinghua Zhang, and Hongye Su (2011). “An adaptive observer for joint estimation of states and parameters in both state and output equations.” In: *International Journal of adaptive control and signal processing* 25.9, pp. 831–842 (cit. on p. 30).
- Löfberg, J. (2004). “YALMIP : A Toolbox for Modeling and Optimization in MATLAB.” In: *In Proceedings of the CACSD Conference*. Taipei, Taiwan (cit. on pp. 15, 132).
- Martin, Guillaume (2010). “0D - 1D Modeling of the Airpath of IC Engines for Control Purposes.” PhD thesis. Université d’Orléans (cit. on p. 3).
- Mohammadpour, J, M Franchek, and K Grigoriadis (Feb. 2012). “A survey on diagnostic methods for automotive engines.” In: *International Journal of Engine Research* 13.1, pp. 41–64 (cit. on pp. 4, 49, 94).
- Mohammadpour, Javad and Carsten W. Scherer, eds. (2012). *Control of Linear Parameter Varying Systems with Applications*. Springer US (cit. on p. 9).
- Mohammadpour, Javad et al. (June 2010). “LPV decoupling and input shaping for control of diesel engines.” In: *Proceedings of the American Control Conference (ACC)*, pp. 1477–1482 (cit. on pp. 97, 101).
- Moulin, Pierre (2010). “Modélisation et Commande des Systèmes d’Air des Moteurs Suralimentés.” PhD thesis. MINES ParisTech (cit. on pp. 97, 101).

- Nelles, Oliver (2011). *Nonlinear system identification: from classical approaches to neural networks and fuzzy models*. Springer (cit. on p. 102).
- Nguyen, Quan (2016). “LPV approaches for modelling and control of vehicle dynamics: application to a small car pilot plant with ER dampers.” PhD thesis (cit. on p. 130).
- Olin, Peter M. (Apr. 2008). “A Mean-Value Model for Estimating Exhaust Manifold Pressure in Production Engine Applications.” In: SAE Technical Paper (cit. on pp. 94, 101).
- Oliveira, Maurício C. de and Robert E. Skelton (2001). “Stability tests for constrained linear systems.” In: *Perspectives in robust control*. Vol. 268. London: Springer, pp. 241–257 (cit. on p. 128).
- Roche, Emilie (2011). “Commande à échantillonnage variable pour les systèmes LPV : application à un sous-marin autonome.” PhD thesis. Université Grenoble Alpes (cit. on p. 83).
- Rodrigues, M. et al. (Mar. 25, 2015). “Actuator fault estimation based adaptive polytopic observer for a class of LPV descriptor systems.” In: *International Journal of Robust and Nonlinear Control* 25.5, pp. 673–688 (cit. on p. 19).
- Salehi, R. et al. (June 2013). “Nonlinear observer design for turbocharger in a SI engine.” In: *Proceedings of the American Control Conference (ACC)*, pp. 5231–5236 (cit. on pp. 97, 98).
- Scherer, C. W. and C. W. J. Hol (June 2006). “Matrix Sum-of-Squares Relaxations for Robust Semi-Definite Programs.” In: *Mathematical Programming* 107.1, pp. 189–211 (cit. on p. 14).
- Scherer, Carsten and Siep Weiland (2000). “Linear matrix inequalities in control.” In: *Lecture Notes, Dutch Institute for Systems and Control* (cit. on pp. 18, 23, 130).
- Sename, Olivier (2001). “New trends in design of observers for time-delay systems.” In: *Kybernetika* 34.4, pp. 427–458 (cit. on p. 125).
- Sename, Olivier, Peter Gaspar, and József Bokor (2013). *Robust control and linear parameter varying approaches: application to vehicle dynamics*. Vol. 437. Springer (cit. on p. 9).
- Shamma, J. S. and M. Athans (1992). “Gain scheduling: potential hazards and possible remedies.” In: *IEEE Control Systems* 12.3, pp. 101–107 (cit. on p. 11).
- Sivanandam, SN and SN Deepa (2008). *Introduction to Genetic Algorithms*. Berlin, Heidelberg: Springer Berlin Heidelberg (cit. on p. 76).
- Sturm, Jos F (1999). “Using SeDuMi 1.02, a MATLAB toolbox for optimization over symmetric cones.” In: *Optimization methods and software* 11.1-4, pp. 625–653 (cit. on p. 15).
- Tóth, Roland, Peter SC Heuberger, and Paul MJ Van den Hof (2010). “Discretisation of linear parameter-varying state-space representations.” In: *IET control theory & applications* 4.10, pp. 2082–2096 (cit. on p. 83).
- Tütüncü, Reha H, Kim-Chuan Toh, and Michael J Todd (2003). “Solving semidefinite-quadratic-linear programs using SDPT3.” In: *Mathematical programming* 95.2, pp. 189–217 (cit. on pp. 15, 132).
- UNECE (2007). “Global technical regulation No. 4.” In: *ECE/TRANS/180/Add.4* (cit. on p. 151).
- VARRIER, Sébastien (2013). “Détection de situations critiques et commande robuste tolérante aux défauts pour l’automobile.” PhD thesis. Université Grenoble Alpes (cit. on p. 24).
- Verhaegen, M. and P. Van Dooren (Oct. 1986). “Numerical aspects of different Kalman filter implementations.” In: *IEEE Transactions on Automatic Control* 31.10, pp. 907–917 (cit. on pp. 30, 47).

- Vu, Van Tan (2017). “Enhancing the roll stability of heavy vehicles by using an active anti-roll bar system.” PhD thesis. Université Grenoble Alpes (cit. on p. 76).
- Vu, Van-Tan et al. (2016). “Optimal selection of weighting functions by genetic algorithms to design H_∞ anti-roll bar controllers for heavy vehicles.” In: *15th International Conference on Vehicle System Dynamics, Identification and Anomalies (VSDIA 2016)* (cit. on p. 76).
- White, Andrew P., Guoming Zhu, and Jongeun Choi (2013). *Linear Parameter-Varying Control for Engineering Applications*. Springer London (cit. on p. 26).
- Wu, Fen (1995). “Control of Linear Parameter Varying Systems.” PhD thesis. University of California at Berkeley (cit. on p. 14).
- Xu, Shengyuan and James Lam (Dec. 2008). “A survey of linear matrix inequality techniques in stability analysis of delay systems.” In: *International Journal of Systems Science* 39.12, pp. 1095–1113 (cit. on p. 129).
- Yamamoto, Kazusa (2017). “Control of Electromechanical Systems, Application to Electric Power Steering Systems.” PhD thesis. Université Grenoble Alpes (cit. on p. 24).
- Yamamoto, Kazusa et al. (Dec. 2015). “Driver torque estimation in Electric Power Steering system using an H_∞/H_2 Proportional Integral observer.” In: *IEEE*, pp. 843–848 (cit. on p. 19).
- Yue-Yun Wang and Ibrahim Haskara (June 2010). “Exhaust pressure estimation and its application to variable geometry turbine and wastegate diagnostics.” In: *Proceedings of the American Control Conference (ACC)*, pp. 658–663 (cit. on p. 94).
- Zhang, Ke, Bin Jiang, and Vincent Cocquempot (2008). “Adaptive observer-based fast fault estimation.” In: *International Journal of Control, Automation, and Systems* 6.3, pp. 320–326 (cit. on pp. 19–21).
- Zhang, Ke, Bin Jiang, and Peng Shi (2012). *Observer-based fault estimation and accomodation for dynamic systems*. Vol. 436. Springer (cit. on p. 19).
- Zhang, Qinghua and Arnaud Clavel (2001). “Adaptive observer with exponential forgetting factor for linear time varying systems.” In: *Decision and Control, 2001. Proceedings of the 40th IEEE Conference on*. Vol. 4. IEEE, pp. 3886–3891 (cit. on pp. 30, 41).
- Zhu, Yucai (Sept. 2002). “Estimation of an N–L–N Hammerstein–Wiener model.” In: *Automatica* 38.9, pp. 1607–1614 (cit. on p. 101).

Observation et diagnostic pour les véhicules poids lourds

Résumé — Pour répondre à la fois aux nouvelles normes législatives et aux exigences du client, la complexité des camions s'est vue fortement augmentée au cours de ces dernières décennies. En plus de réduire les émissions de polluants, ces nouvelles normes imposent la mise en place d'un système de diagnostic des systèmes anti-pollution. Cela implique donc un contrôle plus fin ainsi qu'une surveillance accrue de ces dits systèmes. Le client quant à lui désire augmenter sa productivité et donc la disponibilité des camions. Afin de remplir ces exigences, le développement d'observateurs (ou capteur logiciel) représente une solution attractive. Ils permettent en effet d'obtenir plus d'informations à partir d'un nombre de capteurs donné, sans coûts supplémentaires pour le constructeur. Au cours de cette thèse, plusieurs observateurs ont été développés pour différents sous-systèmes du camion, dont des observateurs non-linéaires, LPV (Linéaire à Paramètres Variants), et avec retard. Dans un premier temps, dans le cadre de la surveillance et de la maintenance préventive, des observateurs ont été conçus dans le but d'estimer différents coefficients caractéristiques de la dégradation d'équipements tels que : un tendeur de courroie, le refroidisseur d'air de suralimentation et le refroidisseur des gaz d'échappement recirculés (EGR). Un observateur de la pression du collecteur d'échappement a également été développé dans le but de diagnostiquer un défaut du capteur mesurant cette pression. Dans un second temps, l'estimation du débit d'air massique EGR a été utilisée pour tester différentes méthodes d'observation sur banc d'essai, cette variable étant importante dans le contrôle des émissions de polluants. Enfin, dans une optique de réduction de coût, une estimation des débits d'air massiques entrant dans le moteur et celui de l'EGR a été réalisée sur la base d'un capteur soumis à un retard.

Mots clés : Observation, Diagnostic, Poids lourds.

Observation and diagnosis for trucks

Abstract — To meet both new legislative standards and customer requirements, the complexity of trucks has increased significantly in the recent decades. In addition to reducing pollutant emissions, these new standards require on board diagnosis solutions for anti-pollution systems. Therefore it implies a thinner control and increased monitoring of these systems. Besides, the customer wants to increase productivity and therefore the availability of the truck. In order to fulfil these requirements, the development of observers (or virtual sensors) is an attractive solution. Indeed, more information can be obtained from a given number of sensors, without additional cost for the manufacturer. During this thesis, several observers were developed for different truck subsystems, including non-linear, LPV (Variable Parameter Linear) or delay observers. As a first step, from a monitoring and preventive maintenance point of view, observers have been designed to estimate different equipment degradation ratio such as: a belt tensioner, a charge air cooler and an exhaust gas recirculation (EGR) cooler. An observer of the exhaust manifold pressure has also been developed to diagnose a fault of the sensor measuring this pressure. In a second step, the EGR mass flow rate estimation was used to test different observation approaches on a test bench, this variable being important for the pollutant emissions control. Finally, in order to reduce cost, the observation of the inlet air and EGR mass flow rates has been studied with a sensor submitted to a delay.

Keywords: Observation, Diagnosis, Trucks.
